KINETIC INVESTIGATION OF NITRONE CYCLOADDITION REACTIONS FOR BIOORTHOGONAL LABELLING

KAITLYN DANIELLE MARGISON

Thesis submitted to the University of Ottawa in

partial Fulfillment of the requirements for the

Master's degree in Chemistry and Biomolecular Sciences

Department of Chemistry and Biomolecular Sciences

Faculty of Science

University of Ottawa

Abstract

Bioorthogonal chemistry involves the development of chemical reactions that can be used to monitor, quantify and manipulate the roles of biological molecules in their native environments. Although there is a continuous demand to develop reactions with fast kinetics, developing reactions that make use of small "mini tag" functional groups are necessary to avoid perturbing function and to cross cellular membranes. Nitrones are small functional groups that have been shown to be excellent alternative 1,3-dipoles to azides in strain-promoted alkyne-nitrone cycloaddition reactions (SPANC). To further expand on the use of nitrones as reacting partners with other dipolarophiles, the kinetics of a variety of acyclic and cyclic nitrones were evaluated with strained- *trans*-cyclooctene. The reactions of acyclic nitrones were conducted under pseudo first-order conditions using UV-visible spectroscopy. By changing the α-aryl- substituent on acyclic nitrones, a linear free energy relationship shows increased reactivity with electron deficient nitrones. Second order rate constants of cyclic nitrones were found to be similar to those of acyclic nitrones, achieving 95% conversion in less than 20 minutes. Using unnatural D-amino acids tagged with nitrones, and s-TCO-Alexa488, labelling of the bacterial peptidoglycan layer was demonstrated. These new findings expand the bioorthogonal toolbox and allow for TCO reagents to be used in bioorthogonal applications beyond tetrazine ligations.

The optimization of click reactions for biological settings has substantially increased the versatility of these reactions for applications beyond biological labelling such as polymer

synthesis. A strained cyclootadiyne, namely *sym*-dibenzo- 1,5-cyclooctadiene-3,7-diyne (diyne) is a benzylated- strained di-alkyne primed for strained- double-click chemistry for conjugation of molecules containing 1,3-dipoles. The second order rate constants for the consecutive additions of a variety of nitrones onto diyne were established via pseudo first-order kinetics by UV-visible spectroscopy. The kinetics of the double addition of acyclic nitrones onto this diyne show that the second addition occurs with second order rate constants more than 2-fold greater, and rates of the second addition can be increased by using electron deficient nitrones. Mechanistic investigation failed to observe the mono-intermediate, and experiments are outlined for future investigation of this phenomenon. Using the kinetic analysis results, di-nitrone monomers containing cyclic and diaryl-nitrones were designed for use in polymer applications. Based on the reports herein, we anticipate the application of this new double-SPANC reaction for peptide cross-linking, polymer synthesis and conjugation of biological molecules.

Statement of Work

The work presented in this thesis is my own and I take full responsibility for its content. All experiments and analysis were prepared by me, with the exception of the NMR kinetics shown in chapter 2, which were conducted by Farnaz Mahmoudi. Synthesis of molecules not shown, namely D-ala-DMImO and D-ala-CMPO, used in Chapter 2 were done by previous lab members.

Acknowledgements

Finishing my graduate studies at the University of Ottawa in the Pezacki Laboratory is bittersweet in many ways. I feel incredibly blessed to have had the opportunity to work with so many great people over the last two and a half years. Dr. John Pezacki, from the moment I took your class, I've enjoyed your research, your humour and your teaching. You have provided an outstanding lab with so many resources and an environment that promotes independence and teamwork. Thank you for your guidance, patience and words of encouragement over the last couple years. Thank you to my committee members for taking the time to read my thesis and be a part of my master's degree. Special thank you to Dr. Jeffrey Keillor for your help with the kinetic analysis in Chapter 3, I look forward to further discussions on this.

Much of the work in my thesis would not have been achieved without the help and support of so many of my peers in and outside the lab. Didier, you were always there to provide advice, talk about projects and fix things- working with you and learning from you was always a blast and I could never thank you enough. To the others of the chem side, I am so happy we all share the same sass and thank you all for making working in the lab so fun. To the 5 women I shared office space with, you all are amazing, hilarious, and kind! I am going to miss all the chats, the treats and the pictures of cats that were shared. To everyone else I have had the pleasure of working with, thank you for creating such a friendly and collaborative environment. A special thanks to some of my collaborators outside the lab, Dr. Ron Shah and Emily Schaefer of the Pratt lab, thank you

both for your assistance with the HPLC and UPLC. To Dr. Sharon Curtis, thank you for your help with mass spectroscopy experiments.

Anyone that has completed graduate school knows that it could not be possible without the support from family and friends. To my mother and father, thank you for always asking about my research, supporting me (both emotionally and financially) and always encouraging me when I needed it the most. Thank you to my brother and sister for being there and for always making me laugh during the hardest times. Thank you to Craig and his family for providing a home away from home. Craig, I am so lucky to have you in my life, I am forever grateful to you for your constant love, support and patience.

Table of Contents

List of Figures

List of Tables

List of Schemes

List of Abbreviations

ACN	**-**	acetonitrile
Ala	-	alanine
BARAC	-	biarylazacyclooctynone
BCN	-	bicyclo[6.1.0]non-4-yne
CMPO	-	2*H*-Pyrrole-2-carboxylic acid, 3,4-dihydro-2-methyl-,1-oxide
CuAAC	-	Cu(I)-catalyzed 1,3-dipolar azide-alkyne cycloaddition
CuANCR	-	Cu(I)-catalyzed 1,3-dipolar alkyne-nitrone cycloaddition followed by rearrangement
DBCO	-	dibenzoazacyclooctyne
DIBO	-	dibenzocyclooctynol
DIFO	-	difluorinated cyclooctyne
Diyne	-	sym-dibenzo- 1,5-cyclooctadiene-3,7-diyne
d-ala-CMPO	-	2R)-2-amino-3-[(2-methyl-1-oxy-3,4-dihydro-2H-pyrrole-2-carbonyl)-amino]-propionic acid
d-ala-DMimo	-	(2R)-2-amino-3-(2,2-dimethyl-5-oxo-3-oxy-2,5-dihydro-imidazol-1-yl)-propionic acid
DMImO	-	(2R)-2-amino-3-(2,2-dimethyl-5-oxo-3-oxy-2,5-dihydro-imidazol-1-yl)- propionic acid
DMPO	-	5,5-dimethyl-1-Pyrroline-N-Oxide
DMSO	-	dimethyl sulfoxide
D-SPANC	-	double-strain promoted alkyne-nitrone cycloaddition
d-TCO	-	dioxolane-fused *trans*-cyclooctene
EDG	-	electron donating group
EWG	-	electron withdrawing group
FMO	-	frontier molecular orbital
HEK293	-	human embryonic kidney
HOMO	-	highest occupied molecular orbital
HPLC	-	high-performance liquid chromatography
IEDDA	-	inverse-electron demand diels alder
LC-MS/ESI+	-	liquid chromatography-mass spectroscopy/electrospray ionization
LUMO	-	lowest unoccupied molecular orbital
m	-	meta
MFN	-	multifunctional nanoparticles
MW	-	molecular weight

NMR	-	nuclear magnetic resonance
o	-	ortho
OCT	-	cyclooctyne
p	-	para
PBS	-	phosphate buffer saline
PEG	-	polyethylenelglycol
RDS	-	rate determining step
SPAAC	-	strain-promoted azide -alkyne cycloaddition
SPANC	-	strain-promoted alkyne-nitrone cycloaddition
SPANOC	-	strain-promoted alkyne-nitrile oxide cycloaddition
SPDC	-	strain-promoted “double-click”
scFv	-	single chain variable fragment
s-TCO	-	strained – *trans*-cyclooctene
TCO-PNB	-	*trans*-cyclooctene-*p*-nitrobenzyl ester
tet	-	tetrazine
TLC	-	thin layer chromatography
UAA	-	unnatural amino acid
UV- Vis	-	Ultra Violet- visible

Chapter 1

Introduction

1.1 Bioorthogonal Chemistry

Cells, organisms and other biological systems are complex in the components they are composed of, the environments they create, and the roles they play. Despite the difficulties in studying these systems, developing ways to study and manipulate components within these systems is important to increase our understanding of the functioning and interactions found within biological systems. The desire to track a variety of biological molecules individually and specifically, like glycans, lipids, and nucleic acids led to the rise of a field known as chemical biology. Chemical biology is the study of biological systems using chemical techniques, typically synthetic small molecules which will directly interact with molecules of interest to report on or alter function. Since synthetic biological tags and reactive groups can be incorporated into a plethora of biological molecules through methods of genetic manipulation, metabolic pathways and active or passive incorporation , the development of suitable reactive moieties for biological systems also developed into its own field of study; bioorthogonal chemistry.[1]

1.2 Defining Bioorthogonal Chemistry

Bioorthogonal chemistry, as championed by Carolyn Bertozzi,[2] involves the development of reactions that probe or take place in biological systems that are selective enough to avoid perturbing other cellular native processes. Bioorthogonal reactions are used to monitor, quantify and manipulate the roles of glycans, lipids, nucleic acids, proteins and enzymes in their native environments. Optimally, a bioorthogonal reaction will be nontoxic in its reactants and products, high yielding, exhibit fast kinetics at biological pH and temperature, and have a unique mechanism leading to increased specificity so that the reactive groups do not react with surrounding biological nucleophiles, electrophiles, oxidants and reductants.[3]

To build a bioorthogonal reaction for labelling applications, it needs to be paired with an imaging modality (fluorophore or radiolabel), affinity handle (biotin-streptavidin) or perturb function so that its effects can be monitored using classical biochemical assays (i.e. qPCR or western blot). As such, the use of bioorthogonal chemistry for labelling typically proceeds in two steps. First, the natural substrate of interest (i.e. a protein) shown as the yellow circle in **Figure 1.1**, is tagged with a bioorthogonal functional group (red square) and introduced into the cell through some form (genetic encoding, metabolic incorporation). Next a probe (green star), which may be biotin or a fluorophore, containing the complementary functional group (blue square), is added to the cell, and will react with and label the substrate of interest. A fluorophore can be used to track the substrates metabolism and function visually,

whereas biotin can be used to isolate the protein of interest and perform mass spectrometry quantitation.

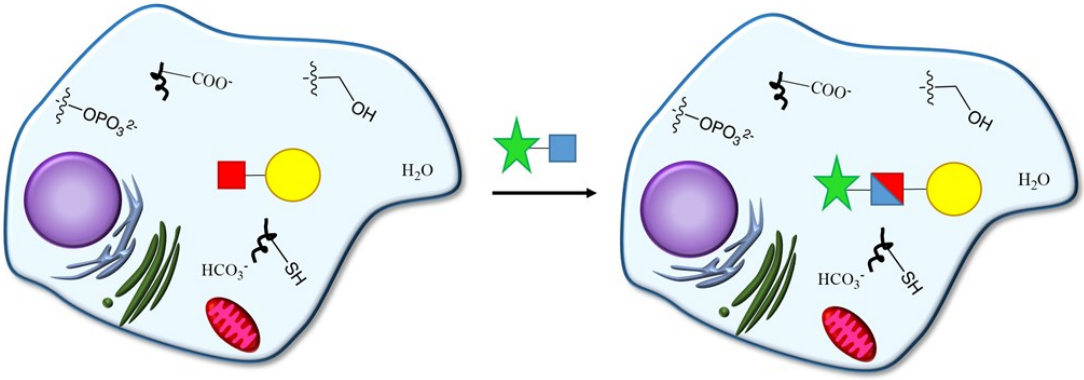

Figure 1.1 A general bioorthogonal reaction scheme occurring intracellularly. Natural substrate of interest (in yellow) is tagged with a reactive group (red), followed by introduction of a probe (green) tagged with a complementary functional group (blue) for labelling substrate of interest.

The key to an effective bioorthogonal reaction is high specificity such that it does not cross-react with other cellular targets, avoiding unspecific labelling. As the cell contains a plethora of nucleophiles and electrophiles, attaining high specificity is quite challenging.[4] Many of the characteristics of bioorthogonal reactions outlined above match those defined by Sharpless of "click" chemistry in 2001, where the click reagents must be mutually exclusive rendering them nearly unreactive to other reactive functionalities that may be present.[5] Naturally, many click reactions have been optimized for bioorthogonal applications or have bioorthogonal potential.

1.3 Click Chemistry

Click chemistry was first described by Sharpless in 2001 as having the goal of creating powerful, selective, and modular "blocks" that can be used in small- and large-scale chemistry. The reactions must fit the criteria of being modular, high yielding, generate innocuous byproducts, and require simple reaction conditions (insensitive to water and oxygen) with simple product isolation. To form these products, they must be "spring-loaded" with a thermodynamic driving force greater than 20 kcal/mol.[5] Cycloadditions of unsaturated species (1,3 dipolar cycloadditions), Diels-Alder reactions, nucleophilic substitution and ring-opening reactions are among some of the many reactions Sharpless identified as fulfilling the criteria outlined above.

One of the first click reactions to satisfy bioorthogonal conditions was the Traceless Staudinger Ligation developed by Bertozzi, where a functionalized phosphine reacts with an azide to form an amide bond through an electrophilic trap. Using azido-sugars and a biotinylated triaryl-phosphine, cell surface labelling was achieved.[6] With neither group naturally found intracellularly, and recognizing that azides could be incorporated into amino acids, this reaction opened the possibility of expanding into intracellular labelling as well.

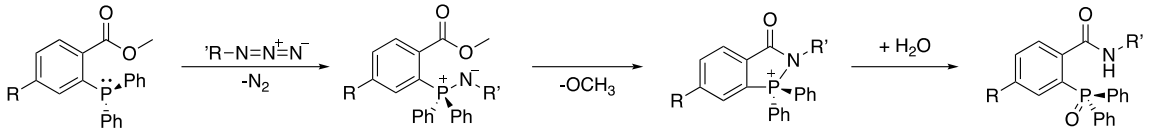

Scheme 1.1 Traceless Staudinger Ligation. R=linker with biotin, R'=mannosamine sugar.

1.4 Copper(I)-catalyzed azide-alkyne cycloaddition (CuAAC)

The first widely used bioorthogonal click reaction is the 1,3 dipolar cycloaddition between a 1,3-dipole and a dipolarophile, first described by Huisgen in 1963 using azides and terminal alkynes (**Scheme 2.2.a**).[7] Although high yields of 88-98% were observed, the reaction suffered from poor regioselectivity and required high temperatures. In 2002, Sharpless and Mendel founded the "copper effect" whereby adding copper(I) to the reaction, the rate increased by 7 orders of magnitude and regioselectivity improved to produce only 1,4 disubstituted 1,2,3- triazoles (**Scheme 1.2b**).[8,9]

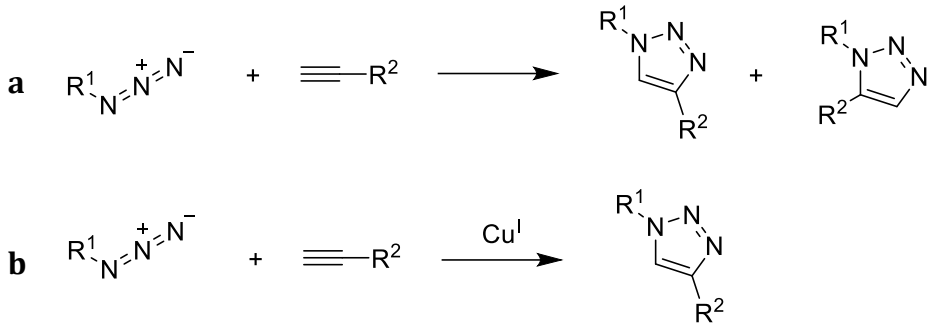

Scheme 1.2 a) Huisgen 1,3-dipolar cycloaddition and b) Cu-catalyzed cycloaddition (CuAAC) between an azide and alkyne to form 1,2,3-trizoles.

To increase the utility of the reaction, different copper ligands, Cu(II) salts with reductants, and preformed Cu(I) catalysts have been explored to increase rate and biological inertness to decrease toxicity.[10,11] To produce Cu(I) species in solution, $CuSO_4 \cdot H_2O$ with sodium ascorbate is often used as it is compatible in water and oxygen. Biological, water soluble ligands like L-proline and L-histidine are also employed to increase inertness by stabilizing the Cu(I) species and reducing concentration of toxic copper ions.[10] Even with these mitigating effects, the overall utility of CuAAC is mainly limited to *in vitro* applications since long-term exposure to copper is cytotoxic to cells.[12]

1.5 Strain-promoted azide-alkyne cycloaddition (SPAAC)

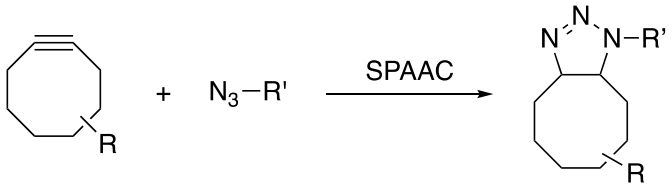

Scheme 1.3 Strain-promoted [3+2] cycloaddition of azides with cyclooctyne.

The strain-promoted [3+2] cycloaddition between cyclooctyne and azides was introduced by Bertozzi and coworkers in 2004.[13] Just two years after the first publications on CuAAC, strain-promoted cycloadditions provided a method to eliminate the need for copper, offering a more biologically inert reaction for *in vivo* studies. The bond angle of the cycloalkyne induces strain accounting for nearly 18 kcal/mol ring strain, causing a destabilization of the ground state versus the transition state. This destabilization greatly increases the rate of reaction compared to that of unstrained alkynes.[5] However, this reaction was very slow in comparison to the copper catalyzed cycloaddition, with a second order rate constant of just of 10^{-3} M^{-1} s^{-1}.[3,14] Modulating electronics and strain of the initial cyclooctyne (OCT) with fluorine substituents or aryl fusion has led to increases in rate from 2-375-fold in comparison to OCT (**Figure 1.2**).[14,15]

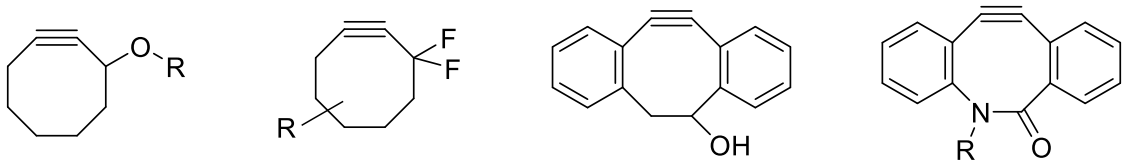

OCT
k_2= 2.4 x 10^{-3}
M^{-1} s^{-1}

DIFO
k_2= 7.6 x 10^{-2}
M^{-1} s^{-1}

DIBO*
k_2= 5.7 x 10^{-2}
M^{-1} s^{-1}

BARAC
k_2= 9 x 10^{-1}
M^{-1} s^{-1}

Figure 1.2 Various cyclooctynes (OCT, DIFO, DIBO, BARAC) and their measured second order rate constants with benzyl azide in acetonitrile. * 3:1 ACN: H_2O.

The overarching goal of investigating different cyclooctynes is to increase the reaction rate of these strain-promoted reactions. The reasoning is twofold, first, by increasing the rate of reaction, the concentration of reagents required can be lowered and still achieve a positive signal, and second, faster rates lower both the risk of toxicity and importantly, the cross-reaction with other biomolecules.[3] With the majority of SPAAC reaction development focused on manipulation of the alkyne, opportunity for alternatives to azides had not been explored until 2010 when the Pezacki laboratory published the first strain-promoted alkyne-nitrone cycloaddition (SPANC) offering an advantageous alternative to azides that can react with the vast number of strained alkynes that had already been developed.[16]

1.6 Nitrones

Nitrones are 1,3-dipoles of the allyl anion type, meaning that they are bent and characterized by three p_z orbitals oriented perpendicular to the plane of the dipole.[17] Nitrones are easily synthesized by a range of chemical reactions including oxidation

of secondary amines,[18] *N,N*-disubstituted hydroxylamines,[19] and isoxazolidines,[20,21] as well as condensation reactions involving hydroxylamines (**Figure 1.3**).[22] Nitrones have typically been used in reactions with nucleophiles[23] or radicals,[24] C-H functionalization,[25,26] and various addition reactions.[27] Nitrones also undergo numerous cycloaddition reactions including [3+3] and [4+2] cycloadditions;[28,29] however, their use in [3+2] cycloadditions with alkenes and alkynes is of most interest in this study.

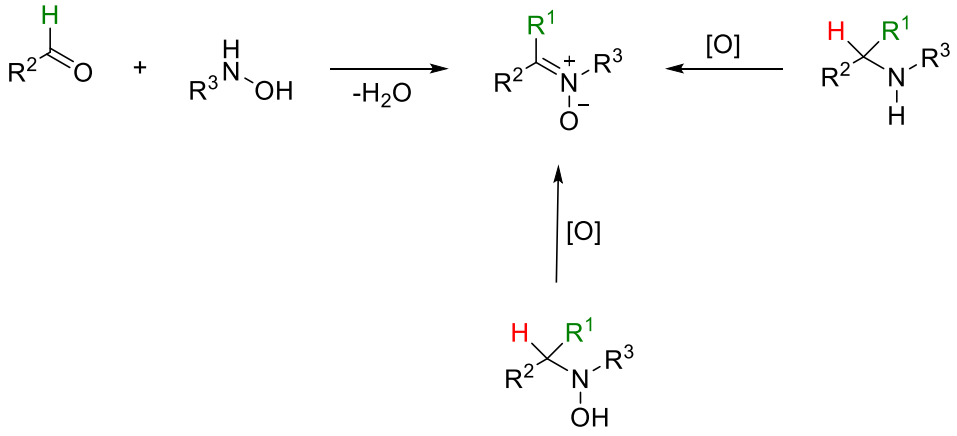

Figure 1.3 Synthesis of nitrones through condensation of hydroxyalmines with aldehydes (right), or oxidation of secondary amines (left) and hydroxyalmines (bottom).

[3+2] cycloadditions occur between a 1,3-dipole (nitrone) and a dipolarophile (alkene or alkyne). The transition state of concerted 1,3-dipolar cycloadditions is controlled by the frontier molecular orbitals (FMOs) of the substrates, whereby decreasing the HOMO-LUMO energy gap increases the reactivity. Governed by the FMO theory, Sustmann classified three types of 1,3-dipolar cycloadditions (**Figure**

1.4).[30] In Type I, also known as "normal electron demand", the transition state is dominated by the interaction of the $HOMO_{dipole}$ with the $LUMO_{dipolarophile}$. In Type II- the similarity of the dipole and alkene FMO energies implies that both HOMO-LUMO interactions are important. Finally, opposite to Type I, Type III, or "inverse electron demand" reactions are dominated by the interaction between the $LUMO_{dipole}$ and $HOMO_{dipolarophile}$.[30] Because of the similarity between the HOMO and LUMO nodal structure of nitrones, reactions of nitrones with alkenes are typically classified as type II, and the reaction type changes to Type I or Type III based on the electronics of the dipolarophile (alkene).[17]

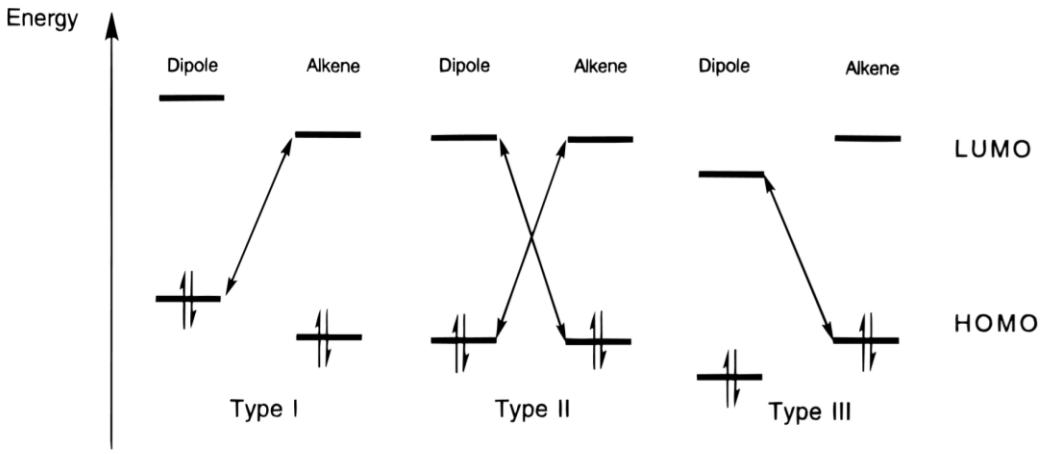

Figure 1.4 Classification of the FMOs for the three types of 1,3-dipolar cycloadditions. Figure was adapted from Gothelf and Jorgensen.[17]

Nitrones are tunable and highly reactive towards alkynes for use in both strain-promoted and copper-catalyzed cycloaddition reactions. They serve as valuable alternatives to azides because they possess three sites for stereo-electronic

modification which allows for the induction of strain or incorporation of a handle or linker to the nitrone (**Figure 1.5b, 1.5c**).[31]

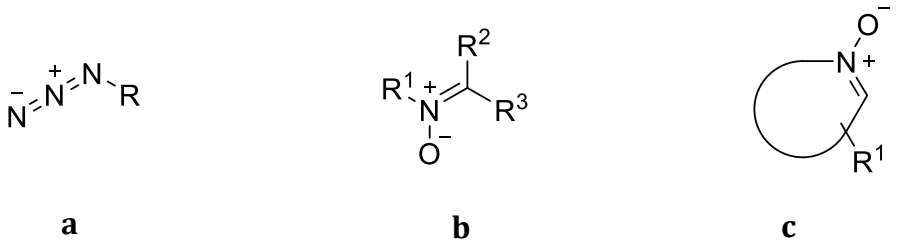

Figure 1.5 General structures of a) azides b) acyclic nitrones and c) cyclic nitrones.

The characterization of both acyclic *N*-phenyl nitrones and endocyclic nitrones with strained and terminal alkynes via copper-catalyzed reactions have been thoroughly investigated.[31,32] Acyclic nitrones can be easily tuned to achieve faster reactivity, however, they are of limited use in aqueous environments. When exposed to acidic and basic conditions, *N*-phenyl nitrone was hydrolyzed to the corresponding hydroxylamine and aldehyde (**Scheme 1.4**). Endocyclic nitrones remain completely stable in acidic and basic conditions, allowing for use in metabolic labelling applications.[33] Nonetheless, investigating the reaction with acyclic nitrones is useful for insight on mechanistic examination and detailing the factors that govern the reactivity of nitrone cycloadditions.

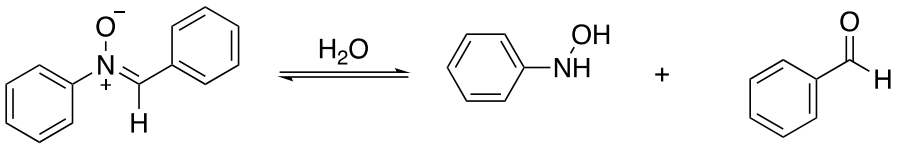

Scheme 1.4 Hydrolysis of C,*N*-phenyl nitrone to the corresponding *N*-phenylhydroxylamine and benzaldehyde.

1.6.1 Copper-catalyzed Alkyne-Nitrone Cycloaddition followed by Rearrangement (CuANCR)

The first report of the copper catalyzed reaction between phenylacetylide and nitrones to form β-lactams, termed the "Kinugasa Reaction", was presented in 1972 by Manubu Kinugasa.[34] This reaction was done in dry pyridine as the solvent and under an inert atmosphere. The nitrogen atmosphere was required to avoid the Glaser coupling that often occurs between two terminal alkynes in the presence of copper.[32,35]

Simultaneous micelle and Cu-catalyzed multicomponent Kinugasa reactions in water were reported by McKay *et al*. from the Pezacki laboratory, along with the proposed reaction mechanism (**Figure 1.6**).[36] The reaction proceeds in two steps- first, the nitrone is synthesized in the micelles from substituted benzaldehydes and *N*-phenylhydroxylamine to form diaryl-nitrones. Next, addition of copper, ligand, sodium ascorbate, alkyne and excess pyridine leads to the 1,3-dipolar cycloaddition and production of the furnished β-lactams with *cis*/*trans* overall yields of about 46%.

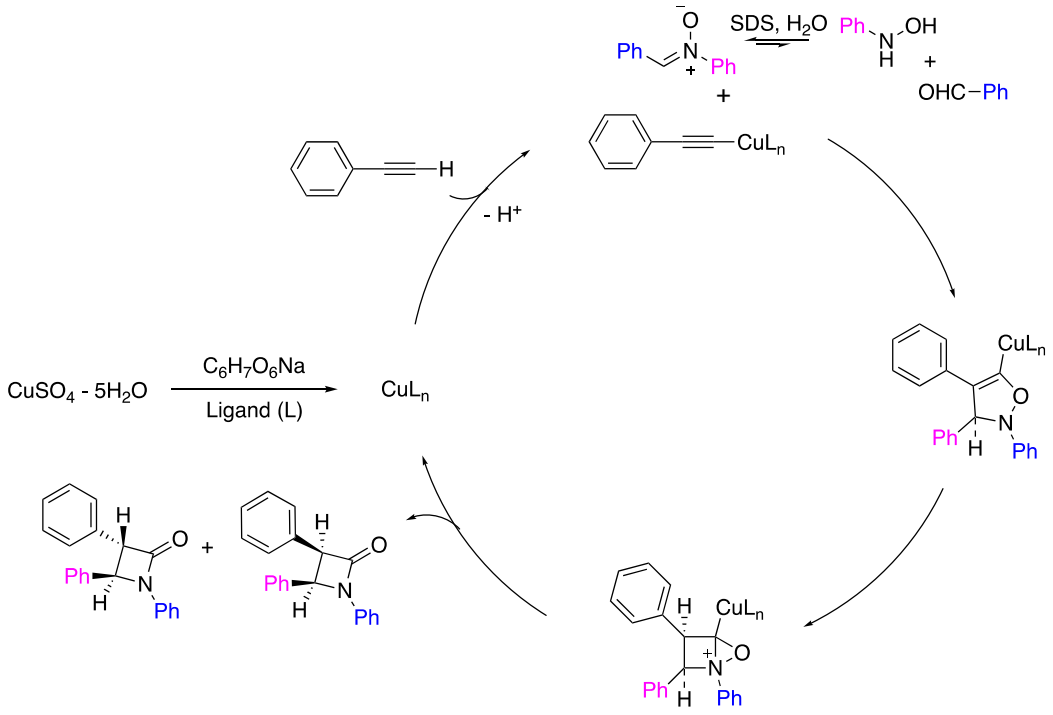

Figure 1.6 Proposed catalytic cycle for micelle catalyzed Kinugsa reaction. Figure adapted from McKay *et al.*[36]

Mammalian cell and bacterial cell labelling was achieved via CuANCR.[37] Human-7 hepatoma (Huh-7) cells were cultured for 72 hours with an alkyne-tagged mannosamine derivative that was incorporated into sialylated glycans on the cell membrane. The sugars were then labelled via CuANCR using biotin-tagged 2*H*-pyrrole-2-carboxylic acid, 3,4-dihydro-2-methyl-,1-oxide (CMPO), L-histidine as the ligand and sodium ascorbate to reduce the Cu(II) species (**Figure 1.7a**). Labelling of gram-negative bacteria was achieved using a similar alkyne-tagged sugar and CMPO-Alexa488 (**Figure 1.7b**). More efficient bacterial labelling was achieved using an unnatural sugar tagged with a nitrone that was incorporated into the

lipopolysaccharide layer (LPS) reacting via CuANCR conditions with an Alexa488-alkyne.

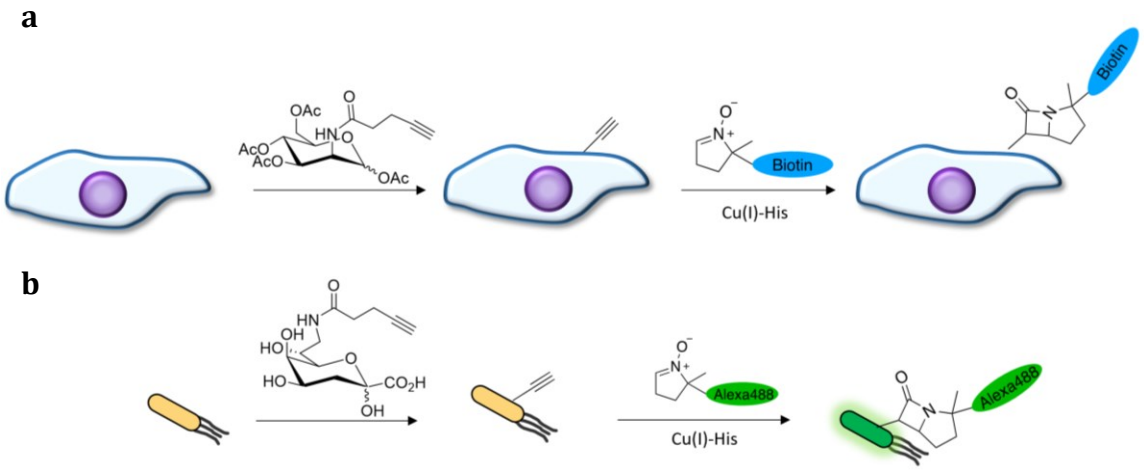

Figure 1.7 a) *In situ* cell surface labelling of Huh-7 cells by CuANCR. b) *In situ* bacterial LPS labelling of *E. coli* by CuANCR.

The significant, yet unexplored advantage of CuANCR over CuAAC is found in the β-lactam products. β-lactams are both primed for further chemistry and make up the core structure of many antibiotics, like penicillin.[38] With further development of the CuANCR reaction for cellular membrane and intracellular environments, this reaction and its products provide the potential for synthesis of β-lactams with antibacterial properties *in situ*. Moreover, β-lactams are useful for the general properties as electrophiles,[39] and therefore can be used for further chemistry to make biomaterials

in situ. More work needs to be done in this area to optimize the reaction conditions for biological contexts to lay the groundwork to explore these applications.

1.6.2 Strain-Promoted Alkyne-Nitrone Cycloaddition (SPANC)

Nearly 10 years ago, the Pezacki lab showed that cyclic nitrones serve as tunable, stable alternatives to azides as reacting partners with cycloalkynes, namely dibenzocycooctyne (DIBO). This reaction was 25 times faster than the parallel reaction with benzyl azide, partially due to the doubly-strained reaction resulting from strain of both the cyclic nitrone and alkyne.[16]

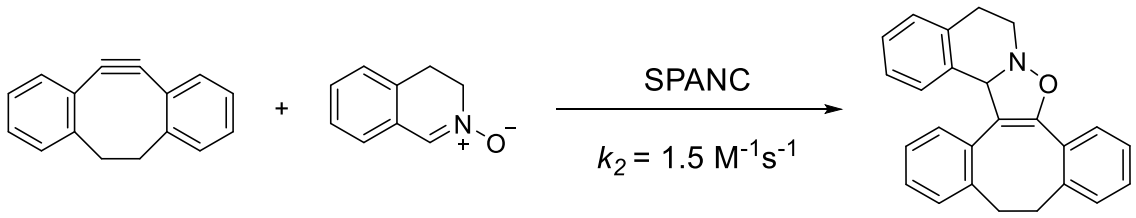

Scheme 1.5 Strain-Promoted Alkyne-Nitrone cycloaddition (SPANC) reaction between DIBO and a cyclic nitrone to form the isoxazoline product.

These initial studies prompted further study of reactions between nitrones and other reactive strained alkynes. In 2010, biarylazacyclooctynone (BARAC) was introduced as a new strained cyclooctyne that demonstrated a rate constant with azides 12-fold larger than that of analogous reaction with DIBO.[40] BARAC was designed according to reports that indicated rate enhancing properties could be achieved through addition of one more sp^2-like centre to DIBO to create a highly reactive ene-yne.[41] However, these compounds are typically very unstable,[42] so to find a balance between

increasing reactivity while maintaining stability, BARAC was designed to possess an amide group which offers double-bond character through its resonance structure. With BARAC showing exceptional kinetics with azides, our group speculated that a similar trend would occur with nitrones, as previously observed with DIFO and DIBO. Indeed, BARAC reacted with cyclic nitrones with rate constants up to 47.3 $M^{-1}s^{-1}$ with 99% conversion in 20 minutes, compared to 0.96 $M^{-1}s^{-1}$ with azides in 99% ACN-H_2O.[43] Accordingly, these reactions were up to 48 times faster than previously reported with benzyl azide, and 14 times faster than previous SPANC reactions (**Table 1.1**).

Using a variety of acyclic nitrones with different α-aryl substituents, a Hammett ρ value of 0.25 ± 0.04 was observed, indicating that the reaction isn't very sensitive to substituent effects, suggesting that BARAC serves as a practical reacting partner to nitrones generally, regardless of electronic character.

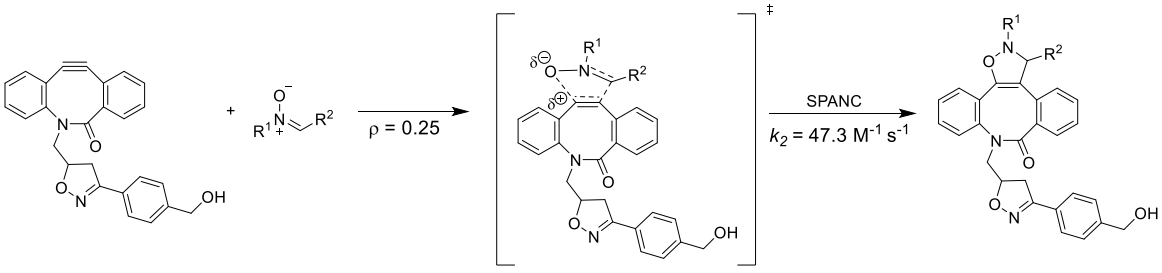

Scheme 1.6 Reaction between BARAC and an acyclic nitrone, showing the likely transition state indicated by a ρ value of 0.25. Figure adapted from *McKay et al*.[43]

Comparatively, ρ values of reactions between nitrones and bicyclo[6.1.0]nonyne (BCN) indicate slightly different results. BCN is a relatively electron rich alkyne making use of a fused cyclopropane ring to increase strain (**Table 1.1**).[44] A larger ρ value of 1.28 ± 0.013 suggests that SPANC reactions involving BCN are more sensitive to electronic changes than BARAC, a consequence of a non-synchronous transition state, and moderate build-up of electron density during the transition state. Thus, nitrones bearing electron deficient substituents like -NO_2 and -CN, reacted with rate constants more than an order of magnitude greater than those with electron donating substituents. In the case of BARAC, the very small rho (near zero) value indicates a more synchronous transition state, with no significant electron density accumulation occurring at the nitrone α-carbon during the transition state compared with the reactant (**Scheme 1.6**), hence, the rate is only slightly accelerated by electron deficient nitrones.

Table 1.1 Rate constants of benzyl azide and cyclic nitrones with DIBO, BARAC and BCN.

Alkyne	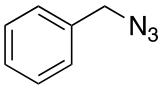	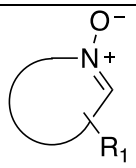
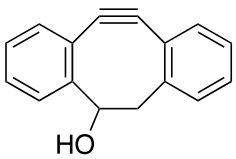 **DIBO,**[45] **2008**	0.062 $M^{-1}s^{-1}$ (C_6D_6)	1.5 $M^{-1}s^{-1}$ (C_6D_6)
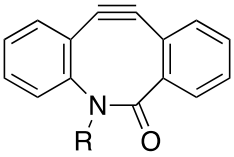 **BARAC,**[40] **2010**	0.96 $M^{-1}s^{-1}$ (acetonitrile)	47.3 $M^{-1}s^{-1}$ (99% acetonitrile: H_2O)
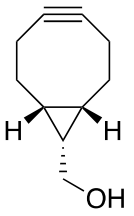 **BCN,**[46] **2010**	0.14 $M^{-1}s^{-1}$ (CD_3CN/D_2O (1:2))	1.5 $M^{-1}s^{-1}$ (MeOH)

The difference in reactivity of nitrones with BCN compared with other alkynes, like DIBO, led to a proof of concept report where two different SPANC reactions could occur in one-pot with minimal cross reactivity. To demonstrate this, solutions of BCN and DIBO were combined with nitrones with opposing electronics 5,5-dimethyl-1-pyrroline N-oxide (DMPO) and (2R)-2-amino-3-(2,2-dimethyl-5-oxo-3-oxy-2,5-dihydro-imidazol-1-yl)- propionic acid (DMImO). Expectedly, BCN exhibited a 5:1 preference for DMImO and DIBO exhibited a 2:1 preference for DMPO over DMImO. These differences result from the difference in alkyne LUMO, where DIBO is similar to BARAC, and is less sensitive to changes in nitrone electronics, compared with BCN which proceeds faster with electronic poor nitrones, like DMImO. It was expected that the appropriate alkyne-nitrone pairs could be used for simultaneous duplex or multiplex labelling.

The duplex reaction concept was then modified for use in a multiplex labelling application.[47] Two gram-positive bacteria, *Listeria (L.) innocua* and *L. lactis* were incubated with unnatural amino acids containing two electronically different nitrones, an electron deficient and an electron rich nitrone, DMImO and CMPO, respectively. The bacteria were then mixed and treated with BCN-CF488 and Dibenzocyclooctyne (DBCO)-TAMRA (**Figure 1.8**). Since DMImO reacts with BCN significantly faster (k_2 two orders of magnitude greater), only *L. innocua* was labelled with BCN-CF488, while both were labelled by DBCO-TAMRA.

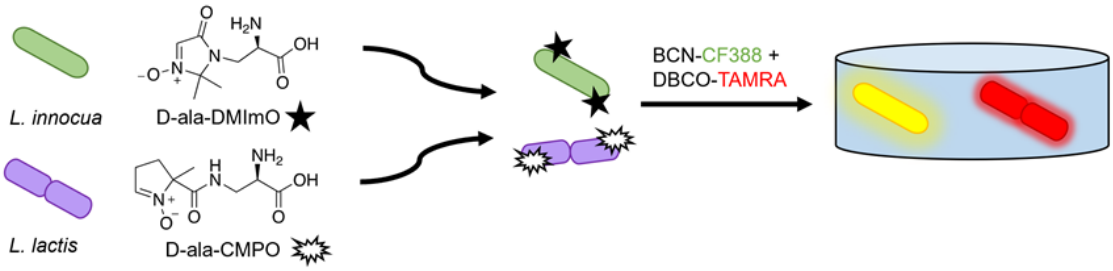

Figure 1.8 Dual SPANC labelling of *L. innocua* and *L. lactis* with D-ala-DMImO and D-ala-CMPO respectively. Figure adapted from Sherratt *et al.*[47]

1.7 Applications of Nitrone Cycloaddition Chemistry

1.7.1 Biology

SPANC was first employed in protein labelling through chemical modification of a peptide to include a nitrone. Van Delft *et al*. demonstrated that peptides containing a N-terminal serine, like interleukin-8 (IL-8), can be chemically modified to contain a nitrone via a one-pot, three step procedure.[31] The N-terminal serine was oxidized with sodium periodate to an aldehyde, followed by treatment with *p*-methoxybenzenethiol, *N*-methylhydroxylamine and *p*-anisidine to afford the nitrone (**Scheme 1.7**).[48] This proof of concept application outlines a method for nitrone incorporation into peptides or other substrates containing carbonyl groups for SPANC labelling.

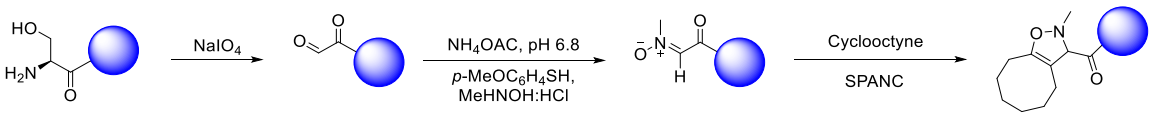

Scheme 1.7 Synthesis of proteins to contain a nitrone functional group for reaction with cyclooctynes via SPANC. A serine residue found on the N-terminal of the peptide (blue sphere) is oxidized to the nitrone for conjugation via SPANC. Figure adapted from Ning *et al*.[48]

The work done by van Delft *et al*. was expanded to a strategy for dual functionalization of peptides and proteins.[4] This was possible because of the orthogonality of SPANC and CuAAC which could be used in tandem. To achieve dual protein labelling, a nitrone was introduced onto the protein as described earlier (**Scheme 1.7**). This nitrone had a propargyl group appended to it in place of the methyl shown in **Scheme 1.7**, providing an alkyne handle for CuAAC. Thus, dual functionalization was achieved on a single protein via CuAAC with azido-fluorescein reacting with the propargyl group, and an orthogonal SPANC reaction between the nitrone with BCN-biotin.

Although metabolic incorporation of nitrones intracellularly remains a challenge, cellular membrane labelling via SPANC has been achieved. The first reports of cell surface labelling via SPANC occurred in 2011 through the modification of epidermal growth factor (EGF) with a cyclic nitrone.[33] Once the nitrone-EGF was bound to the EGF-receptors found on the surface of human breast cancer cells, SPANC labelling

with DIBO-biotin was achieved, followed by visualization using streptavidin-FITC staining (**Figure 1.9**).[33]

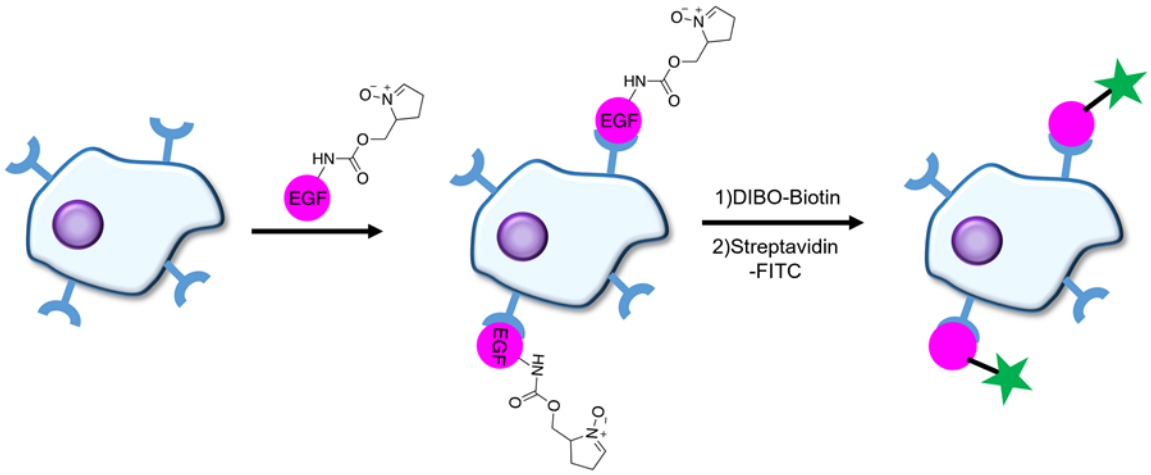

Figure 1.9 Cell surface labelling of human breast cancer cells through EGF receptor labelling via SPANC. Figure adapted from McKay *et al*.[33]

Another promising report of SPANC for cell surface labelling was done using site-specific bioengineering of multifunctional nanoparticles (MFN) with recombinant single chain variable fragment (scFv) antibodies against the human epidermal growth factor receptor 2 (HER2). These antibodies contained a nitrone, introduced far from the antigen binding site via a serine residue. Nanoparticles were functionalized with cyclooctyne ligands which then could react with and tag the nitrone-tagged antibodies without loss of function. The application of SPANC to a scFv antibody resulted in prompt immobilization of MFNs onto the breast cancer cells.[49]

As highlighted above, SPANC reactions have found use in several biological contexts ranging from protein modification, nanoparticle-antibody targeting and even cell surface labelling. These reports indicate the potential of SPANC reactions in more biological contexts, for labelling, targeting and other applications like multiplex labelling.

1.7.2 Materials and Radiolabel Chemistry

Beginning in 2008, SPAAC was already being used in a number of polymer-related applications ranging from side functionalization of polymers to polymeric networks and light-controlled hydrogel formation.[50–52] With SPANC reactions showing faster kinetics, and with nitrones being more structurally diverse than other dipoles such as azides, they offer the potential to provide polymers with broader functionalities. Importantly, they provide a viable alternative to overcome issues occurring with azide polymerization reactions, such as their tendency to react in side reactions resulting in loss of azide functionalities.[53,54]

The first report of nitrone polymerization methods used nitrones in the post-polymerization modification of polymers to form bifunctionalized polymers via SPANC, SPAAC and strain-promoted alkyne-nitrile-oxide cycloaddition (SPANOC) (**Figure 1.10**).[55] However, most of this work focused on oxime group chemistry due to its ease of incorporation into polymers and its stability towards SPAAC reactions. This work was

further expanded in 2014 by Boons *et al*. where polymers were end-functionalized with DIBO to undergo strain-promoted cycloadditions with azides, nitrones and nitrile oxides to make block copolymers. Gold nanoparticles were then functionalized with these DIBO-functionalized polymers for preparation of materials that can be further modified to functional units such as therapeutics or imaging agents by strain promoted cycloadditions.[56] The combination of these reactions not needing a catalyst, and the inherent nature of gold nanoparticles suggest that this tool could be used for biological applications like sensing, drug delivery and imaging.

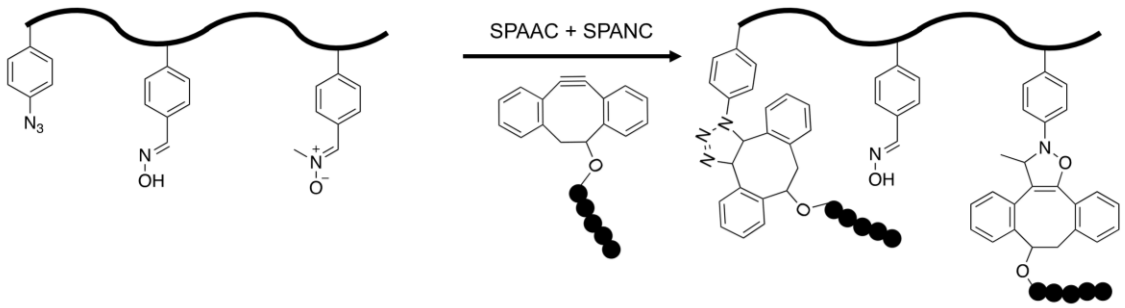

Figure 1.10 Synthesis of co-block polymers from polymers functionalized with azide, oxime and nitrone groups and DIBO-functionalized polymers.[55,56]

The most recent report of SPANC in materials chemistry was reported in 2019, demonstrating the first account of its use in radiolabelled nanomaterials.[57] In this report, the Workentin group designed and characterized a bioorthogonal gold nanoparticle template containing interfacial nitrone functional groups. The synthesis of Gold-Nanoparticle (AuNP)-based radiolabelled probes was achieved through the ability to control the conjugation onto the nitrone-nanoparticle template at the

molecular level. The nitrone on the surface of the nanoparticles undergoes interfacial-SPANC (I-SPANC) with a ^{18}F radiolabelled prosthetic group tagged with a BCN moiety (**Figure 1.9**). Remarkably, these [^{18}F] AuNPs retained their water solubility and tested *in vivo* with broad distribution and low uptake in background organs (liver, kidney, lung), showing the potential for these nanocarriers to be used for targeted PET labelling. This work is one of many that highlight the potential for bioorthogonal reactions to revolutionize radiolabelled probes,[58–60] but importantly, it is a tool that can be used for purposes beyond PET imaging, such as drug delivery or multivalent attachment.

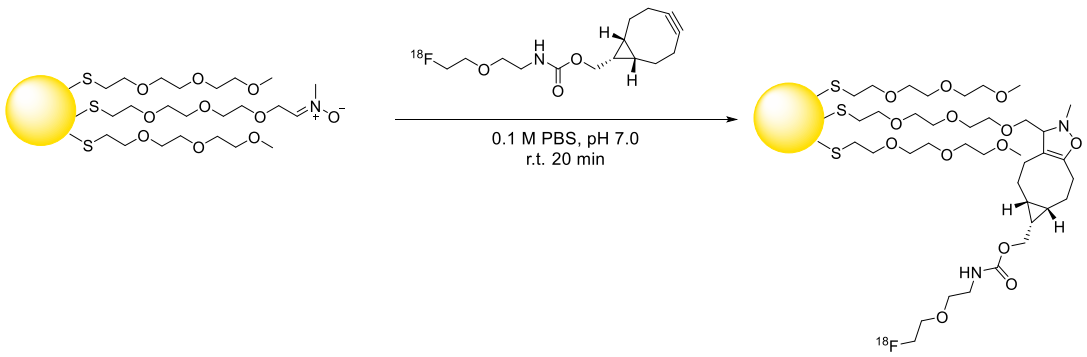

Figure 1.11 Synthesis of [18F]AuNPs via SPANC reaction of AuNP bearing nitrone functionalities and BCN linked with an ^{18}F radiolabel. Figure adapted from Ghiassian *et al.*[57]

1.8 Optimization of Bioorthogonal Chemistry

With a toolbox full of different and efficient bioorthogonal reactions, some might wonder why there is a constant need for more reactions. A major driving force behind

the development and optimization of bioorthogonal reactions has been that of speed, emphasized through the plethora of strained alkynes for that purpose. Faster reactions are necessary because they allow the chemistry to occur on a practical time scale, using a lower concentration of reactants.[3] In the case of creating radiolabelled probes with short half-lives, one can clearly see how achieving the fastest reaction would be more advantageous. Unfortunately, consequences that are often coupled with the fastest reactions are unstable reactants and products.

A key condition of bioorthogonal reactions is the necessity that it not perturb normal functioning of the cell and not interact with untargeted biological reactive groups. To satisfy these conditions, the cell must recognize and treat the tagged substrate as natural, and this condition is most easily achieved by the presence of small reactive groups, such as azides.[3] Cycloalkynes, the classic complementary functional group to azides are typically large and hydrophobic, which can cause unspecific accumulation within membranes, and impact the function of the substrates they are appended to.[3] The design of smaller dipoles and dipolarophiles have been important goals of recent years to make use of highly reactive chemistry, while overcoming limitations of size.[61–63]

Another driving force behind the development of more bioorthogonal reactions is the desire to perform multiplex chemistry and labelling.[64–66] Finding bioorthogonal reactions that are orthogonal to each other while in a complex system is challenging,

yet would allow for labelling of multiple substrates at once, tracking protein interactions, and building molecules within cellular systems.[67] Orthogonal reactions can be achieved through choosing reactions that have unique mechanisms, or vastly different reaction rates.[68] An example of the latter, makes use of two orthogonal reactions, both using methylated cyclopropenes; however, by changing the placement of the methyl from 1,3 disubstituted to 3,3, disubstituted, the authors were able to make use of the different reaction mechanisms, and rates of reactions with tetrazines via the IEDDA reaction and azides via 1,3 dipolar cycloaddition.[69] Since cyclopropenes are small, stable and can react with multiple substrates, the manipulation of rates for multiplex labelling is of high interest, and development of similar small, reactive substrates, such as nitrones should also be investigated to develop a larger toolbox for probing biological systems.

1.9 Outline of Work

The purpose of the work described herein was to demonstrate the use of nitrones in two novel cycloadditions reactions. First, the kinetics of the reaction between strained-*trans*-cyclooctene (s-TCO) and nitrones were evaluated and use of this reaction in metabolic labelling was demonstrated. Rate constants of reactions with acyclic nitrones and s-TCO were obtained by pseudo-first order kinetics using UV-visible spectroscopy at ambient temperature in methanol. Second order rate constants between cyclic nitrones and s-TCO were obtained under second order

conditions in MeOD by ^{1}H NMR. Metabolic labelling was demonstrated by treatment of *L. innocua*, a gram-positive bacterium with unnatural amino acids bearing cyclic nitrones, followed by labelling using a fluorophore tagged with s-TCO. Second, the kinetics of reaction between nitrone and a cycloooctadiyne were evaluated and the reaction mechanism was investigated. Second order rate constants were evaluated under pseudo-first order kinetics by UV-visible spectroscopy and confirmed using mass spectroscopy methods. It is expected that the findings of these reactions will aid in the development of applications for peptide crosslinking and polymer synthesis via this double-strained promoted alkyne-nitrone cycloaddition (D-SPANC) reaction. The variability of nitrones as tools in the bioorthogonal toolbox has been expanded to include strained alkenes and double-strained-alkynes, allowing for a multitude of applications ranging from metabolic labelling to polymer synthesis.

References

1. Sletten, E. M. & Bertozzi, C. R. Bioorthogonal chemistry: Fishing for selectivity in a sea of functionality. *Angew. Chem. Int. Ed.* **48**, 6974–6998 (2009).
2. Hang, H. C., Yu, C., Kato, D. L. & Bertozzi, C. R. A metabolic labeling approach toward proteomic analysis of mucin-type O-linked glycosylation. *Proc. Natl. Acad. Sci. U. S. A.* **100**, 14846–14851 (2003).
3. Devaraj, N. K. The Future of Bioorthogonal Chemistry. *ACS Cent. Sci.* **4**, 952–959 (2018).
4. Temming, R. P., Eggermont, L., Van Eldijk, M. B., Van Hest, J. C. M. & Van Delft, F. L. N-terminal dual protein functionalization by strain-promoted alkyne-nitrone cycloaddition. *Org. Biomol. Chem.* **11**, 2772–2779 (2013).
5. Kolb, H. C., Finn, M. G. & Sharpless, K. B. Click Chemistry: Diverse Chemical Function from a Few Good Reactions. *Angew. Chem. Int. Ed.* **40**, 2004–2021 (2001).
6. Saxon, E. & Bertozzi, C. R. Cell surface engineering by a modified Staudinger reaction. *Science.* **287**, 2007–2010 (2000).
7. Huisgen, R. 1,3 Dipolar Cycloadditions Past and Future. *Angew. Chem. Int. Ed.* **2**, 565–598 (1963).
8. Rostovtsev, V. V., Green, L. G., Fokin, V. V. & Sharpless, K. B. A stepwise huisgen cycloaddition process: Copper(I)-catalyzed regioselective 'ligation' of azides and terminal alkynes. *Angew. Chem. Int. Ed.* **41**, 2596–2599 (2002).
9. Tornøe, C. W., Christensen, C. & Meldal, M. Peptidotriazoles on solid phase: [1,2,3]-Triazoles by regiospecific copper(I)-catalyzed 1,3-dipolar cycloadditions of terminal alkynes to azides. *J. Org. Chem.* **67**, 3057–3064 (2002).

10. Haldón, E., Nicasio, M. C. & Pérez, P. J. Copper-catalysed azide-alkyne cycloadditions (CuAAC): An update. *Org. Biomol. Chem.* **13**, 9528–9550 (2015).

11. Kennedy, D. C. *et al.* Cellular consequences of copper complexes used to catalyze bioorthogonal click reactions. *J. Am. Chem. Soc.* **133**, 17993–18001 (2011).

12. Pickens, C. J., Johnson, S. N., Pressnall, M. M., Leon, M. A. & Berkland, C. J. Practical Considerations, Challenges, and Limitations of Bioconjugation via Azide-Alkyne Cycloaddition. *Bioconjug. Chem.* **29**, 686–701 (2018).

13. Agard, N. J., Prescher, J. A. & Bertozzi, C. R. A strain-promoted [3 + 2] azide-alkyne cycloaddition for covalent modification of biomolecules in living systems. *J. Am. Chem. Soc.* **126**, 15046–15047 (2004).

14. Gordon, C. G. *et al.* Reactivity of biarylazacyclooctynones in copper-free click chemistry. *J. Am. Chem. Soc.* **134**, 9199–9208 (2012).

15. Carell, T. & Vrabel, M. Bioorthogonal Chemistry—Introduction and Overview. *Top. Curr. Chem.* **374**, 1–21 (2016).

16. McKay, C. S., Moran, J. & Pezacki, J. P. Nitrones as dipoles for rapid strain-promoted 1,3-dipolar cycloadditions with cyclooctynes. *Chem. Commun.* **46**, 931–933 (2010).

17. Gothelf, K. V. & Jørgensen, K. A. Asymmetric 1,3-dipolar cycloaddition reactions. *Chem. Rev.* **98**, 863–909 (1998).

18. Mitsui, H., Zenki, S., Shiota, T. & Murahashi, S. I. Tungstate Catalysed Oxidation of Secondary Amines with Hydrogen Peroxide. A Novel Transformation of Secondary Amines into Nitrones. *J.C.S. Chem.Comm* 874–875 (1984).

19. Matassini, C. & Cardona, F. Oxidation of N,N-disubstituted hydroxylamines to nitrones: The search for more sustainable selective and practical stoichiometric oxidants. *Chimia (Aarau).* **71**, 558–561 (2017).

20. LeBel, N. A. & Spurlock, L. A. The Epimeric syn-Bicyclo[3.2.1]octane-2,8-diols. *J. Org. Chem.* **29**, 1337–1339 (1964).

21. Morozov, D. A. *et al.* Synthesis of a chiral C2-symmetric sterically hindered pyrrolidine nitroxide radical via combined iterative nucleophilic additions and intramolecular 1,3-dipolar cycloadditions to cyclic nitrones. *J. Org. Chem.* **77**, 10688–10698 (2012).

22. Lebel, N. A. & Banucci, E. G. Intramolecular Nitrone-Olefin Cycloadditions. The Stereochemistry of Hexahydro-2,l-benzisoxazoline Formation. *J. Org. Chem.* **36**, 2440–2448 (1971).

23. Merino, P. New developments in nucleophilic additions to nitrones. *Comptes Rendus Chim.* **8**, 775–788 (2005).

24. Ueda, M., Miyabe, H., Teramachi, M., Miyata, O. & Naito, T. Diastereoselective intermolecular radical addition to nitrones. *J. Org. Chem.* **70**, 6653–6660 (2005).

25. Dateer, R. B. & Chang, S. Rh(III)-Catalyzed C-H Cyclization of Arylnitrones with Diazo Compounds: Access to N-Hydroxyindolines. *Org. Lett.* **18**, 68–71 (2016).

26. Pi, C., Cui, X. & Wu, Y. Iridium-Catalyzed Direct C-H Sulfamidation of Aryl Nitrones with Sulfonyl Azides at Room Temperature. *J. Org. Chem.* **80**, 7333–7339 (2015).

27. Murahashi, S. I. & Imada, Y. Synthesis and Transformations of Nitrones for Organic Synthesis. *Chem. Rev.* **119**, 4684–4716 (2019).

28. Anderson, L. L. Diverse Applications of Nitrones for the Synthesis of Heterocyclic Compounds. *Asian J. Org. Chem.* **5**, 9–30 (2016).

29. Xu, X. & Doyle, M. P. The [3 + 3]-cycloaddition alternative for heterocycle syntheses: Catalytically generated metalloenolcarbenes as dipolar adducts. *Acc. Chem. Res.* **47**, 1396–1405 (2014).

30. Sustmann, R. Orbital energy control of cycloaddition reactivity. *Pure Appl. Chem.* **40**,

569–593 (1974).

31. MacKenzie, D. A., Sherratt, A. R., Chigrinova, M., Cheung, L. L. W. & Pezacki, J. P. Strain-promoted cycloadditions involving nitrones and alkynes-rapid tunable reactions for bioorthogonal labeling. *Curr. Opin. Chem. Biol.* **21**, 81–88 (2014).

32. Chigrinova, M., MacKenzie, D. A., Sherratt, A. R., Cheung, L. L. W. & Pezacki, P. Kinugasa reactions in water: From green chemistry to bioorthogonal labelling. *Molecules.* **20**, 6959–6969 (2015).

33. McKay, C. S., Blake, J. A., Cheng, J., Danielson, D. C. & Pezacki, J. P. Strain-promoted cycloadditions of cyclic nitrones with cyclooctynes for labeling human cancer cells. *Chem. Commun.* **47**, 10040–10042 (2011).

34. Kinugasa, M. & Hashimoto, S. The Recations of Copper (I) Phenylacetylide with Nitrones. *J.C.S. Chem.Comm.* 466–467 (1972).

35. Ding, L. K. & Irwin, W. J. cis and trans-Azetidin-2-ones from Nitrones and Copper Acetylide. *J.C.S Perkin* **1**, 2382 (1976).

36. McKay, C. S., Kennedy, D. C. & Pezacki, J. P. Studies of multicomponent Kinugasa reactions in aqueous media. *Tetrahedron Lett.* **50**, 1893–1896 (2009).

37. Sherratt, A. R. *et al.* Copper-catalysed cycloaddition reactions of nitrones and alkynes for bioorthogonal labelling of living cells. *RSC Adv.* **4**, 46966–46969 (2014).

38. Stecko, S., Furman, B. & Chmielewski, M. Kinugasa reaction: An 'ugly duckling' of β-lactam chemistry. *Tetrahedron.* **70**, 7817–7844 (2014).

39. Alcaide, B., Almendros, P. & Aragoncillo, C. β-lactams: Versatile building blocks for the stereoselective synthesis of non-β-lactam products. *Chem. Rev.* **107**, 4437–4492 (2007).

40. Jewett, J. C., Sletten, E. M. & Bertozzi, C. R. Rapid Cu-free click chemistry with readily

synthesized biarylazacyclooctynones. *J. Am. Chem. Soc.* **132**, 3688–3690 (2010).

41. Debets, M. F. *et al.* Aza-dibenzocyclooctynes for fast and efficient enzyme PEGylation via copper-free (3+2) cycloaddition. *Chem. Commun.* **46**, 97–99 (2010).

42. Wong, H. N. C., Garratt, P. & Sondheimer, F. Synthesis of sym-Dibenzo-1,5-cyclooctadiene-3,7-diyne and sym-Dibenzo-1,3,5-cyclooctatrien-7-yne, Presumably Planar Conjugated Eight-Membered Ring Compounds. *J. Am. Chem. Soc.* **96**, 5604–5605 (1974).

43. McKay, C. S., Chigrinova, M., Blake, J. A. & Pezacki, J. P. Kinetics studies of rapid strain-promoted [3 + 2]-cycloadditions of nitrones with biaryl-aza-cyclooctynone. *Org. Biomol. Chem.* **10**, 3066–3070 (2012).

44. Mackenzie, D. A. & Pezacki, J. P. Kinetics studies of rapid strain-promoted [3+2] cycloadditions of nitrones with bicyclo[6.1.0]nonyne. *Can. J. Chem.* **92**, 337–340 (2014).

45. Ning, X., Guo, J., Wolfert, M. A. & Boons, G. J. Visualizing metabolically labeled glycoconjugates of living cells by copper-free and fast huisgen cycloadditions. *Angew. Chem. Int. Ed.* **47**, 2253–2255 (2008).

46. Dommerholt, J. *et al.* Readily accessible bicyclononynes for bioorthogonal labeling and three-dimensional imaging of living cells. *Angew. Chem. Int. Ed.* **49**, 9422–9425 (2010).

47. Sherratt, A. R. *et al.* Dual Strain-Promoted Alkyne-Nitrone Cycloadditions for Simultaneous Labeling of Bacterial Peptidoglycans. *Bioconjug. Chem.* **27**, 1222–1226 (2016).

48. Ning, X. *et al.* Protein modification by strain-promoted alkyne-nitrone cycloaddition. *Angew. Chem. Int. Ed.* **49**, 3065–3068 (2010).

49. Colombo, M. *et al.* Site-specific conjugation of ScFvs antibodies to nanoparticles by

bioorthogonal strain-promoted alkyne-nitrone cycloaddition. *Angew. Chem. Int. Ed.* **51**, 496–499 (2012).

50. Lallana, E., Fernandez-Megia, E. & Riguera, R. Surpassing the use of copper in the click functionalization of polymeric nanostructures: A strain-promoted approach. *J. Am. Chem. Soc.* **131**, 5748–5750 (2009).

51. Johnson, J. A., Baskin, J. M., Bertozzi, C. R., Koberstein, J. T. & Turro, N. J. Copper-free click chemistry for the in situ crosslinking of photodegradable star polymers. *Chem. Commun.* 3064–3066 (2008).

52. DeForest, C. A. & Anseth, K. S. Photoreversible patterning of biomolecules within click-based hydrogels. *Angew. Chem. Int. Ed.* **51**, 1816–1819 (2012).

53. Ladmiral, V., Legge, T. M., Zhao, Y. & Perrier, S. 'Click' chemistry and radical polymerization: Potential loss of orthogonality. *Macromolecules.* **41**, 6728–6732 (2008).

54. Ledin, P. A., Kolishetti, N., Hudlikar, M. & Boons, G.-J. Exploring Strain-Promoted 1,3-Dipolar Cycloadditions of End Functionalized Polymers. *Chemistry (Easton).* **20**, 8753–8760 (2014).

55. Ledin, P. A., Kolishetti, N. & Boons, G. J. Multifunctionalization of polymers by strain-promoted cycloadditions. *Macromolecules.* **46**, 7759–7768 (2013).

56. Ledin, P. A., Kolishetti, N., Hudlikar, M. S. & Boons, G. J. Exploring strain-promoted 1,3-dipolar cycloadditions of end functionalized polymers. *Chem. - A Eur. J.* **20**, 8753–8760 (2014).

57. Ghiassian, S. *et al.* Nitrone-Modified Gold Nanoparticles: Synthesis, Characterization, and Their Potential as 18F-Labeled Positron Emission Tomography Probes via I-SPANC. *ACS Omega*. **4**, 19106–19115 (2019).

58. Kim, H. L. *et al.* F-18 labeled RGD probes based on bioorthogonal strain-promoted click reaction for PET imaging. *ACS Med. Chem. Lett.* **6**, 402–407 (2015).

59. Murrell, E., Kovacs, M. S. & Luyt, L. G. A Compact and Synthetically Accessible Fluorine-18 Labelled Cyclooctyne Prosthetic Group for Labelling of Biomolecules by Copper-Free Click Chemistry. *ChemMedChem.* **13**, 1625–1628 (2018).

60. Zhou, Z., Chitneni, S. K., Devoogdt, N., Zalutsky, M. R. & Vaidyanathan, G. Fluorine-18 labeling of an anti-HER2 VHH using a residualizing prosthetic group via a strain-promoted click reaction: Chemistry and preliminary evaluation. *Bioorganic Med. Chem.* **26**, 1939–1949 (2018).

61. Andersen, K. A., Aronoff, M. R., McGrath, N. A. & Raines, R. T. Diazo groups endure metabolism and enable chemoselectivity in cellulo. *J. Am. Chem. Soc.* **137**, 2412–2415 (2015).

62. Yang, J., Šečkute, J., Cole, C. M. & Devaraj, N. K. Live-cell imaging of cyclopropene tags with fluorogenic tetrazine cycloadditions. *Angew. Chem. Int. Ed.* **51**, 7476–7479 (2012).

63. Patterson, D. M., Nazarova, L. A., Xie, B., Kamber, D. N. & Prescher, J. A. Functionalized cyclopropenes as bioorthogonal chemical reporters. *J. Am. Chem. Soc.* **134**, 18638–18643 (2012).

64. Bruins, J. J., Blanco-Ania, D., Van Der Doef, V., Van Delft, F. L. & Albada, B. Orthogonal, dual protein labelling by tandem cycloaddition of strained alkenes and alkynes to: Ortho -quinones and azides. *Chem. Commun.* **54**, 7338–7341 (2018).

65. Xiao, H. *et al.* Genetic incorporation of multiple unnatural amino acids into proteins in mammalian cells. *Angew. Chem. Int. Ed.* **52**, 14080–14083 (2013).

66. Patterson, D. M., Jones, K. A. & Prescher, J. A. Improved cyclopropene reporters for

probing protein glycosylation. *Mol. Biosyst.* **10**, 1693–1697 (2014).

67. Patterson, D. M. & Prescher, J. A. Orthogonal bioorthogonal chemistries. *Curr. Opin. Chem. Biol.* **28**, 141–149 (2015).

68. Colombo, M. *et al.* Protein-assisted one-pot synthesis and biofunctionalization of spherical gold nanoparticles for selective targeting of cancer cells. *Angew. Chem. Int. Ed.* **51**, 9272–9275 (2012).

69. Kamber, D. N. *et al.* Isomeric cyclopropenes exhibit unique bioorthogonal reactivities. *J. Am. Chem. Soc.* **135**, 13680–13683 (2013).

Chapter 2

Cycloadditions of *Trans*-cyclooctenes and Nitrones as Tools for Bioorthogonal Labelling

2.1 Introduction

Reactions need to be fast in biological settings to increase selectivity and allow a practical time scale, while lowering the concentration of reagents necessary to get effective modification.[1] Minimizing toxicity concerns and background labelling are two advantages of rate enhancement through improving the second-order rate constant of the reaction, in contrast to increasing rate through increasing concentrations.[2] Bioorthogonal reactions put additional constraints on reaction optimization, making achieving fast reactions that are stable and biologically inert, a very difficult challenge. The tetrazine-*trans*-cyclooctene ligation is the fastest bioorthogonal reaction to date, employing Inverse-Electron Demand Diels-Alder (IEDDA) chemistry to produce second order rate constants upwards from 10^3 - 10^6 $M^{-1}s^{-1}$. However, efforts to increase bioorthogonality of the reaction while maintaining or increasing speed has proven challenging due to issues of aqueous stability and redox sensitivity of the tetrazine.[3–5]

2.1.1 Inverse-Electron Demand-Diels Alder Reaction

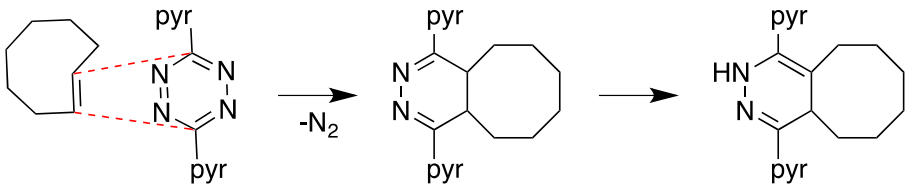

Scheme 2.1 IEDDA reaction between *trans*-cyclooctene and tetrazine. Figure adapted from Yang *et al*.[6]

The reaction between TCO and tetrazine occurs via an Inverse-Electron Demand Diels Alder (IEDDA) reaction; [4+2] addition of the -C=N-N=C- bonds of the tetrazine to the appropriate alkene (**Scheme 2.1**). The first report of the kinetics of the IEDDA reaction between tetrazine and cyclooctene was published by Sauer in 1990 which showed reactions between highly electrophilic tetrazines and a number of strained alkenes.[7] In this report, the TCO-tetrazine reaction occurred 7 orders of magnitude faster than the reaction with *cis*-cyclooctene. Although incredibly fast, the potential of this reaction for use in biological contexts went largely unnoticed because the electron-deficient tetrazine was thought to be too hydrolytically reactive to be useful for bioconjugation. It wasn't until two decades later when its use for bioconjugation reactions was optimized, where in 2008, Fox *et al*. reported a more biocompatible reaction between diaryl-substituted tetrazines and TCO, demonstrating a second order rate constant (k_2) of 2000 M^1s^{-1} in methanol: water mixtures.[6]

The TCO-tetrazine ligation is driven by the electrophilicity of the tetrazine and the high exothermicity of the reaction with alkenes.[8] The Fox lab investigated through computational chemistry, that the TCO could be manipulated to conform to a higher energy chair conformation instead of the crown conformation (**Table 2.1, structure 2**).[9,10] Addition of a cyclopropyl ring on the TCO opposite to the alkene forced this non-crown conformation. Strained-*trans*-cyclooctene (s-TCO) has an alkene approximately 5.9 kcal/mol higher in energy and a reaction rate 160 times faster than the parallel reaction with the unstrained TCO and tetrazine.

To overcome issues of difficult synthesis and stability of s-TCO, computational calculations were used to design a conformationally-strained dioxolane-fused *trans*-cyclooctene (d-TCO).[11] Compared to s-TCO, d-TCO has a simpler synthesis and is more stable, both for long term storage and in aqueous solution where little isomerization was observed. However, d-TCO reacts more slowly under comparable conditions, where rate constants of 3,300,000 $M^{-1}s^{-1}$ and 366,000 $M^{-1}s^{-1}$ were measured for reactions with s-TCO and d-TCO, respectively (**Table 2.1**).

Table 2.1 Reaction rate constants of *trans*-cyclooctene derivates with diphenyl tetrazine in methanol.

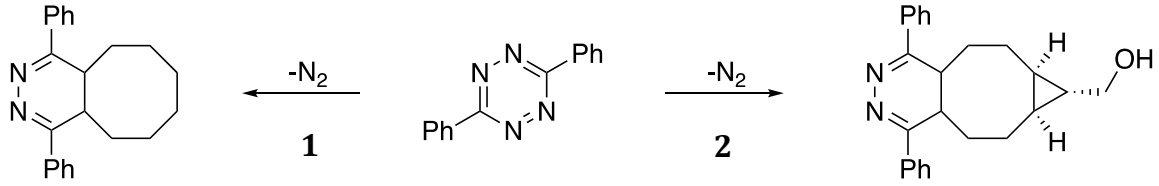

	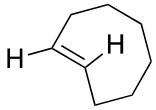	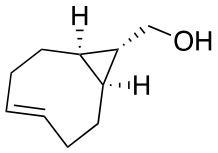	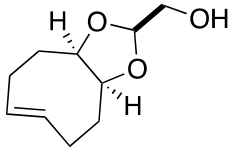
	1[9] (TCO)	**2[9] (s-TCO)**	**3[11](d-TCO)**
$\Delta G^{\ddagger}$ (kcal/mol)	15.4	12.4	13.3
k_2 ($M^{-1}s^{-1}$)	19.1 ± 0.2	3100 ± 50	520 ± 3

To further increase rates and bioorthogonality of the TCO-tetrazine ligation, the stereoelectronics and strain of both the tetrazine and TCO were investigated. Since the tetrazine faces the more significant issue of aqueous stability and redox sensitivity,[3] the substituent effects in positions 3 and 6 have been investigated to optimize stability and reactivity. Tetrazines that display the best long-term *in vivo* stability also appeared to be least reactive,[11,12] or require quite large substituents.[5]

Depending on the use of the reaction, other factors such as size and stability are equally important to that of a fast rate. For example, a reaction sufficient for metabolic labelling requires second order rate constants of 10^{-2} $M^{-1}s^{-1}$ and larger, however,

reactions ideal for *in vivo* applications require rate constants of at least 10^1-10^2 $M^{-1}s^{-1}$.[13] Hence, once a reaction rate is sufficient for the targeted application, focusing on these other factors of stability and size might prove more useful. Since most bioconjugation reactions rely on small reactive groups to get incorporated via natural biological and enzymatic pathways, the reactive groups need to be small enough not to perturb these natural processes. Thus, there has been great effort to develop alternative reagents that overcome the limitations associated with the TCO-tetrazine ligation such as size, aqueous stability and redox sensitivity while still making use of the chemistry and the highly reactive groups.

2.1.2 Alternative Dienophiles to *trans*-cyclooctene

Tetrazines have been used in ligations with other alkenes and alkynes including norbornenes, BCN, acylazetines and cyclopropenes. The reaction between benzylamine-modified tetrazine and norbornene (**Figure 2.1b**), first reported in 2008, occurred in aqueous buffer and fetal bovine serum with second order rate constants of 1.9 and 1.6 $M^{-1}s^{-1}$, respectively. Using this reaction, labelling of antibodies modified with norbornene was achieved using a fluorescently modified tetrazine.[14] In this report, which was published just before the 2008 report on TCO-tetrazine ligation,[6] they also predicted this reaction would occur faster with larger, more strained alkenes like cyclooctene. Although reaction with norbornenes is significantly slower than the TCO-tetrazine ligation, norbornenes have found their place in a

variety of applications including peptide labelling using unnatural amino acids, glycan labelling through norbornene-modified sugars, and antibody labelling.[15]

Interestingly, tetrazines are not limited to reaction with alkenes, as Wang *et al.* demonstrated that the tunability of both strained alkynes and tetrazines allow for even more functionality. Through optimization of the HOMO-LUMO gap guided by computational work, a second order rate constant of 40.9 $M^{-1}s^{-1}$ for the reaction of BCN and an isopropylamide-tetrazine was achieved, up from 0.07 $M^{-1}s^{-1}$ between diphenyltetrazine and cyclooctyne (**Figure 2.1d**).[16] The vast differences in reaction rates (more than 640-fold) between reactions using different alkynes and tetrazines suggests these reactions can be exploited for multiplex labelling.

Cyclooctynes are quite large in size like TCO, so in focusing on overcoming the size and lipophilicity of the TCO group, N-acylazetine was suggested as a suitable alternative, reacting with a second order rate constant of 0.39 ± 0.1 $M^{-1}s^{-1}$ (**Figure 2.1c**).[17] Interestingly, where all other dienophiles relied solely on strain for increasing reactivity (norbornene, BCN, TCO), this group further activated the butene ring by adding a nitrogen atom (electron-donating) to increase reactivity towards tetrazine, an effect reported by Sauer *et al*. in 1990.[7] Application of this reaction was demonstrated by incorporating an N-acylazetine into an activity-based proteasome probe (epoxomicin, a broad-spectrum proteasome inhibitor) and labelling of the constitutive proteome using a fluorescently labelled tetrazine.[17]

An emerging TCO-alternative used to overcome the size and stability issues caused by hydrophobicity and lipophilicity are cyclopropene "*mini tags*".[18] The Devaraj and Presher groups investigated 3-methyl cyclopropenes as new bioorthogonal reporter groups that can be used *in vitro* and *in situ* to react with tetrazines in place of TCO.[5,18,19] Cyclopropenes are highly strained alkenes, not found naturally in biomolecules, and are likely not to perturb the native metabolic pathways. A variety of these 3-methyl cyclopropenes which have been altered for biological sensitivity show second order rate constants on the order of 10^{-2} $M^{-1}s^{-1}$ (**Figure 2.1a**). The IEDDA reaction between cyclopropenes and tetrazines have found use in many biological applications ranging from lipid labelling, protein labelling and oligonucleotides.[18] Although slower than the parallel reactions with TCO, they showed the importance for design and use of small, nonperturbing chemical reporters.

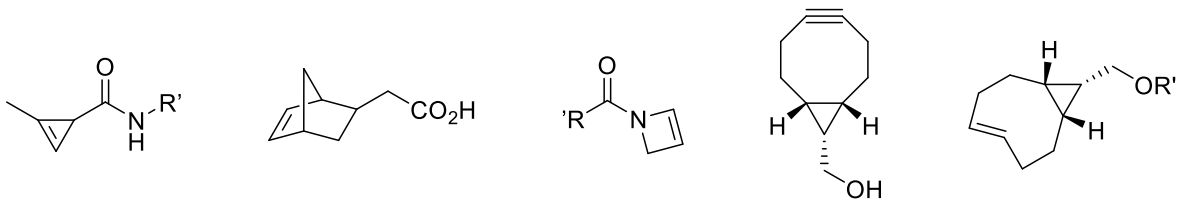

a **b** **c** **d** **e**

k_2 = 10^{-2} $M^{-1}s^{-1}$ k_2 = 0.39 $M^{-1}s^{-1}$ k_2 = 1.9 $M^{-1}s^{-1}$ k_2 = 40.2 $M^{-1}s^{-1}$ $k_2 \geq 3100$ $M^{-1}s^{-1}$

Figure 2.1 Order of increasing reactivity of dienophiles with tetrazines and their measured second order rate constants.

2.1.3 Alternative Dienes to Tetrazines

Tetrazines have been the main diene involved in IEDDA reactions with norbornenes, cyclopropenes and TCOs, with not many alternate dienes having been explored. With the most reactive tetrazines also tending to be the least stable in cells and *in vivo,*[12] overcoming issues of hydrolysis and reactivity with endogenous thiols has led to an increase of size not favourable for chemical reporters.[5,20] In 2015, Presher *et al.* presented 1,2,4-triazines as stable, reactive alternatives to tetrazines.[21] In this paper they showed that triazines are relatively inert to thiols, and although they react much slower than tetrazines, with second order rate constants of 1-7.5 x 10^{-2} $M^{-1}s^{-1}$, the rates are similar to other successful bioorthogonal reactions.[8,22] Interestingly, triazines only reacted with TCOs, and did not react with other tetrazine reactive partners like norbornene and cyclopropene- offering the potential of multiplexing with other orthogonal reactions (**Scheme 2.2**). There have been few reports using triazine chemistry, and consequently, tetrazines remain the dominant diene involved in IEDDA bioorthogonal reactions.

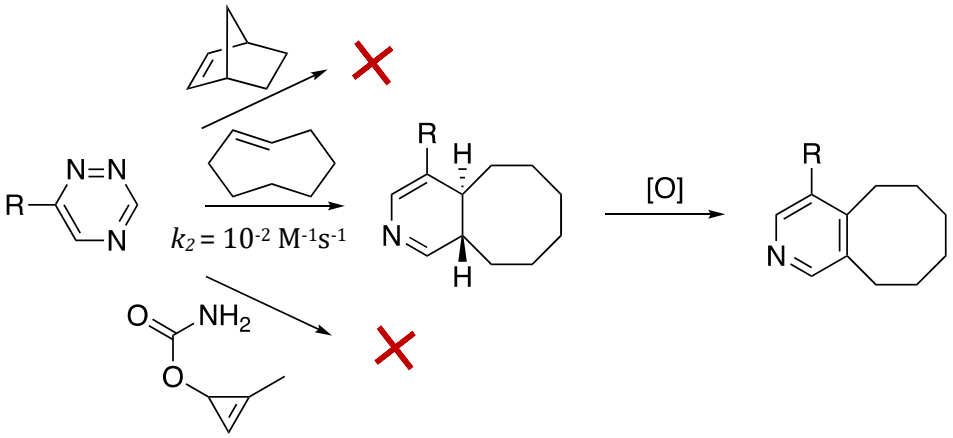

Scheme 2.2 1,2,4-Triazine reactivity with orthogonal reagents norbornene, *trans*-cyclooctene and 3-methyl-cyclopropene. Figure adapted from Kamber *et al.*[21]

2.2 Objective

Inspired by the work of Devaraj and Presher on overcoming limitations of the tetrazine-TCO ligation, our goal was to develop more proficient cycloaddition reactions using nitrones and strained-*trans*-cyclooctene (s-TCO). This was achieved by measuring substituent and strain effects of the nitrone on reaction rates. The optimized nitrones were then tagged as unnatural amino acids (UAAs), incorporated into bacterial membranes and labelled via cycloaddition with TCO- Alexa488.

2.3 Results and Discussion

With the reactions of nitrones and strained alkynes having been well studied and shown to be successful in several SPANC applications, the introduction of strained-*trans*-cyclooctenes offered an alternate dipolarophile to be explored in SPANC chemistry. Investigating alternate reacting partners is important for expanding the bioorthogonal toolbox and potentially revealing new orthogonal bioorthogonal reactions. Prior to characterizing the reactivity of acyclic and cyclic nitrones with s-TCO, the reactivity difference of nitrones with TCO and s-TCO was evaluated.

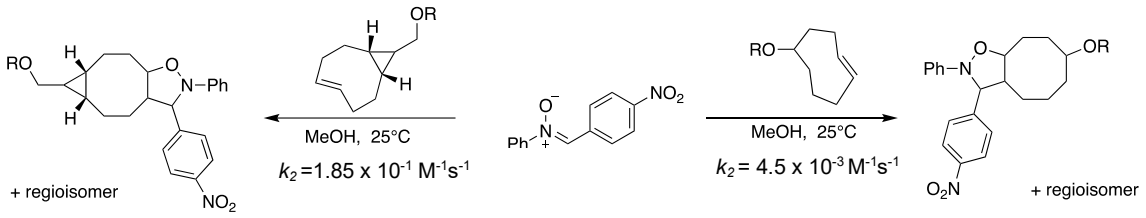

Scheme 2.3 Comparison of the reaction of nitrone **2f** with *trans*-cyclooctene and strained- *trans*-cyclooctene. R= PNB.

We chose nitrone **2a** as the core nitrone due to its stability, ease of synthesis, and ease of handling as all nitrones were solid materials. The second order rate constant for the reaction between the fastest reacting nitrone **2f** with s-TCO was observed to be two orders of magnitude larger than the parallel reaction with the unstrained version of TCO. Thus, we continued our studies using only s-TCO.

2.3.1 Kinetic Studies and Methodology- Acyclic Nitrones

The rate measurements of cycloadditions of s-TCO with various nitrones were performed using UV-visible spectroscopy in methanol at 25 ± 0.1 °C in duplicate. Reactions were done under pseudo-first order conditions with one of the reactants in at least 10-25-fold excess and were monitored by following the decay of the absorbance at the characteristic wavelengths specified in **Table 2.2**.

General procedure for the cycloaddition kinetic studies.

A calculated amount of stock solution of excess reagent (s-TCO) required to achieve the desired final concentration was diluted in a calculated amount of additional methanol in a cuvette. A calculated amount of stock solution of the reacting partner (nitrone) required to achieve the desired final concentration was rapidly mixed with the thermally equilibrated solution and immediately inserted into the UV-vis spectrophotometer. Absorption was measured at pre-set time intervals of 1-2 min and monitored by the wavelength chosen **Table 2.2**. Due to complexity of NMR spectra of the mixture of regio- and diastereomeric products in each reaction, mass spectrometry was used to confirm the formation of products.

Table 2.2 Reaction conditions and absorption wavelengths used to perform UV-Visible kinetic studies of cycloadditions between s-TCO and various nitrones.

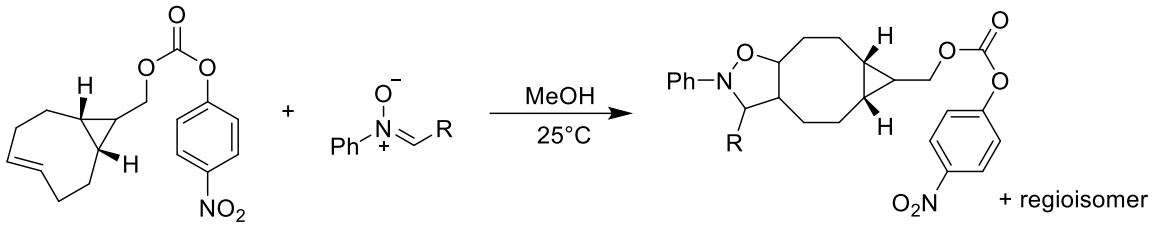

	Nitrone	Wavelength λ (nm)
	s-TCO-PNB	278
2a	R= C_6H_4	312
2b	R= p-$OCH_3C_6H_4$	325
2c	R= p-FC_6H_4	325
2d	R= p-BrC_6H_4	320
2e	R= p-CNC_6H_4	330
2f	R= p-$NO_2C_6H_4$	351

Data analysis of pseudo-first order UV-Visible kinetic experiments. Natural logarithms of relative absorption values were plotted against time (in seconds). Only the linear portion of the regression was used to fit a linear trend line to give a negative slope of which represented the observed rate constant (k_{obs}) for the given experiment at the given concentration of the excess reagent. The observed rate constants of the duplicate reactions were averaged and then plotted against the corresponding excess reagent concentrations. The slope of the linear trend line fitted to the data points represents the second-order rate constant (k_2) for each of the cycloadditions. **Table 2.3** and **Figure 2.2** are shown below as examples, the data for each nitrone is shown in **Appendix A**.

Table 2.3 Observed rate constants for the kinetic studies of cycloadditions of s-TCO-PNB with **2d** C-(4-bromophenyl)-*N*-phenylnitrone correlated to the tested concentrations of s-TCO-PNB in methanol.

Nitrone	Concentration of TCO (10^{-4} M)	k_{obs} (10^{-5} s^{-1})
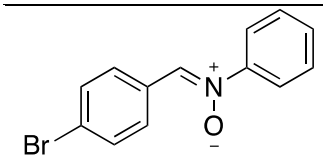	2.00	1.14 ± 0.05
	3.00	1.57 ± 0.08
	4.00	1.82 ± 0.11
	5.00	2.10 ± 0.08

All reactions were done in methanol at 25 °C

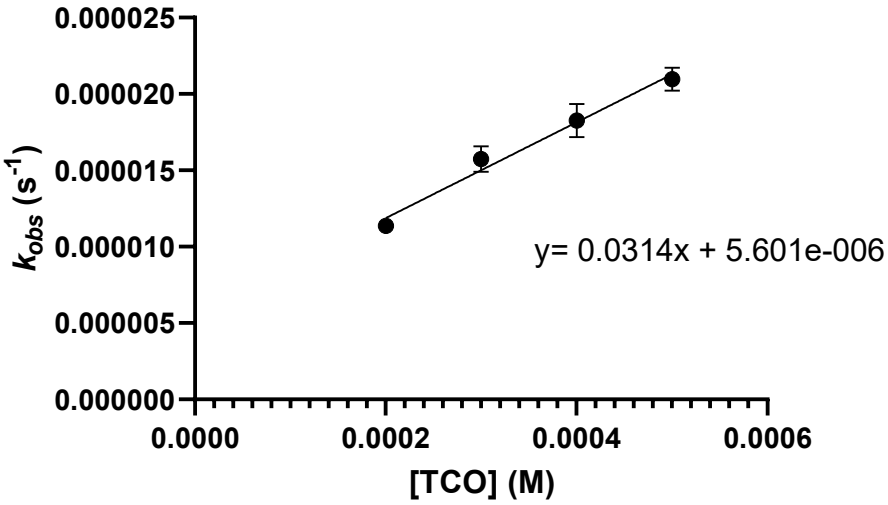

Figure 2.2 Pseudo first-order rate constants of cycloadditions of **2d** C-(4-bromophenyl)-*N*-phenylnitrone with s-TCO plotted against the tested concentrations of s-TCO. Error bars represent the difference of the replicate reactions. $R^2 = 0.96$.

2.3.2 Cycloadditions of s-TCO with Acyclic Nitrones

Table 2.4 Kinetic evaluation of cycloaddition reactions of acyclic nitrones with s-TCO.

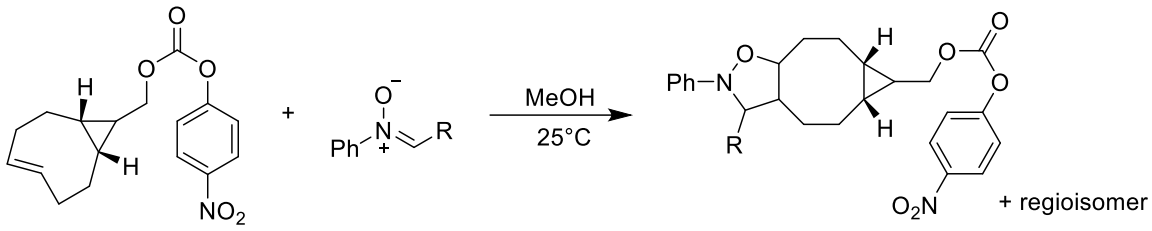

	Nitrone	k_2 (10^{-2} $M^{-1}s^{-1}$)[a, b]
2a	R= p-$OMeC_6H_4$	too slow
2b	R= C_6H_5	1.40 ± 0.09[b]
2c	R= *p*-FC_6H_4	1.70 ± 0.31[a]
2d	R= *p*-BrC_6H_4	3.14 ± 0.27[a]
2e	R= *p*-CNC_6H_4	14.6 ± 1.5[a]
2f	R= *p*-$NO_2C_6H_4$	18.5 ± 1.1[a]

[a] Nitrone **2a**, **c-f** and **s-TCO-PNB** were mixed in a molar ratio of 1:10-25 respectively,[14,15] in MeOH at 25°C. k_2 was determined by UV-visible spectroscopy under pseudo-first order conditions. [b]Initial rate of nitrone **2b** and **s-TCO-OH** was calculated via second order conditions (equimolar ratio (25 mM) in CD_3OD at 25°C) by NMR, this rate constant was subsequently confirmed using methodology a.

To investigate the effect of substituents on the nitrone, nitrones **2b-f** were synthesized and kinetics with s-TCO were tested by UV-vis. By increasing the electron withdrawing character of the nitrone substituent, an increase in rate was observed. This is characteristic of the IEDDA reaction observed between the tetrazine-TCO ligation. With IEDDA, the LUMO of the electron poor diene (tetrazine) and HOMO of the electron rich dienophile (TCO) reacts. By adding an EWG to the diene, the LUMO is lowered, which decreases the energy gap of the reaction.[15] This is also consistent with SPANC reactions involving the HOMO of BARAC and the LUMO of nitrones, where only slight rate accelerations were observed with nitrones bearing EWGs which lowered the LUMO of the nitrone.[23]

2.3.3 Structure-Activity Relationships

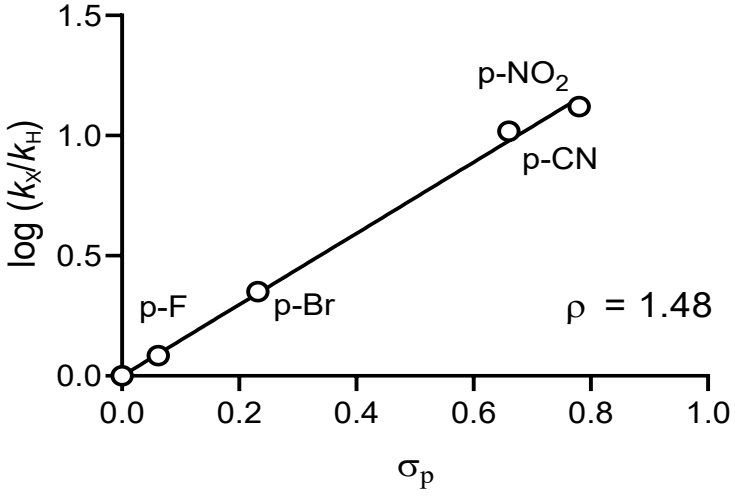

Figure 2.3 Hammett plot depicting the substituent effects on the cycloadditions of acyclic nitrones **2b-f** with s-TCO. R^2= 0.997.

To further evaluate the stereoelectronic sensitivity of the reaction of s-TCO with nitrones, a Hammett plot was constructed (**Figure 2.3**) using nitrones **2a-f** bearing different electron-withdrawing (EWG) and electron-donating groups (EDG) on the *para* position of the α-aryl substituent. The line of best fit was achieved with σ_p parameters (R^2= 0.997), with the resonance structures between the nitrone functional group and *para*-substituents of electron donating and electron-withdrawing character depicted in **Scheme 2.4**.[23] A relatively small Hammett rho (ρ) value of 1.48 ± 0.04 suggests some sensitivity to substituent and a stabilization of the transition state by an EWG directly attached to the nitrone α-aryl substituent. Comparatively, nitrones reacted with BARAC with a ρ =0.25, which is significantly lower than that observed with BCN (ρ =1.28) and TCO (ρ =1.48) (**Table 2.5**), signifying that reactions with BCN and TCO are more sensitive to electronic changes. This suggests that these reactions occur via a non-synchronous transition state where the new nitrone-alkyne C-C σ bond formation occurs in advance of nitrone C-N π bond cleavage, resulting in accumulation of electron density on the nitrone α-carbon during the transition state (**Scheme 2.5**).

Hammett ρ values have been used in the past to confirm the mechanism of reaction. Generally, larger values suggest a large accumulation of charge resulting in an intermediate involved in a step-wise mechanism, and smaller values indicate less accumulation of charge, more consistent with a concerted mechanism. This ρ value is moderately small, indicating that there is not a significant accumulation of electron

density during the transition state, suggesting this reaction proceeds via a concerted reaction mechanism. However, other nitrone-cycloaddition reactions described as concerted have ρ values smaller than 1,[23,37] and therefore, computational studies of the transition state are required to verify the mechanism of addition.

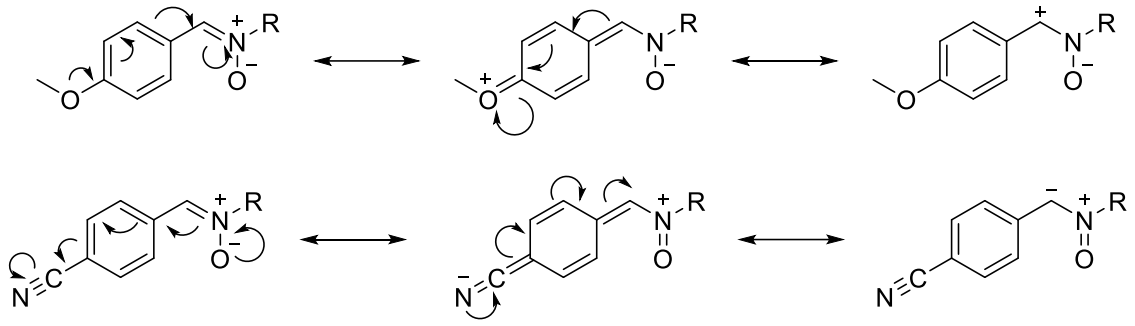

Scheme 2.4 Resonance interactions of acyclic nitrones with electron donating (top) and electron withdrawing groups (bottom) at the *para* position of the α-aryl substituent of the nitrone. Figure adapted from McKay *et al*.[23]

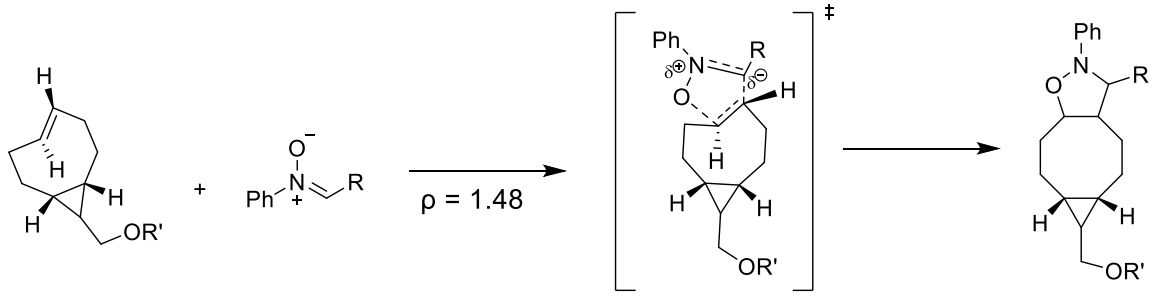

Scheme 2.5 Reaction between s-TCO and an acyclic nitrone with a substituted α-carbon, the suggested transition state shown is based off a ρ value of 1.48.

Table 2.5 Reaction rate parameter, ρ, for SPANC reactions between nitrones and BARAC, BCN and s-TCO.

Nitrone Reaction	Reaction rate parameter, ρ
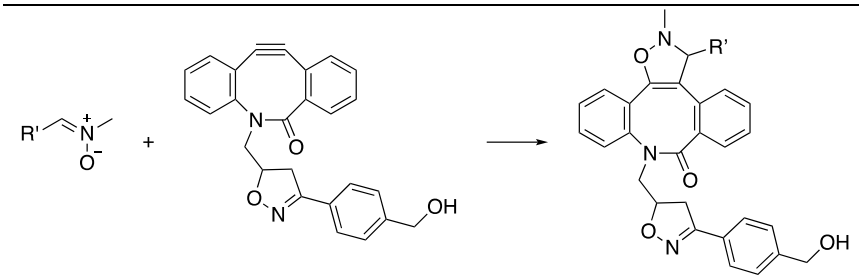 **BARAC**[23]	0.25
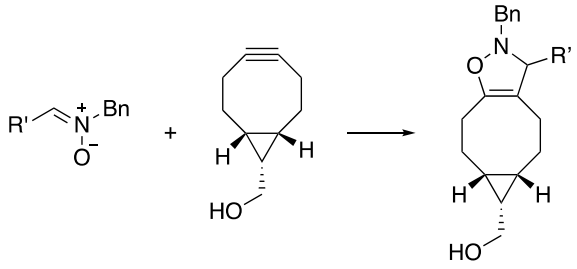 **BCN**[24]	1.28
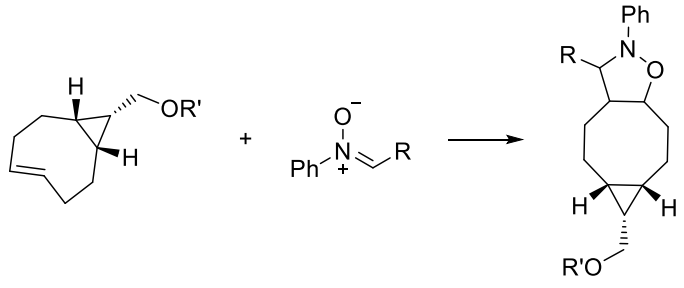 **s-TCO**	1.48

2.3.4 Kinetic Studies and Methodology-Cyclic Nitrones

* Cycloaddition reactions of s-TCO with cyclic nitrones were conducted by Farnaz Mahmoudi.

Kinetic studies of s-TCO and cyclic nitrones by NMR

Both nitrone and s-TCO-OH were pre-dissolved in 0.3 mL of methanol-d4 (~50 mM) and mixed at equimolar concentrations of 25 mM at 25 °C in an NMR tube. To decrease the error of weight measurement, a stock solution of each reagent in the desired concentration was made prior to each trial. The reaction was monitored by ^{1}H NMR. 1,3,5-trimethoxybenzene was used as an internal standard in all experiments.

Second order rate constants (k_2) in units of $M^{-1}s^{-1}$ were calculated using the NMR integration by plotting 1/[nitrone] or 1/[TCO] versus time and subsequently analyzed by linear regression (**Appendix B**). The reaction between the nitrones **2f-i** and s-TCO-OH were tested in two or three trials and each time the same product was obtained (determined by integration at multiple chemical shifts in the ^{1}H NMR).

The ^{1}H NMR stack spectra of **s-TCO-OH (1b)** and nitrone **2i** as starting materials, and the reaction between **TCO** and **2i** (before and after completion) are shown in **Figure 2.4** as an example for these cycloaddition reactions.

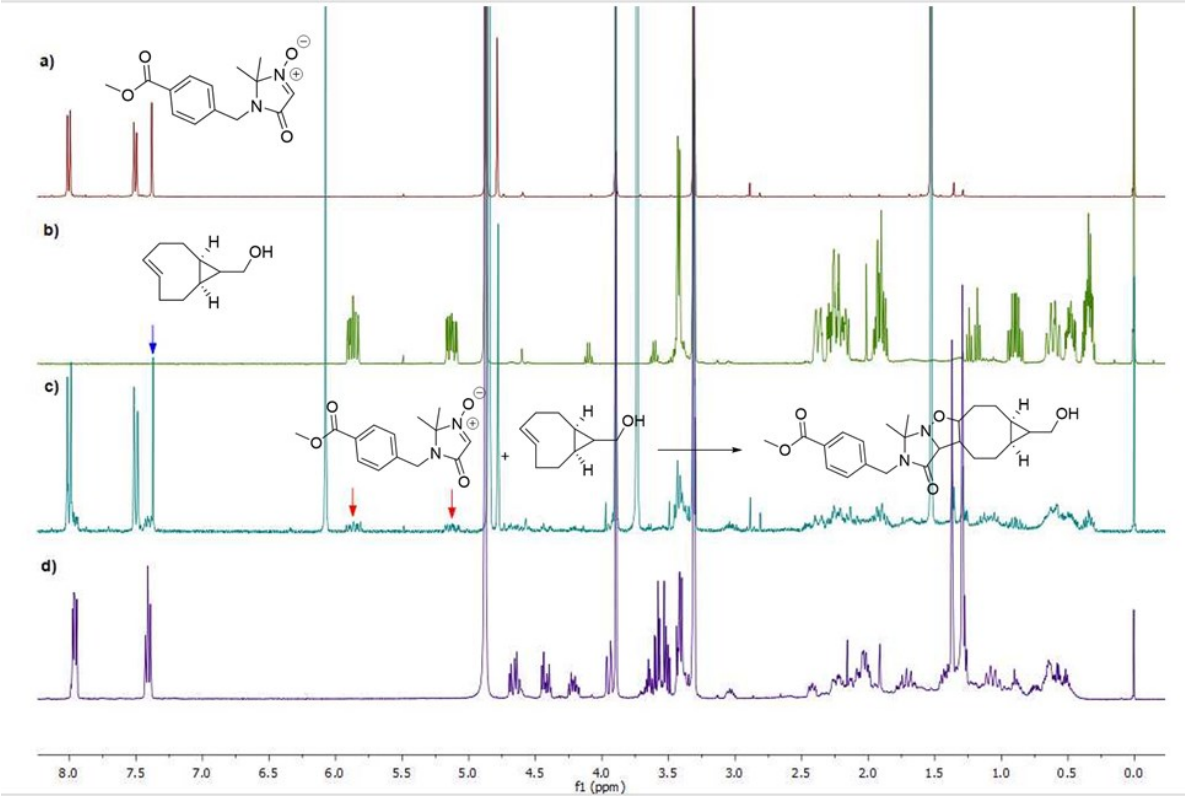

Figure 2.4 ^{1}H NMR spectra (300 MHz, CD_3OD) of a) s-TCO-OH (**1b**), b) nitrone **2i**, c) reaction solution at the beginning time of the reaction, (the red arrows represent the double-bond of s-TCO-OH (**1b**), and the blue arrows represent the hydrogen next to N-O bond in nitrone **2i**, indicating the peaks used to track reaction completion and d) isolated product after complete reaction between s-TCO-OH (**1b**) and nitrone **2i**.

2.3.5 Cycloadditions of s-TCO with Cyclic Nitrones

Cyclic nitrones are more stable to hydrolysis than acyclic nitrones under aqueous conditions and are better suited for functionalizing proteins and cell surfaces and metabolic labeling applications compared with acyclic nitrones.[25] We sought to establish a kinetic profile of cyclic nitrones with s-TCO to determine utility in metabolic labelling. Bimolecular rate constants, k_2 were determined by NMR spectroscopy under second order reaction kinetics for a series of nitrones bearing different sterics, stereoelectronics and ring size (**2g-2i**). Reactions with cyclic nitrones yielded fast conversions in under 20 minutes. Nitrone **2i** demonstrated the greatest promise for metabolic labelling as it demonstrated fast kinetics, stability to hydrolysis, and easy conjugation to amino acids.

Table 2.6 Kinetic evaluation of cycloaddition reactions of cyclic nitrones with s-TCO.

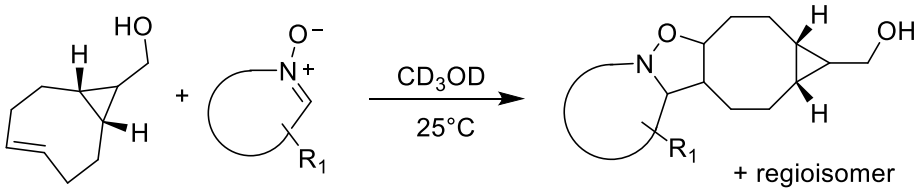

1b **2g-i**

	Nitrone	k_2 (10^{-2} $M^{-1}s^{-1}$)	Time to 95% completion (min)
2g	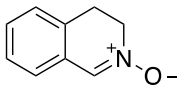	8.17 ± 0.05	10-12
2h	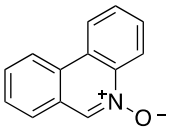	3.60 ± 0.03	20
2i	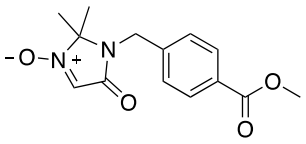	7.23 ± 0.05	10-12

Nitrone **2g-i** and **s-TCO-OH** were mixed in an equimolar ratio (25 mM) in CD_3OD at 25 °C. k_2 was determined by ^1H NMR under second order conditions. 1,3,5-trimethoxybenzene was used as an internal standard. The k_2 ($M^{-1}s^{-1}$) values were calculated from linear regression of plots of 1/[nitrone] or 1/[TCO] vs. time.

2.3.6 Bacterial Labelling Using Nitrones and s-TCO

General metabolic labelling of bacterial cells via nitrone-TCO cycloaddition.

L. innocua were cultured in BHI medium until mid-log phase growth, and then treated with 1.5 μL DMSO, or 5 mM of the indicated UAA for 1 hour at 30 °C. Cells were washed in PBS before and after cycloaddition reaction with ~50 μM TCO-Alexa488 (10 minutes at 30 °C), followed by fluorescence microscopy.

Fluorescence microscopy. All microscopy images herein were acquired using Nikon Ni-U Ratiometric Fluorescence Microscope with Dual Excitation Sources. The microscope was equipped with a 60x objective lens and a 2x relay lens. Average background fluorescence obtained in absence of D-ala-UAA is shown. Scale bar indicates 5 μm.

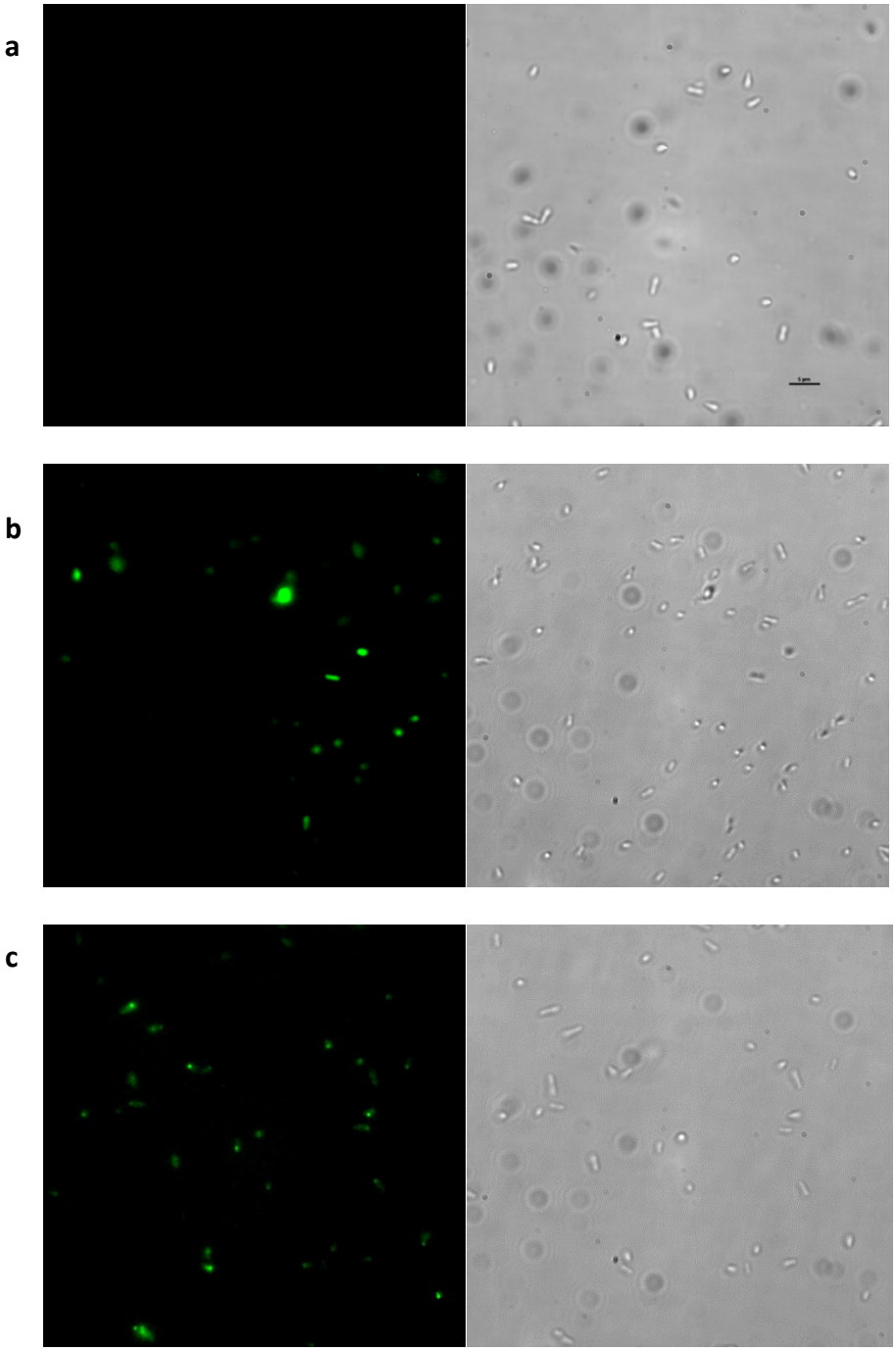

Figure 2.5 Images showing incorporation of UAA by *L. innocua.* Cells were cultured in the presence of (a) DMSO or 5 mM of (b) D-ala-CMPO or (c) D-ala-DMImO for 1 hour at 30 °C, washed with PBS before and after reaction with ~50 μM TCO-Alexa488 for 10 minutes at 30 °C. Brightfield is on the right, fluorescence is on the left. An above background signal obtained for cells cultured in the presence of DMSO with identical TCO-Alexa488 treatment is shown. Scale bar= 5 μm.

Targeting the bacterial peptidoglycan wall is of high interest as it provides an accessible opportunity to gain insight into bacterial growth and division.[26,27] The bacterial peptidoglycan wall is composed of interlinked glycans and peptides, providing structural rigidity and a protective layer.[28] Labelling the peptidoglycan layer requires small reactive groups with a biological handle, such as an amino acid. We have previously shown that nitrones are small enough to be tagged onto unnatural amino acids and glycans and readily incorporated into the peptidoglycan wall and cell membrane respectively.[30,34] As the UAAs bearing nitrones proved to be stable and demonstrated robust incorporation, our present work expands the SPANC labelling toolbox to incorporate fluorophores bearing a s-TCO moiety.

The bioorthogonal potential of the TCO-nitrone cycloaddition was investigated using unnatural amino acids bearing cyclic nitrones and an Alexa-488 fluorophore appended to s-TCO. UAAs bearing DMImO and CMPO were chosen as they represent stable compounds with opposing electron deficiency. *Listeria innocua* was chosen as a model organism as it is gram positive and thus does not contain an outer cell membrane and is a non-pathogenic model of the common food pathogen *L. monocytogenes. L. innocua* were treated with excess of UAA for 1 hour, washed with PBS and labelled with TCO-Alexa488 for 10 minutes followed by more PBS washes prior to imaging (**Figure 2.5**). Treatment with both of the UAAs demonstrated robust labelling, consistent with conversion times in **Table 2.6**.

Furthermore, the labelling of model bacteria occurred rapidly enough that significant amounts of fluorescence were observed following treatment with the TCO-dye conjugate, confirming both the bioorthogonality of the reaction, (no reaction in the absence of nitrone), (**Figure 2.5a**) and the useful rates of cycloaddition. Thus, we show a new application for s-TCO in bioorthogonal TCO-nitrone cycloadditions and open- up new chemistries beyond ligations with tetrazine.

2.4 Conclusion

In conclusion, we have shown for the first time that both acyclic and cyclic nitrones serve as good reaction partners for s-TCOs in bioorthogonal applications. These cycloadditions react with rate constants on the order of 10^{-2} to 10^{-1} $M^{-1}s^{-1}$, comparable to other rate constants of IEDDA alternative reactions to TCO-tetrazine ligation. Furthermore, we demonstrate the effects of nitrone substituents on reactivity, highlighting that electron deficient nitrones give rise to faster kinetics. We have expanded the bioorthogonal toolbox to include the reaction between nitrones and strained-TCO, demonstrating the utility of nitrones to replace azides, and now tetrazines for metabolic imaging applications. These reactions expand the utility of TCO reagents and overcome some of the limitations of tetrazine reagents such as size or redox stability. The TCO-nitrone ligation shown here offers the advantage of a smaller inherent dipole for easier metabolic incorporation than for analogous reactions involving tetrazine. These results reinforce the utility of nitrones as small,

tunable metabolic labelling agents. Future work will investigate the potential of the nitrone-TCO cycloaddition for multiplex labelling applications.

2.5 Materials and Experimental Details

All commercially available reagents were purchased from Alfa Aesar and Sigma Aldrich and were used without further purification. Alexa 488 hydrazide was purchased from Fischer Scientific. Strained-*trans*cyclooctene (hydroxyl and PNB ester versions) were received from the Fox group (Department of Chemistry at University of Delaware, USA). All deuterated solvents were purchased from Cambridge Isotopes and were used as received, except for deuterated chloroform that was neutralized by passing through a pad of basic alumina (such treated $CDCl_3$ will be signaled below by an asterisk, i.e. '$CDCl_3$*'). Thin layer chromatography was performed on Analtech Uniplate® silica gel (60 A F254, layer thickness 250 μm). Flash chromatography was performed using silica gel (60 A, particle size 40-63 μm). LC-MS spectra were obtained using Acquity UPLC class H equipped with Waters PDA diode array detector and connected to Waters XEVO TQD mass spectrometer equipped with pneumatically assisted electrospray ionization source, operating in both positive and negative mode. Samples were run with gradient elution of 50/50 MeOH/H_2O to 100% acetonitrile on the Acquity UPLC BEH C18 (2.1 x 50mm, 1.7 μm) column with flow rate of 0.2 mL/min. Preparative HPLC was performed on a Waters

2695 using XBridge prep column (19x50 mm, 5 μm OBD). Column effluents were monitored at wavelength specified in respective procedures.

All ^{1}H and ^{13}C NMR spectra were obtained using 300 MHz, and 400 MHz Bruker NMR spectrometers and processed using MestReNova iNMR 4.2.0 software. The units of the NMR spectra peaks are ppm and referenced against the residual solvent peak. Multiplicity of peaks recorded as abbreviated form: s = singlet, d = doublet, t = triplet, m = multiplet or unresolved, br = broad and J = coupling constants in Hz.

2.5.1 Synthesis of Reagents

General Nitrone Synthesis A

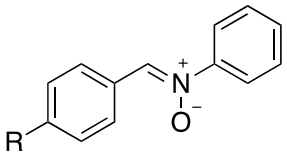

300 mg (2.8 mmol) of phenylhydroxylamine and 3 mmol of *para*-substituted benzaldehyde were added to a dry 25 mL round-bottom flask. 5 mL of dry ethanol was added to the flask and the mixture was stirred for 2 hours at 35 °C. Pure products were obtained following filtration of the precipitated crude product and recrystallization from warm ethanol and hexanes.

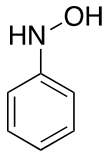

N-Phenylhydroxylamine. A mixture of nitrobenzene (10.8 mL, 0.105 mol), NH_4Cl (6.5 g, 0.12 mol) and degassed H_2O (200 mL) under argon at r.t. was stirred vigorously while zinc dust (15.4 g, 0.21 mol) was added portion wise over 20 min. After addition was complete, the reaction mixture was stirred for an additional 20 minutes and was filtered while still warm. The resultant filter cake was washed with hot distilled water (50 mL) and the combined filtrate was saturated with NaCl and extracted with 3x100 mL of EtOAc. The organic layers were combined, dried over Na_2SO_4 and concentrated under reduced pressure. The crude N-phenyl hydroxylamine was recrystallized from petroleum ether / ethyl acetate (8.2 g, 72 %), dried thoroughly and stored under an atmosphere of argon at -20 °C. ^1H NMR and MS data are in agreement with that reported previously.[31]

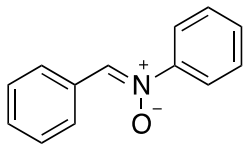

C, *N*-diphenylnitrone. The nitrone was synthesized according to General Nitrone Synthesis A. The product was obtained in 50% yield. **^{1}H NMR** (300 MHz; $CDCl_3$): δ 8.42-8.39 (m, 2H), 7.93 (s, 1H), 7.80-7.77 (m, 2H), 7.50-7.48 (m, 6H). Spectral data was consistent with previously reported data.[32]

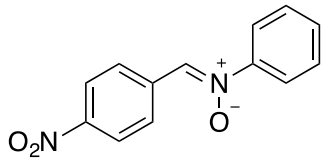

C-(4-nitrophenyl)-*N*-phenylnitrone. The nitrone was synthesized according to General Nitrone Synthesis A. The product was obtained in 75% yield. **^{1}H NMR** (300 MHz; $CDCl_3$): δ 8.58-8.53 (m, 2H), 8.34-8.30 (m, 2H), 8.07 (s, 1H), 7.80-7.77 (m, 2H), 7.53 (dd, *J* = 4.2, 2.5 Hz, 3H). Spectral data was consistent with previously reported data.[32]

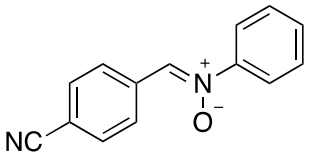

C-(4-cyanophenyl)-*N*-phenylnitrone. The nitrone was synthesized according to General Nitrone Synthesis A. The product was obtained in 52% yield. **^{1}H NMR** (400 MHz; $CDCl_3$): δ 8.48 (d, *J* = 8.4 Hz, 2H), 8.00 (s, 1H), 7.78-7.74 (m, 4H), 7.52 (t, *J* = 3.3 Hz, 3H). Spectral data was consistent with previously reported data.[32]

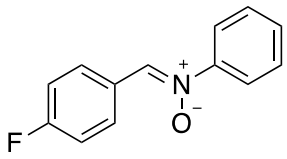

C-(4-fluorophenyl)-*N*-phenylnitrone. The nitrone was synthesized according General Nitrone Synthesis A. The product was obtained in 54% yield. **^{1}H NMR** (300 MHz; $CDCl_3$): δ 8.48-8.43 (m, 2H), 7.91 (s, 1H), 7.79-7.76 (m, 2H), 7.52-7.48 (m, 3H), 7.20-7.15 (m, 2H). Spectral data was consistent with previously reported data.[32]

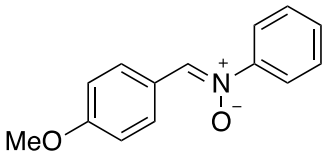

C-(4-methoxyphenyl)-*N*-phenylnitrone. The nitrone was synthesized according to General Nitrone Synthesis A. The product was obtained in 77% yield. **^{1}H NMR** (300 MHz; $CDCl_3$): δ 8.43-8.39 (m, 2H), 7.86 (s, 1H), 7.80-7.76 (m, 2H), 7.51-7.44 (m, 3H), 7.02-6.99 (m, 2H), 3.89 (s, 3H). Spectral data was consistent with previously reported data.[32]

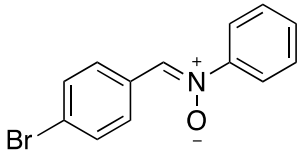

C-(4-bromophenyl)-*N*-phenylnitrone. The nitrone was synthesized according General Nitrone Synthesis A. **^{1}H-NMR** (400 MHz; $CDCl_3$): δ 8.30 (d, *J* = 8.5 Hz, 2H), 7.91 (s, 1H), 7.77 (d, *J* = 9.8 Hz, 2H), 7.62 (d, *J* = 8.6 Hz, 2H), 7.50 (dd, *J* = 5.1, 1.9 Hz, 3H). Spectral data was consistent with previously reported data.[38]

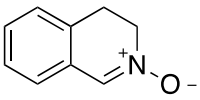

3,4-Dihydroisoquinoline *N*-oxide. Synthesized according to previously reported literature.[33] **^{1}H-NMR** (300 MHz; $CDCl_3$): δ 7.76 (s, 1H), 7.29-7.26 (m, 2H), 7.22 (q, *J* = 4.4 Hz, 1H), 7.14-7.11 (m, 1H), 4.11 (t, *J* = 7.3 Hz, 2H), 3.18 (t, *J* = 7.8 Hz, 2H).

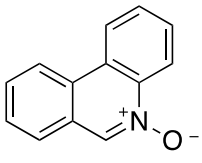

Phenanthridine 5-oxide. Synthesized according to previously reported literature.[29] Accordingly, phenanthridine (50 mg, 0.28mmol, 1 eq) was dissolved in acetonitrile (200 µL) and hydrogen peroxide (83 µL, 0.84mmol, 3 eq, 30% in water) was added dropwise, followed by phosphomolybdic acid (25 µL of freshly prepared 0.2M solution in EtOH, 0.005 mmol, 1.8 mol%), also dropwise. The reaction was allowed to proceed at 50 °C overnight. The mixture was cooled to room temperature, diluted with saturated ammonium chloride and extracted with dichloromethane twice. The organic extracts were combined, dried over Na_2SO_4 and concentrated under reduced pressure. The crude mixture was purified by column chromatography (0-20% MeOH gradient in 3:7/Hex:EtOAc) to yield the product as a pale beige powder (40 mg, 0.21mmol, 73%, Rf= 0.16 in 100% EtOAc). **^{1}H-NMR** (400 MHz, $CDCl_3$): δ 8.88 (ddd, J=1.5, 7.8 Hz, 1H), 8.82 (s, 1 H), 8.49 (d, J=7.6 Hz, 1 H), 8.41 (s, 1 H), 7.73 (m, 4 H), 7.60 (t, J=7.4 Hz, 1 H); **^{13}C-NMR** (100 MHz, $CDCl_3$): δ 139.3, 134.5, 129.5, 129.4, 129.3, 128.8, 126.6, 126.5, 126.0, 122.7, 122.0, 120.6. **MS (ESI+)** calcd ($C_{13}H_9NO$): 195.0684, $[M+H]^+$ found 196.0757.

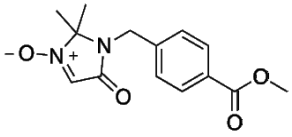

Methyl 4-[(2,2-dimethyl-3-oxido-5-oxo-2,5-dihydro-1*H*-imidazol-1-yl)methyl]benzoate. Synthesized according to a modified version of

previously reported literature.[34] The product was obtained in 26.4% yield over 5 steps. **^{1}H NMR** (400 MHz, $CDCl_3$) δ 8.04 – 7.94 (m, 2H), 7.42 – 7.34 (m, 2H), 7.09 (s, 1H), 4.69 (s, 2H), 3.90 (s, 3H), 1.47 (s, 6H); **^{13}C NMR** (100 MHz, $CDCl_3$) δ 166.52, 162.27, 141.76, 130.20, 130.08, 127.89, 123.49, 90.48, 52.23, 43.36, 25.06; **HRMS (EI)** calcd for ($C_{14}H_{16}N_2O_4$): 276.11101, [M] found 276.10923.

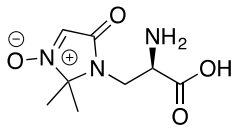

(2R)-2-Amino-3-(2,2-dimethyl-5-oxo-3-oxy-2,5-dihydro-imidazol-1-yl)-propionic acid(D-Ala-DMImO). Synthesized according to previously described literature procedures.[34,35] **^{1}H-NMR** (400 MHz, CD_3OD): δ 7.37 (s, 1H), 4.39 (dd, J=4.7, 6.6 Hz, 1H), 4.03 (m, 2H), 1.70 (s, 3H), 1.68 (s, 3H); **^{13}C-NMR** (100 MHz, CD_3OD): δ 169.4, 166.3, 125.3, 92.4, 54.4, 42.1, 24.4, 24.3; **LRMS (ESI+)** m/z calcd for ($C_8H_{13}N_3O_4$): 216.09 $[M+H]^+$, found 216.3.

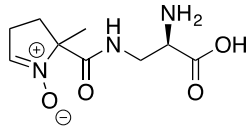

(2R)-2-Amino-3-[(2-methyl-1-oxy-3,4-dihydro-2H-pyrrole-2-carbonyl)-amino]-propionic acid (D-Ala-CMPO). Synthesized according to previously described literature procedure.[34] **^{1}H-NMR** (300 MHz; MeOD): δ 7.27 (s, 1H), 4.17 (dt, *J* = 6.5, 4.4 Hz, 1H), 3.76 (m, 2H), 2.72-2.65 (m, 3H),2.24-2.12 (m, 1H), 1.69 (s, 3H); **MS (ESI+)** m/z calcd for ($C_9H_{15}N_3O_4$): 230.11 $[M+H]^+$, found 230.3.

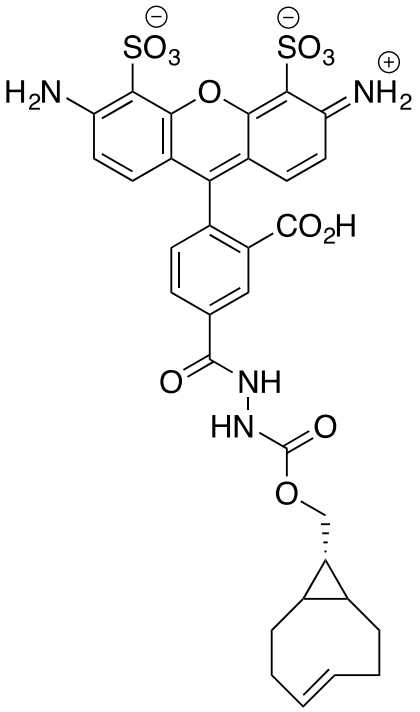

Synthesis of TCO-Alexa488. Synthesis was based on the literature procedure.[36] (1R, 8 S, 9 R, 4 E)-Bicyclo [6.1.0] non-4-em-9-ylmethyl(4-nitrophenyl) carbonate (2.8mg, 8.86 μmol) was added to a vial containing Alexa Fluor 488 hydrazide (1.0 mg, 1.75 μmol). A DMF solution (200 μL, anhydrous) containing N, N, -diisopropylethylamine (3.5 μmol) and 4-Dimethylaminopyridine (DMAP) (0.88 μmol) was added to the vial. The mixture was stirred overnight at room temperature and purified with reverse phase HPLC elution gradient 1:1 MeOH: H_2O to 100% ACN over 30 minutes, at 6mL/min (λ 488 nm) generating the product as a yellow solid. **MS (ESI+)** m/z calcd for ($C_{32}H_{29}N_4O_{12}S_2^-$): 725.1229 $[M+H]^+$ found 726.3797 (**Appendix C**) confirmed the identification of the compound with a mass of 0.47mg.

Kinetic studies procedure

All kinetic experiments were conducted following the general method outlined in **Section 2.3.1**, varying the concentration and wavelength chosen according to the values found in **Table 2.2**. The concentrations of nitrones used can be found in **Appendix B**.

Stock solutions of s-TCO (1 mM) and nitrone (2 mM) were prepared in screw cap vials in OptimaGrade Methanol and stored at -20 °C. Fresh stocks of nitrone were made prior to each run, s-TCO stocks were made prior to replicate runs. The cuvettes used were 1.5 mL Quartz cuvettes with stoppers (10 mm pathlength). Before preparation of each reaction, UV-vis cuvettes were cleaned with acetone 4 times and let dry for 20 minutes. Cuvettes were wiped with Kimwipes prior to reading to remove any residue on the outer surface.

Prior to reactions, the UV-vis spectrophotometer was blanked with 1 mL of methanol. Next, reactions were set up with addition of methanol and s-TCO (**Table 3.5**), followed by quick addition of nitrone, inverting the cuvette to mix the reaction, and it was immediately inserted for wavelength reading.

In order to choose a wavelength for product monitoring, the following spectra (200 nm to 800 nm) were obtained over the entire reaction period:

- Solvent only as baseline
- s-TCO (200-500 μM)
- Nitrone (20 μM)
- Reaction mixture containing 20 μM nitrone, 200-500 μM Nitrone and remaining amount of methanol according to the volumes shown in **Table 3.5**.

Table 2.7 Volume of stock solutions used for the pseudo-first order kinetics of acyclic nitrones with s-TCO.

Reaction	Vol. of 2 mM nitrone stock (μL)	Vol. of 1mM s-TCO stock (μL)	Vol. of methanol (μL)	Total Volume of reaction (μL)
20 μM Nitrone 200 μM s-TCO	10	200	790	1000
20 μM Nitrone 300 μM s-TCO	10	300	690	1000
20 μM Nitrone 400 μM s-TCO	10	400	590	1000
20 μM Nitrone 500 μM s-TCO	10	500	490	1000

References

1. Devaraj, N. K. The Future of Bioorthogonal Chemistry. *ACS Cent. Sci.* **4**, 952–959 (2018).
2. Baskin, J. M. & Bertozzi, C. R. Copper-free click chemistry: Bioorthogonal reagents for tagging azides. *Aldrichimica Acta.* **43**, 15–23 (2010).
3. Sauer, J. *et al.* 1,2,4,5-Tetrazine: Synthesis and Reactivity in [4+2] Cycloadditions. *European J. Org. Chem.* 2885–2896 (1998).
4. Yang, J., Šečkute, J., Cole, C. M. & Devaraj, N. K. Live-cell imaging of cyclopropene tags with fluorogenic tetrazine cycloadditions. *Angew. Chem. Int. Ed.* **51**, 7476–7479 (2012).
5. Yang, J., Liang, Y., Šečkute, J., Houk, K. N. & Devaraj, N. K. Synthesis and reactivity comparisons of 1-methyl-3-substituted cyclopropene mini-tags for tetrazine bioorthogonal reactions. *Chem. A Eur. J.* **20**, 3365–3375 (2014).
6. Blackman, M. L., Royzen, M. & Fox, J. M. Tetrazine ligation: Fast bioconjugation based on inverse-electron-demand Diels-Alder reactivity. *J. Am. Chem. Soc.* **130**, 13518–13519 (2008).
7. Thalhammer, F., Wallfahrer, U. & Sauer, J. Reaktivität einfacher offenkettiger und cyclischer dienophile bei Diels-Alder-reaktionen mit inversem elektronenbedarf. *Tetrahedron Letters.* vol. 31 6851–6854 (1990).
8. Devaraj, N. K. & Weissleder, R. Biomedical applications of tetrazine cycloadditions. *Acc. Chem. Res.* **44**, 816–827 (2011).
9. Taylor, M. T., Blackman, M. L., Dmitrenko, O. & Fox, J. M. Design and synthesis of highly reactive dienophiles for the tetrazine-trans-cyclooctene ligation. *J. Am. Chem. Soc.* **133**, 9646–9649 (2011).
10. Bach, R. D. Ring strain energy in the cyclooctyl system. the effect of strain energy on [3 + 2] cycloaddition reactions with azides. *J. Am. Chem. Soc.* **131**, 5233–5243 (2009).
11. Darko, A. *et al.* Conformationally strained trans-cyclooctene with improved stability and excellent reactivity in tetrazine ligation. *Chem. Sci.* **5**, 3770–3776 (2014).
12. Šečkute, J. & Devaraj, N. K. Expanding room for tetrazine ligations in the in vivo chemistry toolbox. *Curr. Opin. Chem. Biol.* **17**, 761–767 (2013).
13. Liu, F., Liang, Y. & Houk, K. N. Bioorthogonal Cycloadditions: Computational Analysis with the Distortion/Interaction Model and Predictions of Reactivities. *Acc. Chem. Res.* **50**, 2297–2308 (2017).

14. Devaraj, N. K., Weissleder, R. & Hilderbrand, S. A. Tetrazine-based cycloadditions: Application to pretargeted live cell imaging. *Bioconjug. Chem.* **19**, 2297–2299 (2008).

15. Oliveira, B. L., Guo, Z. & Bernardes, G. J. L. Inverse electron demand Diels-Alder reactions in chemical biology. *Chem. Soc. Rev.* **46**, 4895–4950 (2017).

16. Chen, W., Wang, D., Dai, C., Hamelberg, D. & Wang, B. Clicking 1,2,4,5-tetrazine and cyclooctynes with tunable reaction rates. *Chem. Commun.* **48**, 1736–1738 (2012).

17. Engelsma, S. B. *et al.* Acylazetine as a dienophile in bioorthogonal inverse electron-demand Diels-Alder ligation. *Org. Lett.* **16**, 2744–2747 (2014).

18. Ravasco, J. M. J. M., Monteiro, C. M. & Trindade, A. F. Cyclopropenes: A new tool for the study of biological systems. *Org. Chem. Front.* **4**, 1167–1198 (2017).

19. Patterson, D. M., Nazarova, L. A., Xie, B., Kamber, D. N. & Prescher, J. A. Functionalized cyclopropenes as bioorthogonal chemical reporters. *J. Am. Chem. Soc.* **134**, 18638–18643 (2012).

20. Row, R. D. & Prescher, J. A. Constructing New Bioorthogonal Reagents and Reactions. *Acc. Chem. Res.* **51**, 1073–1081 (2018).

21. Kamber, D. N. *et al.* 1,2,4-Triazines Are Versatile Bioorthogonal Reagents. *J. Am. Chem. Soc.* **137**, 8388–8391 (2015).

22. Jewett, J. C., Sletten, E. M. & Bertozzi, C. R. Rapid Cu-free click chemistry with readily synthesized biarylazacyclooctynones. *J. Am. Chem. Soc.* **132**, 3688–3690 (2010).

23. McKay, C. S., Chigrinova, M., Blake, J. A. & Pezacki, J. P. Kinetics studies of rapid strain-promoted [3 + 2]-cycloadditions of nitrones with biaryl-aza-cyclooctynone. *Org. Biomol. Chem.* **10**, 3066–3070 (2012).

24. Mackenzie, D. A. & Pezacki, J. P. Kinetics studies of rapid strain-promoted [3+2] cycloadditions of nitrones with bicyclo[6.1.0]nonyne. *Can. J. Chem.* **92**, 337–340 (2014).

25. McKay, C. S., Blake, J. A., Cheng, J., Danielson, D. C. & Pezacki, J. P. Strain-promoted cycloadditions of cyclic nitrones with cyclooctynes for labeling human cancer cells. *Chem. Commun.* **47**, 10040–10042 (2011).

26. Gautam, S., Gniadek, T. J., Kim, T. & Spiegel, D. A. Exterior design: Strategies for redecorating the bacterial surface with small molecules. *Trends Biotechnol.* **31**, 258–267 (2013).

27. Fura, J. M., Sabulski, M. J. & Pires, M. M. D-amino acid mediated recruitment of endogenous antibodies to bacterial surfaces. *ACS Chem. Biol.* **9**, 1480–1489 (2014).

28. Heijenoort, J. van. Recent advances in the formation of the bacterial peptidoglycan monomer unit. *Nat. Prod. Rep.* **18**, 503–519 (2001).

29. Strmiskova, M., Bilodeau, D. A., Chigrinova, M. & Pezacki, J. P. Phenanthridine-based nitrones as substrates for strain-promoted alkyne-nitrone cycloaditions. *Can. J. Chem*. **97**, 1-6 (2019) .

30. McKay, C. S., Blake, J. A., Cheng, J., Danielson, D. C. & Pezacki, J. P. Strain-promoted cycloadditions of cyclic nitrones with cyclooctynes for labeling human cancer cells. *Chem. Commun.* **47**, 10040–10042 (2011).

31. Chatterjee, A., Maiti, D. K. & Bhattacharya, P. K. Water Exclusion Reaction in Aqueous Media: Nitrone Formation and Cycloaddition in a Single Pot. *Org. Lett.* **5**, 3967–3969 (2003).

32. Luo, Q., Cao, C. T., Cao, Z. & Cao, C. Influence of the side-group at C=N bridging bond of bis-aryl Schiff bases on the wavelength of absorption maximum of ultraviolet absorption spectra. *J. Phys. Org. Chem.* **29**, 406–413 (2016).

33. Gella, C. *et al.* A metal-free general procedure for oxidation of secondary amines to nitrones. *J. Org. Chem.* **74**, 6365–6367 (2009).

34. MacKenzie, D. A., Sherratt, A. R., Chigrinova, M., Kell, A. J. & Pezacki, J. P. Bioorthogonal labelling of living bacteria using unnatural amino acids containing nitrones and a nitrone derivative of vancomycin. *Chem. Commun.* **51**, 12501–12504 (2015).

35. Dai, X., Miller, M. W. & Stamford, A. W. Formal Olefination and Acylaziridination of Imidazolones. *Org. Lett.* **12**, 2718–2721 (2010).

36. Zhang, H., Dicker, K. T., Xu, X., Jia, X. & Fox, J. M. Interfacial bioorthogonal cross-linking. *ACS Macro Lett.* **3**, 727–731 (2014).

37. Lorello, G.R., Legault, M.C.B., Rakic, B., Bisgaard,K., Pezacki, J.P. Synthesis and bioorthogonal coupling chemistry of a novel cyclopentenone-containing unnatural tyrosine analogue. *Bioorg. Chem*. **36**, 105- (2008)

38. Tian, Z., Xu, J., Liu, B., Tan, Q. & Xu, B. Copper-Catalyzed Synthesis of Polysubstituted Pyrroles through [3+1+1] Cycloaddition Reaction of Nitrones and Isocyanides. *Org. Lett.* **20**, 2603–2606 (2018).

Chapter 3

Double Strain-Promoted Alkyne-Nitrone Cycloadditions

3.1 Introduction

The rise of bioorthogonal chemistry has led to the optimization of many click reactions that render them useful for purposes outside of biological applications. For instance, polymer synthesis using 1,3 dipolar cycloadditions first occurred in the late 1960s,[1–3] but it wasn't until the rise of bioorthogonal chemistry where the limitations of these reactions (poor reaction efficiency, unavoidable side products, and harsh reaction conditions) were overcome, allowing for increased versatility.[4] A recent example shows the synthesis of a polymer using two different monomers, one; a bifunctional strained cyclooctyne formed by connecting two Dibenzoazacyclooctynes (DBCOs) together, and a second monomer with two azides appended via different linkers. Though the preparation of di-azido monomers was quite facile, they found synthesis of the DBCO monomers quite difficult, in terms of finding a linker that provided optimal solubility and stability.[5] The *sym*-dibenzo- 1,5-cyclooctadiene-3,7-diyne (diyne) shown in **Scheme 3.1**, which is similar to DIBO with two alkynes, can be more easily synthesized and offers greater versatility.[6,7]

A report which investigates the use of diyne in SPAAC chemistry, termed the strain-promoted "double-click" (SPDC) reaction was recently characterized and utilized for

labelling applications (**Scheme 3.1**).[8] Interestingly, in this report, the mono-intermediate was never isolated nor detected over the course of the reaction, suggesting that the monoyne is significantly more reactive than the unreacted diyne. The explanation for this observation was best found in the difference between the activation energies of the first and second cycloaddition. The activation energy calculated for the first cycloaddition was +12.4 kcal/mol, and for the second cycloaddition, where the alkyne bond is expected to be highly distorted, was calculated to be +8.8kcal/mol and +9.5 kcal/mol for the *trans*- and *cis*- adducts, respectively.[8] A second-order rate constant of 6.29 ± 0.05 x 10^{-2} $M^{-1}s^{-1}$ in MeOH, 25°C was determined for the rate-determining step (RDS); the first reaction between the diyne with benzyl azide.[8]

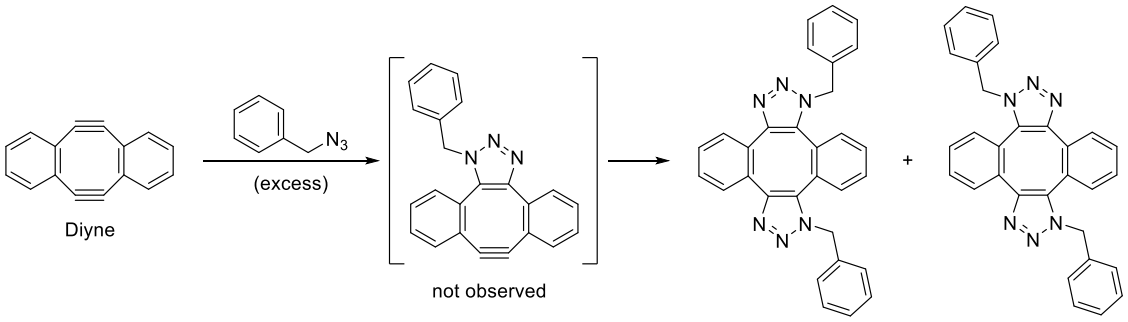

Scheme 3.1 Strain-promoted double-click reaction between benzyl azides and diyne.

Using this new reaction tool, cell surface labelling of HEK293 cells was attained. To achieve labelling, a three-step protocol was used. First, an azido-mannosamine was

incorporated into the membrane, followed by quick treatment with diyne and then labelling with an azide-tagged fluorophore.[8] This SPDC reaction has also found use in peptide stapling applications where it can increase peptide stability or activity,[7,9] and polymer chemistry.[10]

3.1.1 Strain-Promoted-Double Click Reactions with Nitrones

During the preparation of this work investigating the reaction of diyne and nitrones, an example of reactions with di-nitrones and diyne had been published by Zhang *et al.* which investigated SPDC reactions of diyne with diazo, syndone and nitrone monomers for use in polymer synthesis.[4] In this report, they found that with the second addition being faster than the first, it created a self-accelerating property to the reaction. By using this property and developing a novel kind of stoichiometric imbalance with the diyne in excess, high molecular weight (MW) (> 10^5 g/mol) polymers were prepared. The effect of the monomer ratio ($S = [Diyne]_0/[M]_0$) on the step-growth polymerization was evaluated and found that by increasing the monomer ratio from 0.91 to 1.1, higher MW polymers were observed, with polymerization complete in 30 minutes. Where the polymers formed from diazo and syndone groups showed high stability, polymers formed from nitrones, containing isoxazoline rings in the polymer backbone, demonstrated self-degradation behaviour.[4] Since the only difference between the nitrone polymer and the others was the heterocyclic ring formed, the degradation of this polymer was explained by the cleavage of the isoxazoline ring of the polymer backbone. The degradation of the

isoxazoline ring by the pathway shown in **Scheme 3.2** is mainly due the low thermochemical stability of the N-O bond associated with the π system.[11,12] Since this group only studied the polymer reaction using one nitrone, a C-phenyl-*N*-methyl nitrone, we hypothesized that alternate nitrones such as cyclic nitrones might produce more stable polymers.

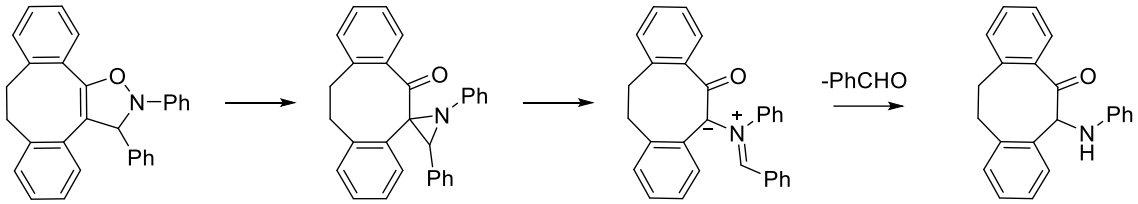

Scheme 3.2 Thermal decomposition of isoxazoline to the α-amino-ketone and benzaldehyde.

3.2 Objective

The objective was to expand on the utility of the SPANC reaction to include double-strain promoted alkyne-nitrone cycloadditions (D-SPANC) using *sym*-dibenzo- 1,5-cyclooctadiene-3,7-diyne (diyne). The kinetics of the cycloaddition between diyne and acyclic nitrones were analyzed and compared with reported data. Kinetic data will be used to develop reactions where the reactivity of diyne can be controlled based on nitrone selectivity. Guided by mechanistic investigation of these reactions shown herein, the utility of these reactions for applications in peptide crosslinking, modular connecting of biological molecules and polymer synthesis will be explored.

3.3 Results and Discussion

With little mechanistic information available about the structure-activity relationships of the SPDC reaction with nitrones and diyne,[4] we sought out to determine the effects of nitrone electronics on the reaction rate. Herein, the reaction kinetics were investigated between several acyclic nitrones bearing different α-carbon substituents. Monitoring kinetics using second-order conditions by NMR was attempted; however, due to peak overlap in the aromatic region, and the fact that only one proton would be changing significantly (**Scheme 3.3** in red), monitoring NMR changes in reaction over time was difficult. Kinetic scanning by UV-vis monitored all changes in reaction over time, allowed visualization of starting material and product peaks, and provided a more accurate method to measure both additions. The nitrone was used in excess as at least 2 equivalents of nitrone are needed form the di-product and having the nitrone in excess pushed the reaction to completion, providing a chance to monitor both additions simultaneously.

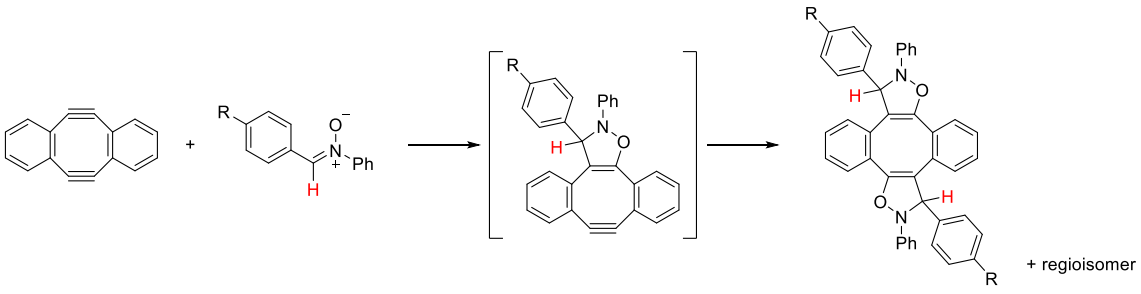

Scheme 3.3 Double strain-promoted alkyne-nitrone cycloaddition.

3.3.1 Kinetics Studies and Methodology

The rate measurements of cycloadditions of diyne with various nitrones were performed using UV-visible spectroscopy in methanol at 25 ± 0.1 °C in duplicate. Reactions were done under pseudo-first order conditions with the nitrone in 20 - 100-fold excess of the diyne and were monitored by following the increase of the absorbance at the characteristic wavelengths specified in **Table 3.1.** Note that due to spectral overlap and difficulties observing individual reactant peaks, the absorbance changes used for kinetic analyses are assumed to be those associated with the formation of the double-addition product.

Table 3.1 Reaction conditions and absorption wavelengths used to perform UV-Visible kinetic studies of cycloadditions between diyne and nitrones.

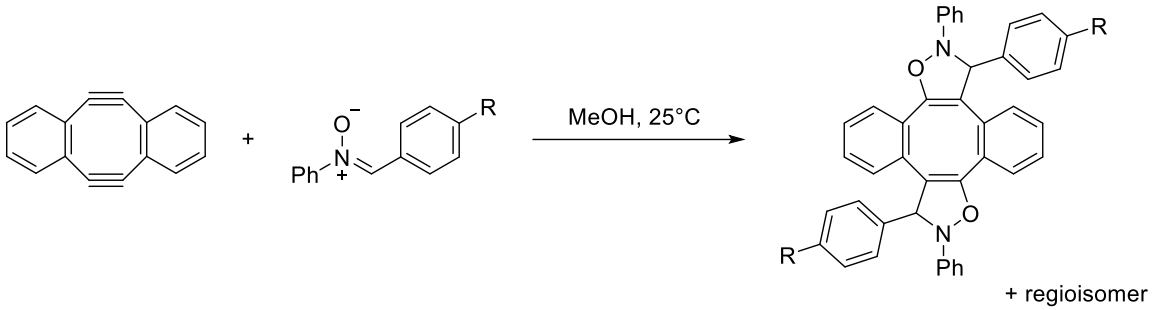

	Nitrone	Product Wavelength λ (nm)
3a	R= H	380
3b	R= p-OCH_3	402
3c	R= p-F	384
3d	R= p-Br	384
3e	R= p-CN	402
3f	R= p-NO_2	450

General procedure for the double cycloaddition kinetic studies.

A calculated amount of stock solution of nitrone (excess reagent) required to achieve the desired final concentration was diluted in a calculated amount of additional methanol in a cuvette. A calculated amount of stock solution of diyne required to achieve the desired final concentration was rapidly mixed with the thermally equilibrated solution and immediately inserted into the UV-vis spectrophotometer.

Absorption was measured at pre-set time intervals of 2 minutes until it reached a plateau at the wavelength chosen as shown in **Table 3.1**. Due to complexity of NMR spectra of the mixture of regio- and diastereomeric products in each reaction, mass spectrometry was used to confirm the formation of products.

Data analysis of pseudo-first order UV-Visible kinetic experiments.

Data analysis was done using rate laws and explicit equations provided by Dr. Jeffrey Keillor. To determine k_1 and k_2 the following rate laws and explicit equations used are outlined in **Table 3.2.**

Table 3.2 Rate laws and corresponding explicit equations used to determine kinetics of the SPDC reactions.

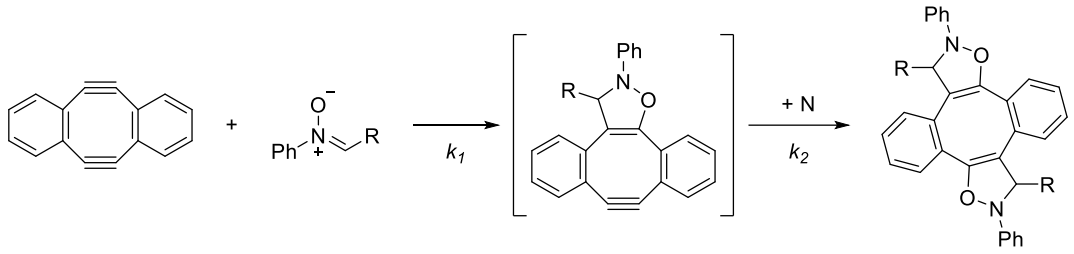

D N I P

Rate law	**Explicit Equation**
d[D]/dt= - k_1'[D]	[D]= $[D]_0$- $k1't$
d[N]/dt ≈ 0, where N >> D	[N] = $[N]_0$ - [I] - 2[P]
d[I]/dt = k_1'[D] – k_2'[I]	[I]= - k_1' $[D]_0$ / (k_2'- k_1') $(k1't-k2't)$
d[P]/dt = k_2'[I]	[P]= $[D]_0$ - [D] – [I]

Absorbances were first corrected by subtracting the lowest absorbance from all values. The corrected absorbances and the initial concentrations of nitrone (1-2.5 mM), diyne (25 μM), intermediate (0 μM) product (0 μM) were used with the above equations to predict concentrations for nitrone, diyne, intermediate and product throughout the reaction based on product absorbance. The curves of best fit to the data were determined by a least square fitting model. **Figure 3.5** shows a graph obtained from a consecutive first-order fitting of the reaction between nitrone **3a** at 1000 μM and 25 μM diyne. Given that this is a consecutive pseudo-first order fitting, a few assumptions were made: 1) the concentrations of the intermediate (**I**) and product (**P**) at time 0 seconds were 0 μM, and 2) since the equations could not

determine which reaction was faster, it was assumed that the smaller rate constant corresponded to the first addition, based off data from azide-diyne reactions that k_2 was faster than k_1.[8]

The observed rate constants for the slow and fast reactions (k_1' and k_2') were then plotted against the corresponding excess reagent concentrations. The slope of the linear trend line fitted to the data points represents the second-order rate constant (k_1 and k_2) for each of the cycloadditions. **Table 3.3** and **Figure 3.1** are shown below as examples, the data for each nitrone is shown in the appendix.

Table 3.3 Observed rate constants for the consecutive pseudo-first-order kinetic studies of cycloaddition reactions of nitrone **3a** with diyne, correlated to tested concentrations of nitrone in methanol.

Nitrone	Concentration of Nitrone (10^{-3} M)	k_1' (10^{-4} s^{-1})	k_2' (10^{-4} s^{-1})
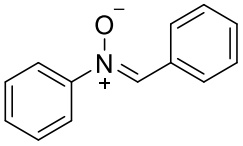	1.00	3.44 ± 0.02	8.52 ± 0.74
	1.25	4.05 ± 0.45	9.04 ± 0.03
	1.50	4.37 ± 0.15	10.4 ± 0.92
	2.00	5.18 ± 0.08	12.5 ± 1.95

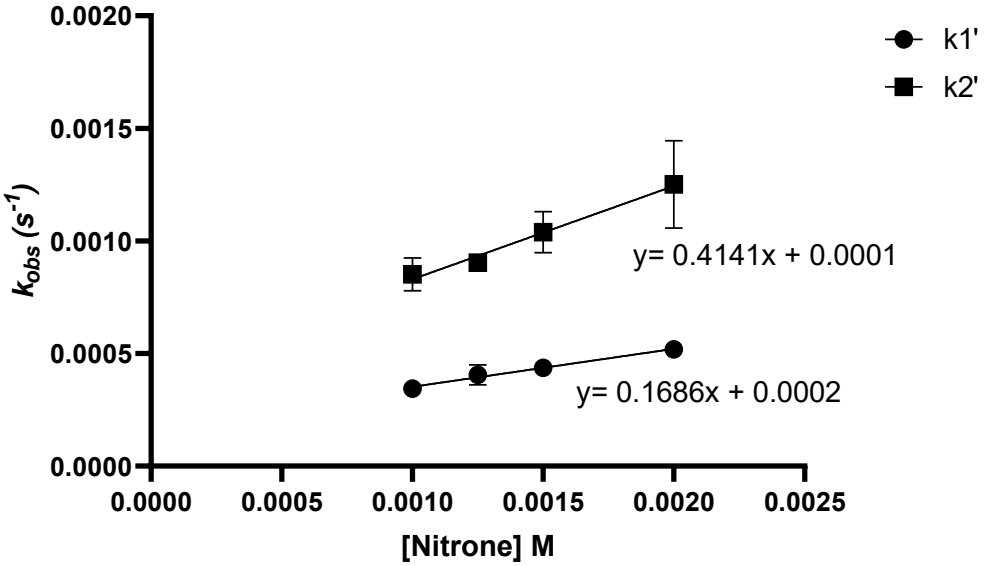

Figure 3.1 Pseudo-first order rate constants (k_1 and k_2) of C-*N*-diphenylnitrone with diyne cycloadditions. Determined by plotting the k_{obs} (s^{-1}) of each cycloaddition against concentration of nitrone used (M). Error bars represent the difference of the replicate reactions. R^2 (k_1') = 0.92, R^2 (k_2') = 0.77.

3.3.2 Cycloadditions of Diyne with Acyclic itrones

Based on the assumptions mentioned above ($k_2 > k_1$, and [I]=0, [P]=0) and equations in **Table 3.2,** a graph demonstrating the apparent reaction flux over time (s) of the reaction between 1000 μM **3a** and 25 μM diyne was simulated in **Figure 3.2**. Using this model, it is predicted that the concentration of the mono-intermediate (I) would reach a maximum at about 1700 seconds, reaching a peak of only 20% the initial concentration of diyne (D), at which point the concentration of di-product (P) is exponentially increasing. If the reaction followed this pathway, it is likely that observing the mono-intermediate would be difficult. If, however, $k_2 < k_1$, as shown in **Figure 3.3**, a build-up of mono-intermediate (I) to approximately 50% the concentration of initial diyne (D) would be expected at about 1000 seconds after reaction began. Importantly, in this case, di-product (P) would only account for 20% of the products, indicating that the mono-intermediate would more easily be observed. Before investigating the reaction pathways further by mass spectroscopy, comparison of the second order rate constants calculated using this method were compared to the literature.

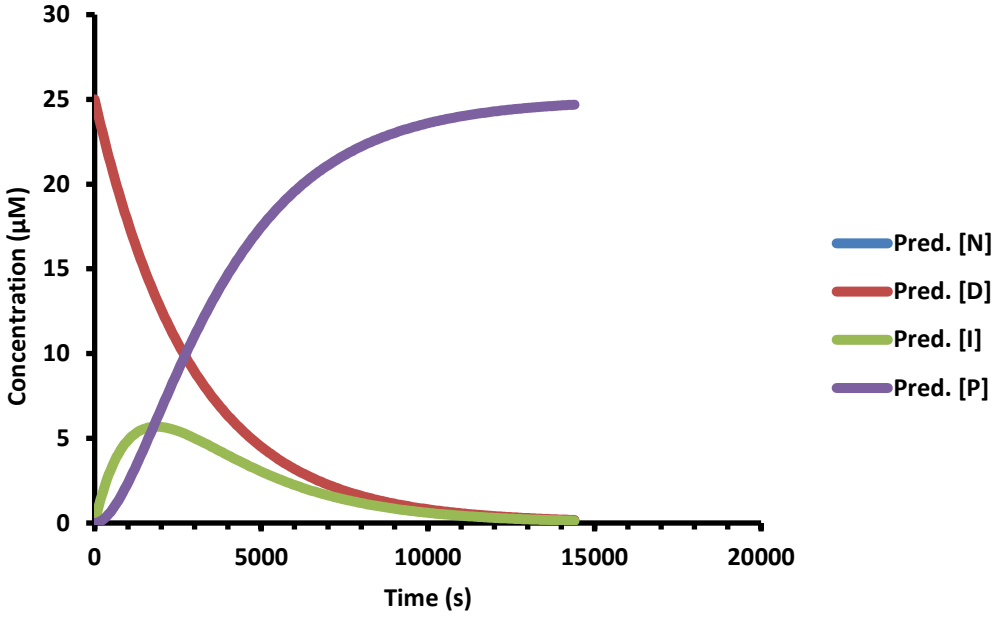

Figure 3.2 Predicted reaction flux of 1000 μM C-*N*-diphenylnitrone with 25 μM diyne based on explicit equations in Table 3.2, assuming $k_1' < k_2'$.

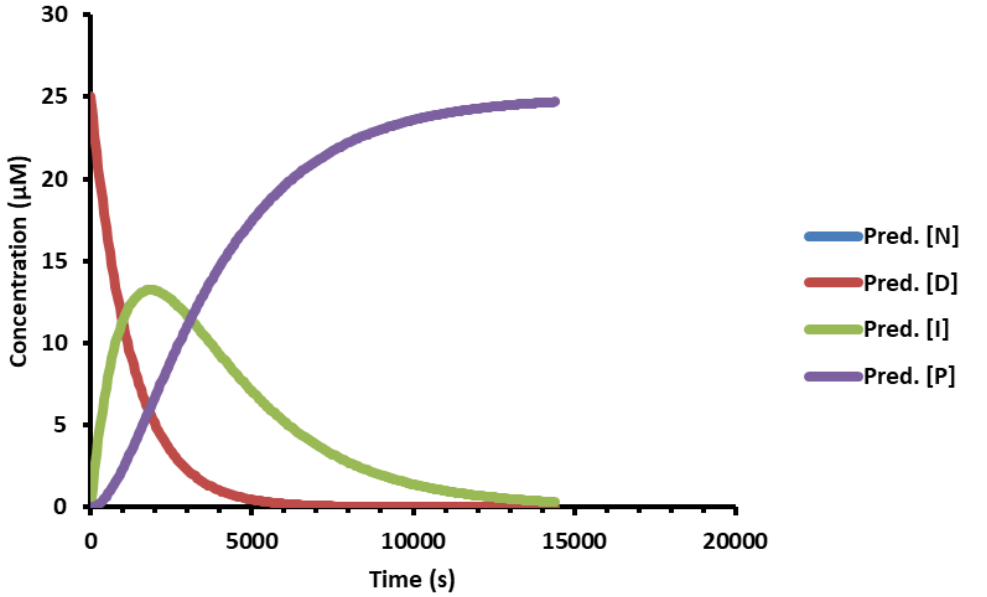

Figure 3.3 Predicted reaction flux of 1000 μM C-*N*-diphenylnitrone with 25 μM diyne based on explicit equations in Table 3.2, assuming $k_2' < k_1'$.

Table 3.4 Kinetic evaluation of cycloaddition reactions of diyne with acyclic nitrones.

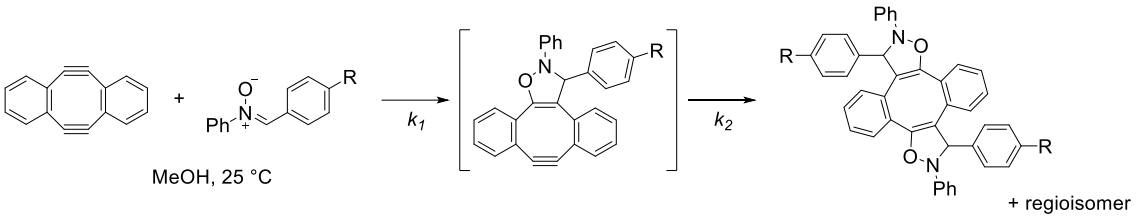

Nitrone		k_1 (M^{-1} s^{-1})	k_2 (M^{-1} s^{-1})	Rate constant ratio ($r = k_2/k_1$)
3a	R= H	0.17 ± 0.02	0.41 ± 0.09	2.41
3b	R= OCH_3	0.09 ± 0.01	0.07± 0.04	0.78
3c	R= F	0.19 ± 0.02	0.47 ± 0.06	2.47
3d	R= Br	0.17 ± 0.02	0.53 ± 0.10	2.94
3e	R= CN	0.20 ± 0.01	7.16 ± 0.13	35.8

In the investigation into the kinetics of the reaction between diyne and nitrones, two interesting trends were observed (**Table 3.4**). First, there exists a general difference in reaction rate between the first (k_1) and the second (k_2) addition. Second, there is a trend of increasing rate of the second addition with increasing the electron withdrawing character of the nitrone substituent. The first trend is not surprising, as it has also been observed with the reactions of diyne and other 1,3 dipoles.[4,8] Moreover, in a recent report which investigated the reaction of α-phenyl-*N*-methylnitrones with diyne, a rate constant ratio ($r = k_2/k_1$) of 230 was calculated, with

a second order rate constant for the first addition (k_1) = 1.14×10^{-1} $M^{-1}s^{-1}$. Although this second order rate constant mirrors our reports where the average k_1 of reaction with diphenyl nitrones was ~1.64×10^{-1} $M^{-1}s^{-1}$, our calculated rate constant ratios (r) are significantly smaller (**Table 3.4**).[8]

In both cases, the mono-intermediate was neither isolated nor observed (more on this below), which suggests that the second addition is in fact faster than the first addition. However, looking at **Figure 3.2** and **Figure 3.3** the formation of the di-product experiences a small lag phase before rising exponentially; a trend observed with typical consecutive first-order reactions,[13] and should not be treated as a simple first-order reaction. This lag phase was observed for all reactions except those where $k_2 >>> k_1$, for example with the p-CN **(Table 3.4)** and p-NO_2 (data not shown). Therefore, in the cases of reactions where $k_2 >>> k_1$, it is more likely that the mono-intermediate would not be observed, and the reaction proceeds more like a simple first-order reaction (not-consecutive). Potentially, in the cases where reaction rates have similar second order rate constants, such as the case with nitrone **3b**, the mono-intermediate could be observed. To investigate these trends further, mass spectroscopy is required (**Section 3.3.4**).

The second trend observed from these reactions is that with increasing the electron withdrawing character of the nitrone substituent, increases in the rate of the second

addition was also observed, with no significant impact on the first addition. This trend was further analyzed by construction of Hammett plots.

3.3.3 Structure-Activity Relationships

Hammett plots report on the sensitivity of the reaction to substituent effects, as explained in chapter 2. To investigate these effects over the course of the reaction, a Hammett plot for each addition reaction was constructed (**Figure 3.4 and Figure 3.5**). The line of best fit for each addition was achieved with σ_p parameters, allowing for reaction comparison to the ρ values of previously studied SPANC reactions. Hammett ρ values of 0.28 and 2.08 were observed for the first and second additions, respectively.

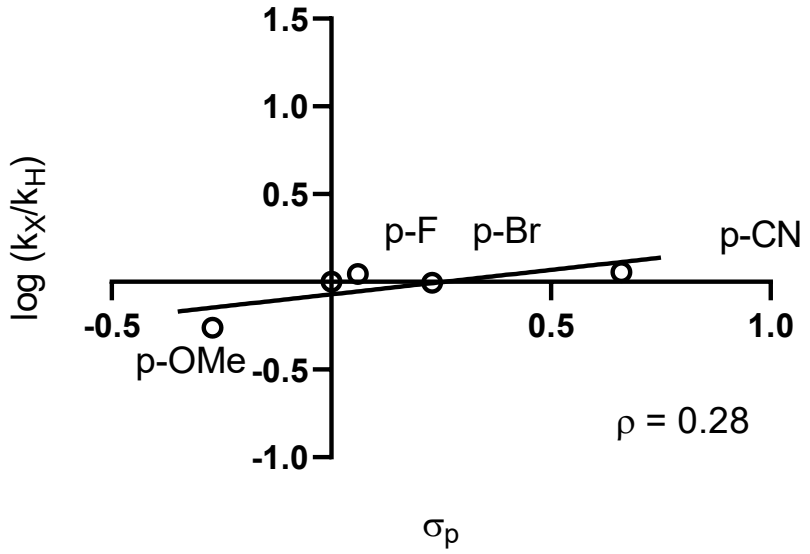

Figure 3.4 Hammett plot depicting the substituent effects on the first (*k1)* cycloaddition of acyclic nitrones **3a-e** with diyne. R^2= 0.54.

The first addition was expected to follow suit with other SPANC reactions, and in general, the rates are on par with that of DIBO *(k_2* = 0.13 ± 0.01 $M^{-1}s^{-1}$), as expected through their structural and electronic similarities. Since a Hammett plot was not constructed for reactions using DIBO, BARAC was used as a comparison model since DIBO and BARAC are both electron-deficient alkynes, with high levels of conjugation and delocalized electron density. A ρ value of 0.28 for the first addition mirrors what was observed between BARAC with nitrones with a determined ρ value of 0.25 (shown in chapter 2 **Table 2.6**). This low value indicates that the first addition is not very sensitive to electronic changes on the nitrone substituent, though it is slightly accelerated by electron-withdrawing groups. Additionally, similar to the reaction mechanism of BARAC, there is little to no buildup of electron density during the transition state, consistent with a concerted reaction mechanism (**Scheme 3.4**).

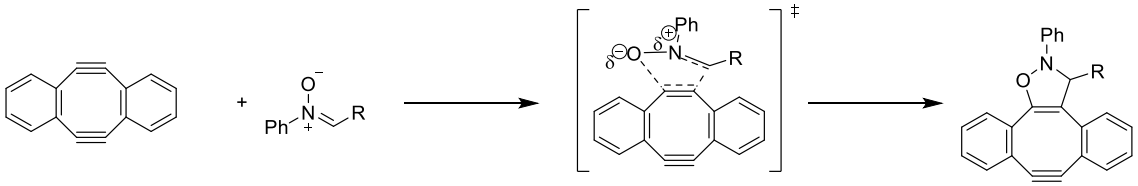

Scheme 3.4 First addition of nitrone to diyne, showing the likely transition state indicated by a ρ value of 0.28.

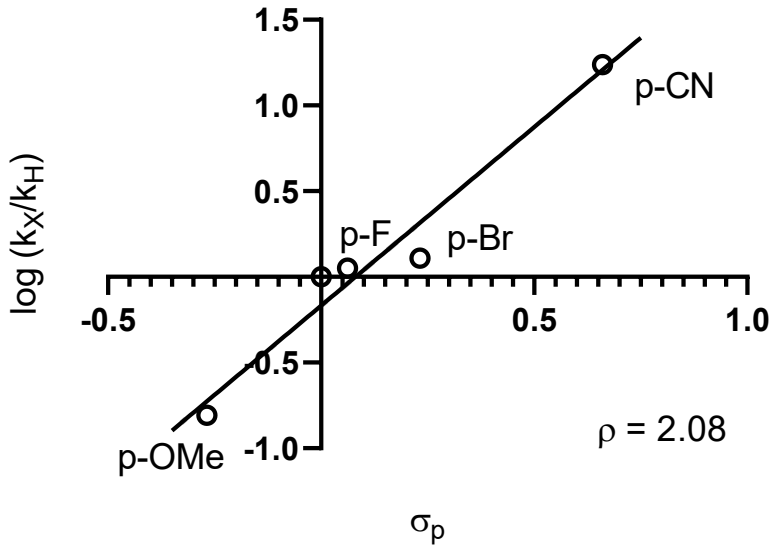

Figure 3.5 Hammett plot depicting the substituent effects on the second (*k2)* cycloaddition of acyclic nitrones **3a-e** with diyne. R^2=0.96.

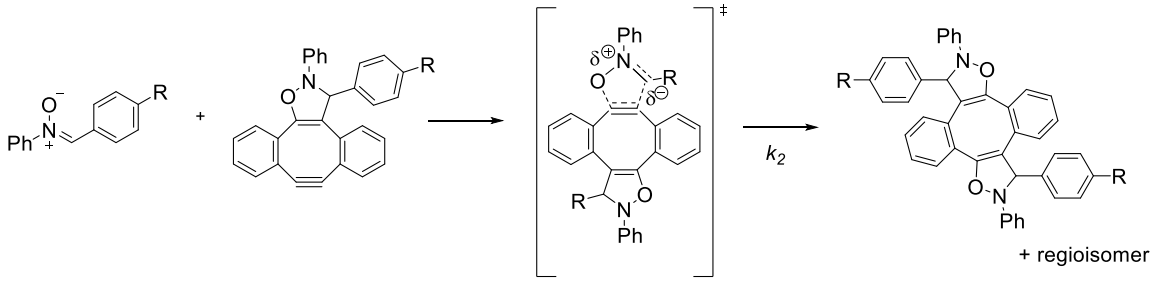

Scheme 3.5 Second addition of nitrone to diyne, showing the likely transition state indicated by a ρ value of 2.08.

Comparatively, a high ρ value of 2.08 indicates that the second addition is more sensitive to electronic changes on the nitrone, suggesting a significant build-up of electron density during the transition state, as observed with BCN (1.30) and TCO (1.48) shown in **Scheme 3.5**. In the case with BCN, the increased sensitivity was

explained as a result of the higher LUMO energy and increased electron density of the alkyne of BCN. Similarly, in the report with azide-diyne reaction, Kohn-Sham orbital amplitude plots from the HOMO and LUMO of transition structures show that the orbital coefficients of the monoyne intermediate (LUMO) are localized at the alkyne carbons, a possible explanation for the increased sensitivity.[8]

However, given that this value is significantly higher than others for nitrone-cycloadditions, it is possible that the accumulation of charge could be in the form of an intermediate forming during the second addition. To properly understand the difference in electronic sensitivity between the first and second addition, computational studies of the transition states and structure of the intermediate are currently being investigated.

3.3.4 Reaction Progression via Mass Spectroscopy

To further investigate the reaction progression, mass spectroscopy was used to visualize the formation and disappearance of mass ions of the reactants and products. A TOF mass spectrophotometer was used allowing the separation of the lower molecular weight ions (starting materials) from the mid-MW ions (mono-intermediate) and the high-MW ions (di-products).

General procedure for the double cycloaddition mass spectroscopy studies.

Both nitrone and diyne were pre-dissolved in 5.0 mL of acetonitrile (~200 μM) and mixed at equimolar concentrations of 100 μM at room temperature in a vial, then the reaction was taken up with a 5 mL syringe and continuously injected via syringe pump directly into the Synapt Mass Spectrometer at a rate of 50 μL/min for about 60-70 minutes. A summary of 50 scans of peak intensity were taken of the masses of both the product and the nitrone at time points over the course of the reaction and plotted as a function of time (s). Data is of one trial.

Data analysis of mass spectroscopy studies

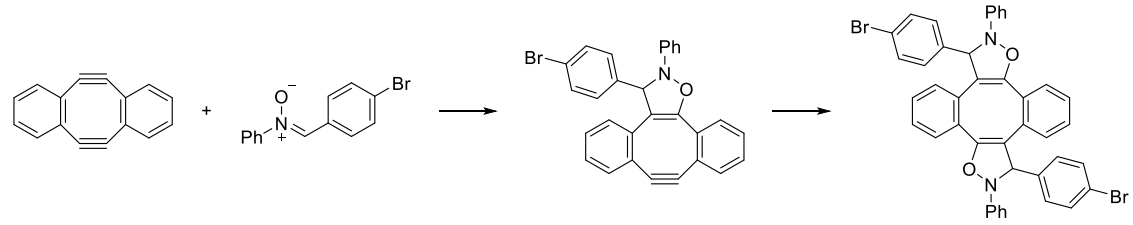

a

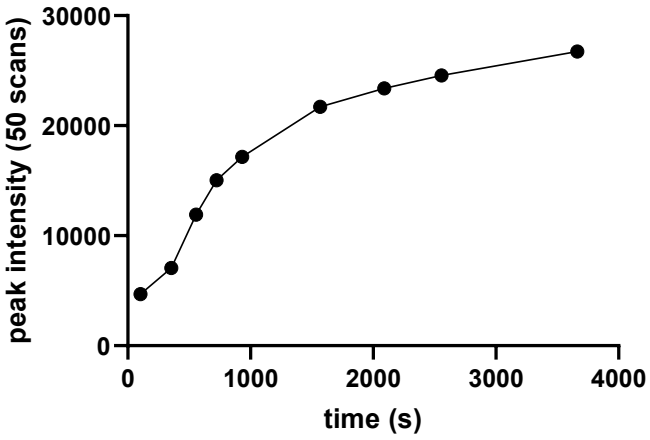

b

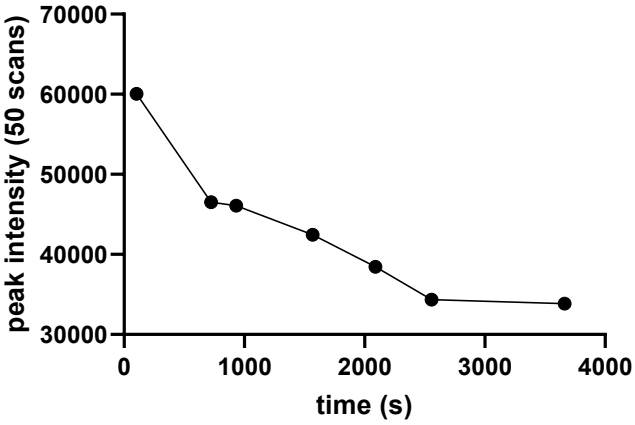

Figure 3.4 Graph of the peak intensities (50 scans) representing a) product $(M+H)^+$ = 750, 751 $(M+Na)^+$ = 775, 777 and b) nitrone peak $(M+H)^+$ = 276, 278, $(M+Na)^+$= 298, 300 over the course of the reaction in (s).

C-(4-bromophenyl)-*N*-phenylnitrone was chosen as the model nitrone as its isotopes make it easy to identify by mass spectroscopy, especially with the known difficulties in observing the mono-intermediate. Only the disappearance of the nitrone and formation of the product were followed as the ionization of diyne was not achieved. The appearance of product follows the disappearance of nitrone, showing similar changes in intensity: 22 050 and 26 208, respectively. Over the course of the reaction, the mono-intermediate was not accurately observed, further confirming that the second addition of nitrone to diyne is significantly faster than the first.

Further mass spectroscopy studies are needed to investigate the kinetics of reaction. To accurately measure appearance and disappearance of products and reactants, the reaction double addition product must be isolated and properly characterized (^{1}H NMR, ^{13}C NMR, mass spectroscopy, UV-vis). The dibromo-product would be ideal, as it is significantly heavier than many of the other D-SPANC products, so it will not interfere with quantitation. Additionally, separation by liquid chromatography prior to mass spectroscopy (LC-MS) would allow better peak resolution which may resolve the mono-intermediate more readily.

Additional mass spectroscopy experiments of more nitrones will be conducted to confirm the rate constants calculated. To further investigate the rate constants and ρ values, a competitive reaction using two nitrones with vastly different rate constants: **3b** (k_1 = 0.09 $M^{-1}s^{-1}$, k_2 = 0.07 $M^{-1}s^{-1}$) and **3e** (k_1 = 0.20 $M^{-1}s^{-1}$, k_2 = 7.16 $M^{-1}s^{-}$

[1]) can be used to confirm the rate constants calculated. Since both have relatively similar k_1 but very different k_2, we would only expect to see the mass of two products: the mixed di-product, where the first addition occurred by **3b** and the second addition by **3e**, and the second product where both additions were by nitrone **3e**. The ratio of products could be used to confirm the ratio of rate constants.

3.4 D-SPANC Polymer Synthesis Outline

There has been a great rise in the use of bioorthogonal reactions for polymer synthesis; however, the presence of nitrones in these reactions is lacking. In a recent report, the authors noted that the polymers synthesized from SPANC chemistry began to degrade at higher concentrations and at higher temperatures.[4] To further investigate the potential of nitrones in polymerization reactions, we hypothesized that di-aryl nitrones (**3a-3e)** or cyclic nitrones would produce more stable products towards thermal decomposition, as opposed to the C-phenyl-*N*-methylnitrones used in their study. Examples of the predicted D-SPANC polymers are shown in **Scheme 3.6**.

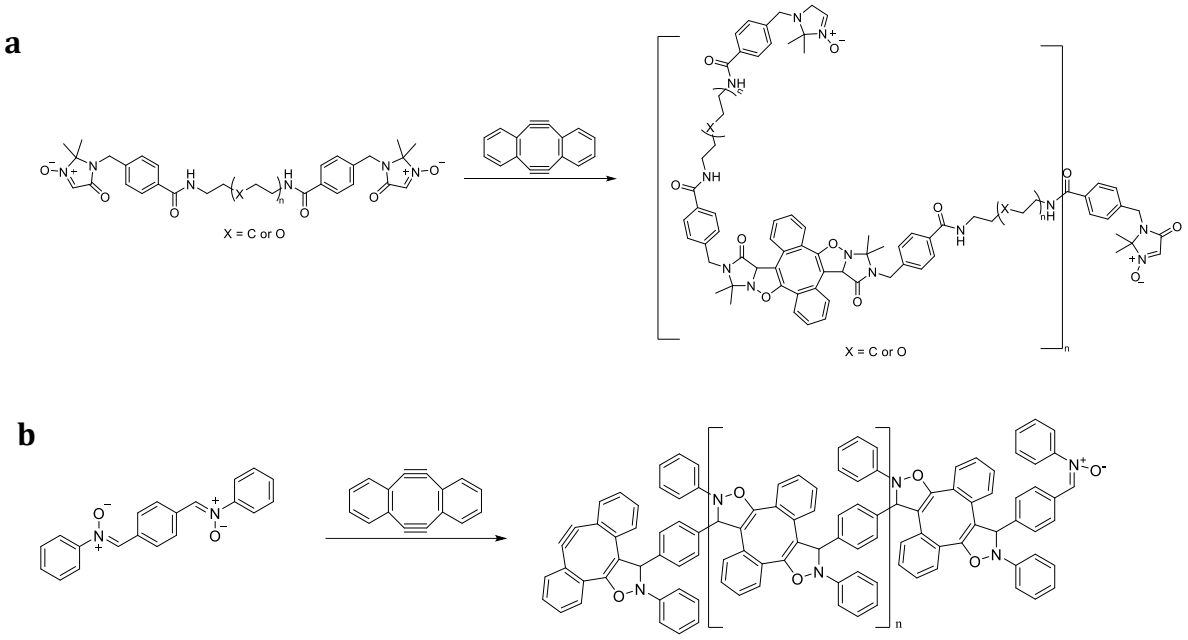

Scheme 3.6 Predicted polymer products from reaction of diyne with a) cyclic and b) acyclic nitrone-monomers.

Since kinetics with acyclic nitrones showed that electron deficient nitrones react significantly faster than electron-rich nitrones, DMImO, an electron deficient cyclic nitrone, was chosen as the nitrone for exploration of polymer synthesis (**Scheme 3.6a**). Depending on solubility, two different linkers will be explored of varying length: straight aliphatic ones (X=C) and polyethylenelglycol (PEG)-based linkers (X=O) shown in **Scheme 3.6a**. These di-DMImO monomers are expected to be easily synthesized via HATU coupling with diamines to form amide linkages (**Scheme 3.7a**). For the di-aryl nitrone-based monomers, the simplest linker; a benzyl group was chosen, as the di-nitrone is easily synthesized via a condensation reaction with hydroxylamine, as previously reported (**Scheme 3.7b**).[14]

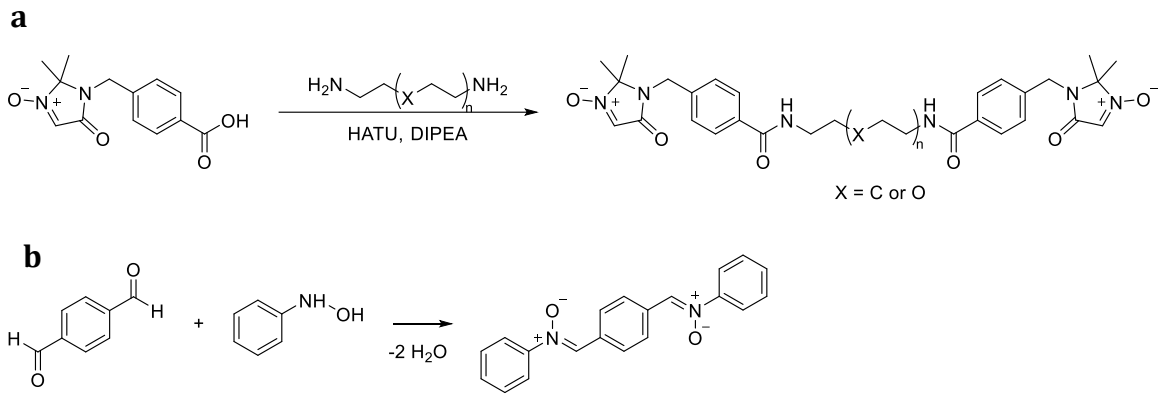

Scheme 3.7 Proposed synthesis of the di-nitrone monomers.

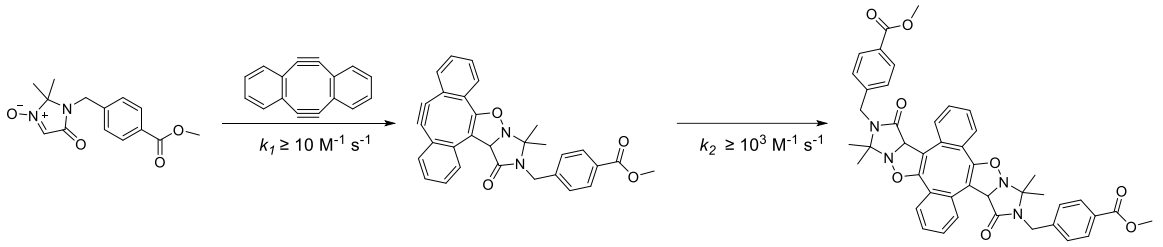

Scheme 3.8 SPDC of DMImO with diyne and calculated second order rate constants for each addition reaction.

Second order rate constants (k_1 *a*nd k_2) for the SPDC reaction of DMImO and diyne (**Scheme 3.8**) were determined via pseudo first-order kinetics using methods described in **Section 3.3.1**. Due to issues obtaining satisfactory k_2, the second order rate constant for the first addition, k_1, was calculated using one-phase association model using GraphPad Prism 8.3.1. k_1 was determined to be ~0.08 M^{-1} s^{-1} and k_2 was determined to be larger than 10^3 $M^{-1}s^{-1}$. However, it is important to note that there was great error in this calculation between replicates, indicating that this reaction needs to be monitored under more precise and slower conditions. Given these

findings, we suggest that the second order rate constant for the first addition is actually larger than 10 $M^{-1}s^{-1}$, estimated from the rate constant observed between DMImO and BARAC of 40 $M^{-1}s^{-1}$.[15]

The large k_2 for the second addition is presumably a result of the extra strain induced by the cyclic nitrone upon first addition. Recalling the first reports of the reaction with diyne and azides, the mono-intermediate was expected to have a highly distorted alkyne bond which arose from steric repulsion between the substituent on the triazole ring and the hydrogen atom on the benzene ring.[8] With DMImO, two new rings are added to the diyne- inducing a much greater amount of distortion upon the unreacted alkyne. Prior to beginning the polymerization reactions, the product in **Scheme 3.8** must be isolated and fully characterized to later allow for proper characterization of linked polymers.

Polymer reactions will be done to optimize polymer synthesis and compare to previous SPDC-polymers. Polymers bearing different MWs are expected to be observed by changing the ratios of monomers, similar to what has been reported.[4] Confirmation of polymer growth will be achieved by gel permeation curve (GPC) and size exclusion chromatography (SEC). Moreover, to compare the thermal stability of the di-aryl nitrone and the cyclic nitrone polymers, GPC curves of fresh and heated polymers will be compared to determine whether the polymer has degraded with exposure to heat.

3.5 Future Directions

Future work will begin with computational studies of the reaction between nitrones and diyne to look at the transition states of each addition to confirm that the activation energy required for the second addition is smaller than the first, further confirming the results herein that show that the second addition is faster. Computational work will also aid in teasing out the mechanism of additions and explain the large difference in Hammett values calculated for each addition with electronically different nitrones. Moreover, computational work of the transition state of the mono-intermediate with cyclic nitrones would test the assumption that the presence of two heterocycles onto the diyne distorts the mono-yne significantly so that the second addition proceeds with a second order rate constant > 10^3 $M^{-1}s^{-1}$.

Initial mass spectroscopy experiments showed in **Section 3.3.4** will be repeated in duplicate with nitrone **3b, 3d** and **3e** to properly ascribe rate constants and to determine if the assumption $k_2 > k_1$ remains true for all nitrones. With this data, experiments will be developed to control nitrone-addition onto the diyne. The ability to control addition would be useful for polymerization applications and cell-surface labelling.

Work described in **Section 3.4** will expand on the use of nitrones in polymerization reactions, with aims of designing a more stable polymer reaction.

3.6 Conclusions

In conclusion, we have established the second order rate constants for the consecutive additions of a variety of nitrones onto diyne and studied the structure-activity relationships via Hammett plots. Results show that the addition of the second nitrone to the mono-intermediate occurs significantly faster than the first, however, not as fast as previously reported.[4] The rate of second addition increases with electron deficient nitrones, as demonstrated by a large ρ value of 2.08, suggesting that the reaction rate can be controlled by nitrone selectivity. Using the kinetic analysis results, di-nitrone monomers containing cyclic and diaryl-nitrones will be designed for use in polymer applications. A polymer formed from a cyclic nitrone is expected to be more stable than polymers previously formed by acyclic nitrones.

3.7 Materials and Experimental Details

All reagents, solvents and equipment utilized are described in Chapter 2 **Section 2.5**. All nitrones (**3a-e**) were prepared as described in chapter 2. Diyne was purchased from VWR chemicals.

Kinetic studies procedure

All kinetic experiments were conducted following the general method outlined, varying the concentration and wavelength chosen according to the values found in **Table 3.1**. The concentrations of nitrones used can be found in **Appendix B**.

Stock solutions of diyne and nitrone were prepared as 5 mM stocks in screw cap vials in OptimaGrade Methanol and stored at -20 °C. Diyne was then diluted down to 1 mM in methanol and covered with aluminum foil. The cuvettes used were 1.5 mL Quartz screw cap (10mm pathlength). Before preparation of each reaction, UV-vis cuvettes were cleaned with acetone 4 times and let dry for 20 minutes. Cuvettes were wiped with Kimwipes prior to reading to remove any residue on the outer surface.

Prior to reactions, the UV-vis spectrophotometer was blanked with a 1 mL of methanol. Next, reactions were set up with addition of methanol and nitrone (**Table 3.5**), followed by quick addition of diyne, mixing of the reaction by inverting the cuvette and immediate insertion for wavelength reading.

In order to choose a wavelength for product monitoring, the following spectra (200 nm to 800 nm) were obtained over the entire reaction period:

- Solvent only as baseline
- Diyne (25 μM)
- Nitrone (1000- 2500 μM)
- Reaction mixture containing 25 μM Diyne, 500-2500 μM Nitrone and remaining amount of methanol according to the volumes shown in **Table 3.5**.

Table 3.5 Volume of stock solutions used for the pseudo-first order kinetics of acyclic nitrones with diyne.

Reaction	Vol. of 1 mM Diyne stock (μL)	Vol. of 5mM nitrone stock (μL)	Vol. of methanol (μL)	Total Volume of reaction (μL)
25 μM Diyne 500 μM Nitrone	25	100	875	1000
25 μM Diyne 1000 μM Nitrone	25	200	775	1000
25 μM Diyne 1500 μM Nitrone	25	300	675	1000
25 μM Diyne 2000 μM Nitrone	25	400	575	1000
25 μM Diyne 2500 μM Nitrone	25	500	475	1000

Once reaction was complete, indicated by a plateau at the indicted wavelength, the highest point of the peak was chosen as the wavelength to use to kinetic calculations. The absorbances at the wavelength chosen over the course of the reaction (in seconds) were then input into an excel spreadsheet designed by Dr. Jeffrey Keillor. Using a least square fitting model of consecutive first-order reactions, a line of best fit based off predicted absorbance over time in seconds was used to determine k_1' and k_2'. An example of this fitting is shown in **Figure 3.5** of the reaction between 1000 μM C-*N*-diphenylnitrone with 25 μM Diyne.

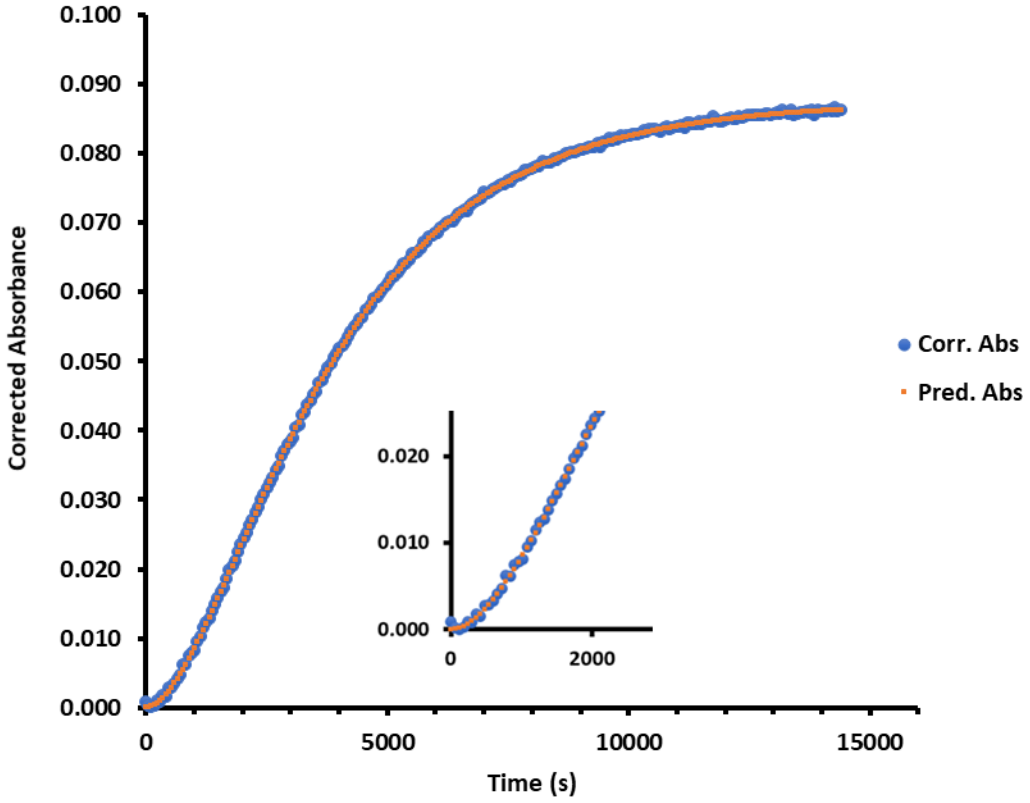

Figure 3.5 Sequential first order fitting by least squares fitting model of the reaction between 1000 μM C-*N*-diphenylnitrone with 25 μM Diyne, with the corrected and predicted Abs. First 2000s zoomed in to highlight lag period.

Mass Spectroscopy Procedure

Mass Spectroscopy was performed at the University of Ottawa John L. Holmes Mass Spectroscopy Facility in assistance with Dr. Sharon Curtis. Waters Synapt High Definition Mass Spectrophotometer with TriWave which uses quadrapole time-of-flight mass spectrometry was used with positive electrospray ionization (ESI^+).

First, two stocks of Diyne (5mM) and nitrone (5mM) were prepared in OptimaGrade ACN and filtered through 0.2 μm nylon syringe filters. 400 μl of each stock was then diluted to 200 μM in a 9.6 mL of ACN. The reagents were mixed in an equimolar ratio (100 μM), taken up with a 5mL glass syringe and injected via syringe pump into the mass spectrometer.

Molecular ions representing the C-(4-bromophenyl)-*N*-phenylnitrone and the di-product were tracked over the course of the reaction, with 50 scan summaries of intensities from each chromatogram taken over the period of the reaction, as shown in **Appendix C**.

References

1. Iwakura, Y., Uno, K., Hong, S.-J. & Hongu, T. A Novel Synthesis of Polyisoxazoline and Polyisoxazole, The Reaction of Terephthalohydroxamoyl Chloride with Bisdipolarophiles. *Polym. J.* **2**, 36–42 (1971).

2. Overberger, C. G. & Fujimoto, S. Polycycloaddition of terephthalonitrile oxide. *J. Polym. Sci. Part C Polym. Symp.* **16**, 4161–4168 (1967).

3. Stille, J. K. & Bedford, M. A. Polymers from 1,3-dipole addition reactions: The sydnone dipole. *J. Polym. Sci.* **6**, 2331–2342 (1968).

4. Liu, X., Xiang, L., Li, J., Wu, Y. & Zhang, K. Stoichiometric imbalance-promoted step-growth polymerization based on self-Accelerating 1,3-dipolar cycloaddition click reactions. *Polym. Chem.* **11**, 125–134 (2019).

5. McNelles, S. A., Pantaleo, J. L., Meichsner, E. & Adronov, A. Strain-Promoted Azide-Alkyne Cycloaddition-Mediated Step-Growth Polymerization. *Macromolecules.* **52**, 7183–7187 (2019).

6. Orita, A., Hasegawa, D., Nakano, T. & Otera, J. Double elimination protocol for synthesis of 5,6,11,12-tetradehydrodibenzo[a,e]cyclooctene. *Chem. A Eur. J.* **8**, 2000–2004 (2002).

7. Sharma, K. *et al.* Water-soluble, stable and azide-reactive strained dialkynes for biocompatible double strain-promoted click chemistry. *Org. Biomol. Chem.* **17**, 8014–8018 (2019).

8. Kii, I. *et al.* Strain-promoted double-click reaction for chemical modification of azido-biomolecules. *Org. Biomol. Chem.* **8**, 4051–4055 (2010).

9. Lau, Y. H. *et al.* Double Strain-Promoted Macrocyclization for the Rapid Selection of Cell-Active Stapled Peptides. *Angew. Chem. Int. Ed.* **54**, 15410–15413 (2015).

10. Sun, P., Chen, J., Liu, J. & Zhang, K. Self-Accelerating Click Reaction for Cyclic Polymer. *Macromolecules.* **50**, 1463–1472 (2017).

11. Baldwin, J. E., Pudussery, R. G., Qureshi, A. K. & Sklarz, B. Valence Rearrangement of Hetero Systems. The 4-Isoxazolines. *J. Am. Chem. Soc.* **90**, 5325–5326 (1968).

12. Pinhoe Melo, T. M. V. D. 4-Isoxazolines: Scaffolds for organic synthesis. *European J. Org. Chem.* 3363–3376 (2010).

13. Erdoğdu, F. & Şahmurat, F. Mathematical fundamentals to determine the kinetic constants of first-order consecutive reactions. *J. Food Process Eng.* **30**, 407–420 (2007).

14. Heaney, F., Rooney, O., Cunningham, D. & McArdle, P. Simultaneous double 1,3-dipolar cycloaddition reactions involving bisnitrones or bisdipolarophiles. 1H NMR investigation of the conformational preferences of N-methyl- and N-phenyl-isoxazolidines. *J. Chem. Soc. Perkin Trans. 2* 373–378 (2001).

15. McKay, C. S., Chigrinova, M., Blake, J. A. & Pezacki, J. P. Kinetics studies of rapid strain-promoted [3 + 2]-cycloadditions of nitrones with biaryl-aza-cyclooctynone. *Org. Biomol. Chem.* **10**, 3066–3070 (2012).

Appendix A

Kinetic Analysis for Chapter 2

UV-Vis pseudo first-order kinetic analysis

Table S1. Observed rate constants for the kinetic studies of cycloadditions of s-TCO with **2a** C-*N*-phenylnitrone correlated to the various concentrations of s-TCO in methanol.

Nitrone	Concentration of TCO (10^{-4} M)	k_{obs} (10^{-6} s^{-1})
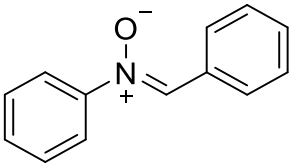	2.00	1.70 ± 0.39
	3.00	1.65 ± 0.78
	4.00	3.83 ± 0.32
	5.00	4.72 ± 0.07

All reactions were done in Methanol at 25 °C

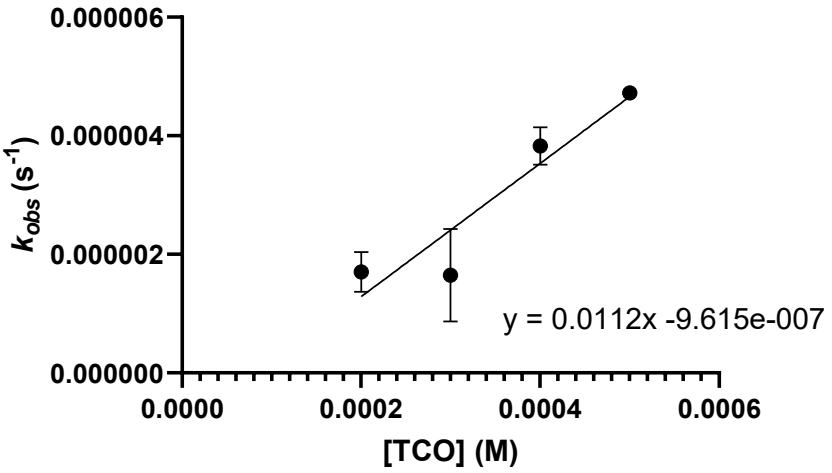

Figure S1. Pseudo first-order rate constants of cycloadditions of **2a** C,*N*-diphenylnitrone with s-TCO plotted against the tested concentrations of s-TCO. Error bars represent the difference of the replicate reactions. R^2= 0.83.

Table S2. Observed rate constants for the kinetic studies of cycloadditions of s-TCO with **2c** C-(4-fluorophenyl)-*N*-phenylnitrone correlated to the tested concentrations of s-TCO in methanol.

Nitrone	Concentration of TCO (10^{-4} M)	k_{obs} (10^{-6} s^{-1})
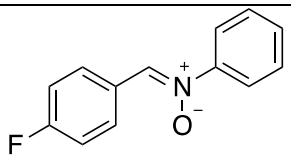	2.00	3.00 ± 1.09
	3.00	5.57 ± 0.01
	4.00	7.10 ± 0.00
	5.00	8.46 ± 1.23

All reactions were done in Methanol at 25 °C

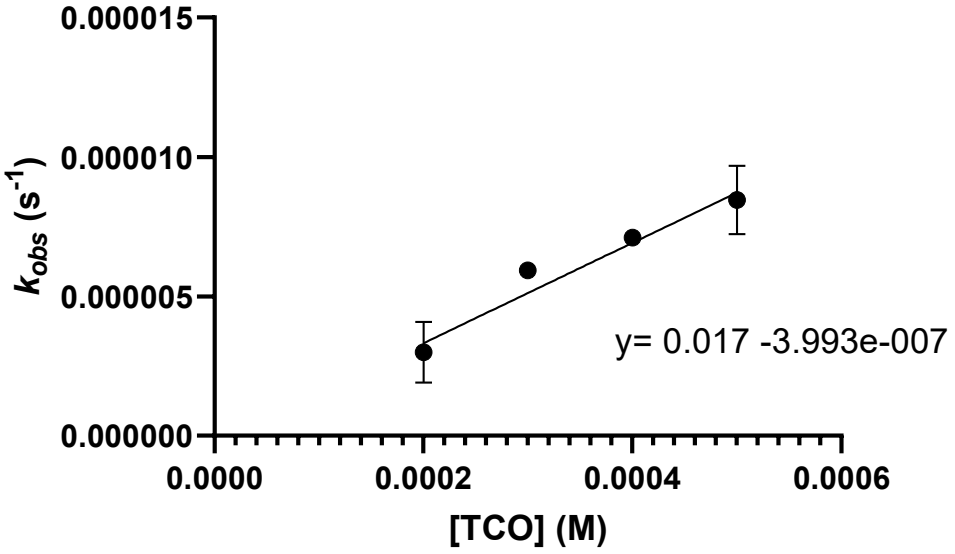

Figure S2. Pseudo first-order rate constants of cycloadditions of **2c** C-(4-fluorophenyl)-*N*-phenylnitrone with s-TCO plotted against the tested concentrations of s-TCO. Error bars represent the difference of the replicate reactions. R^2= 0.89.

Table S3. Observed rate constants for the kinetic studies of cycloadditions of s-TCO with **2d** C-(4-bromophenyl)-*N*-phenylnitrone correlated to the tested concentrations of s-TCO in methanol.

Nitrone	Concentration of TCO (10^{-4} M)	k_{obs} (10^{-5} s^{-1})
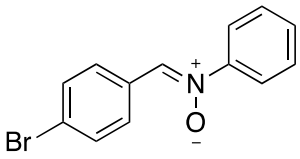	2.00	1.14 ± 0.05
	3.00	1.57 ± 0.08
	4.00	1.82 ± 0.11
	5.00	2.10 ± 0.08

All reactions were done in Methanol at 25 °C

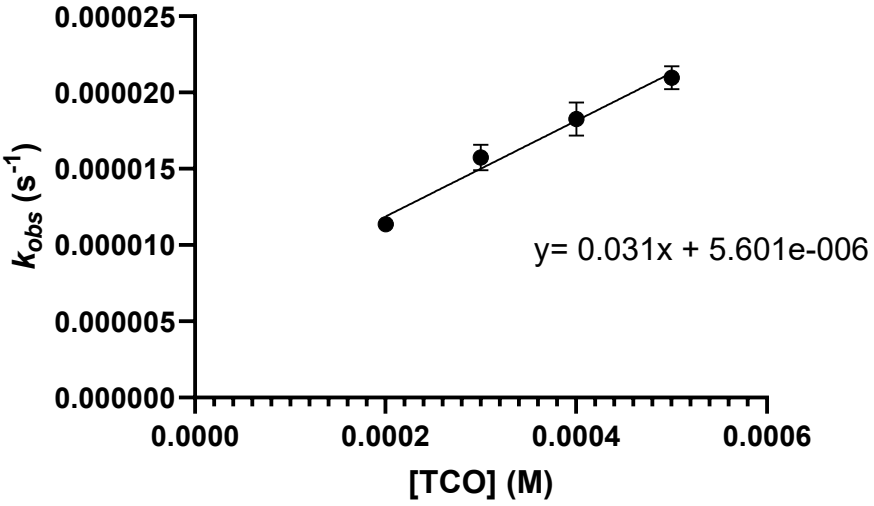

Figure S3. Pseudo first-order rate constants of cycloadditions of **2d** C-(4-bromophenyl)-*N*-phenylnitrone with s-TCO plotted against the tested concentrations of s-TCO. Error bars represent the difference of the replicate reactions. R^2= 0.96.

Table S4. Observed rate constants for the kinetic studies of cycloadditions of s-TCO with **2f** C-(4-nitrophenyl)-*N*-phenylnitrone correlated to the tested concentrations of s-TCO in methanol.

Nitrone	Concentration of TCO (10^{-4} M)	k_{obs} (10^{-5} s^{-1})
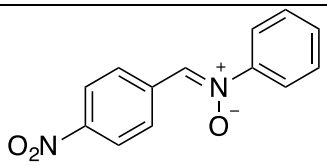	2.00	5.45 ± 0.07
	3.00	6.07 ± 0.05
	4.00	7.59 ± 0.42
	5.00	11.1 ± 3.63

All reactions were done in Methanol at 25 °C.

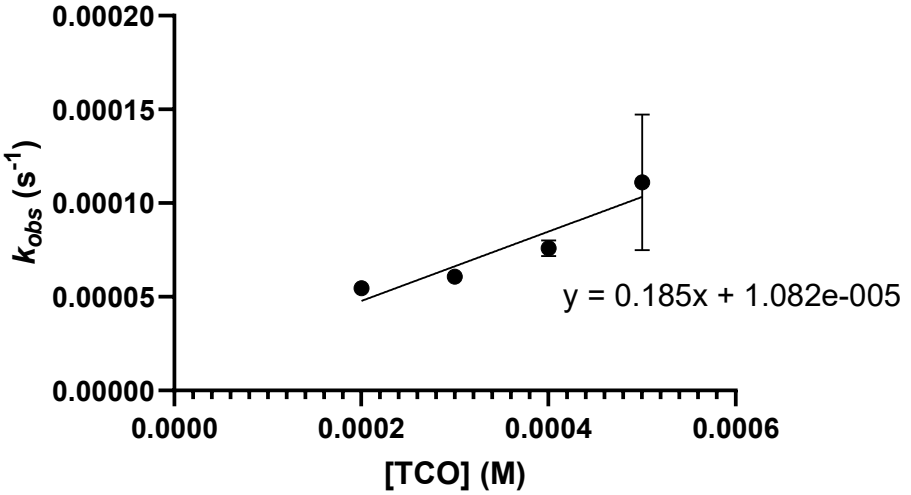

Figure S4. Pseudo first-order rate constants of cycloadditions of **2f** C-(4-nitrophenyl)-*N*-phenylnitrone with s-TCO plotted against the tested concentrations of s-TCO. Error bars represent the difference of the replicate reactions. R^2= 0.66.

Table S5. Observed rate constants for the kinetic studies of cycloadditions of s-TCO with **2e** C-(4-cyanophenyl)-*N*-phenylnitrone correlated to the tested concentrations of s-TCO in methanol.

Nitrone	Concentration of TCO (10^{-4} M)	k_{obs} (10^{-5} s^{-1})
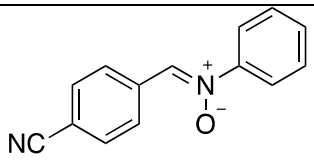	2.00	5.39 ± 0.31
	3.00	7.64 ± 0.12
	4.00	8.39 ± 0.66
	5.00	10.0 ± 0.36

All reactions were done in Methanol at 25 °C

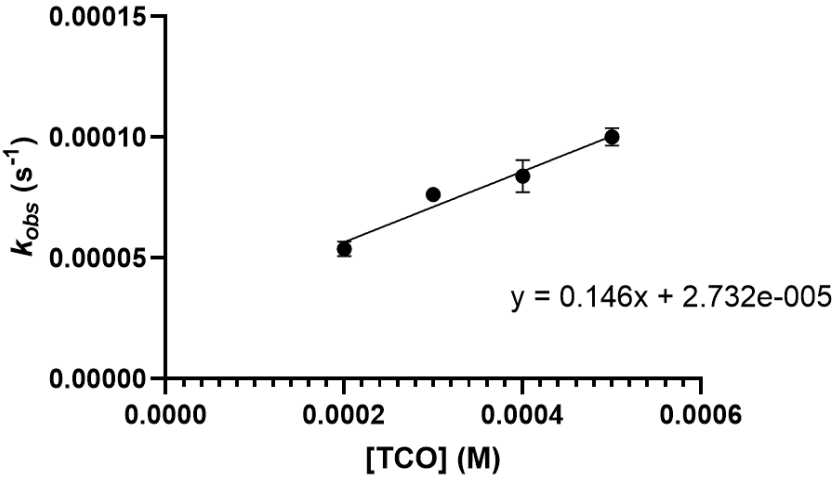

Figure S5. Pseudo first-order rate constants of cycloadditions of **2e** C-(4-cyanophenyl)-*N*-phenylnitrone with s-TCO plotted against the tested concentrations of s-TCO. Error bars represent the difference of the replicate reactions. R^2= 0.94.

Table S6. Observed rate constants for the kinetic studies of cycloadditions of unstrained-TCO with **2f** C-(4-nitrophenyl)-*N*-phenylnitrone correlated to the tested concentrations of unstrained-TCO in methanol.

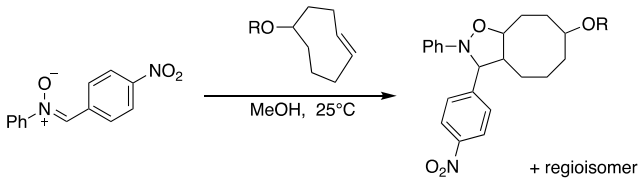

Nitrone	Concentration of TCO (10^{-4} M)	k_{obs} (10^{-6} s^{-1})
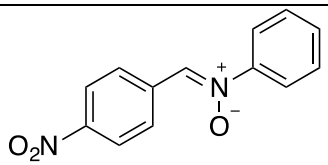	2.00	0.91 ± 0.08
	3.00	1.28 ± 0.40
	4.00	1.86 ± 0.19
	5.00	2.20 ± 0.33

All reactions were done in Methanol at 25 °C

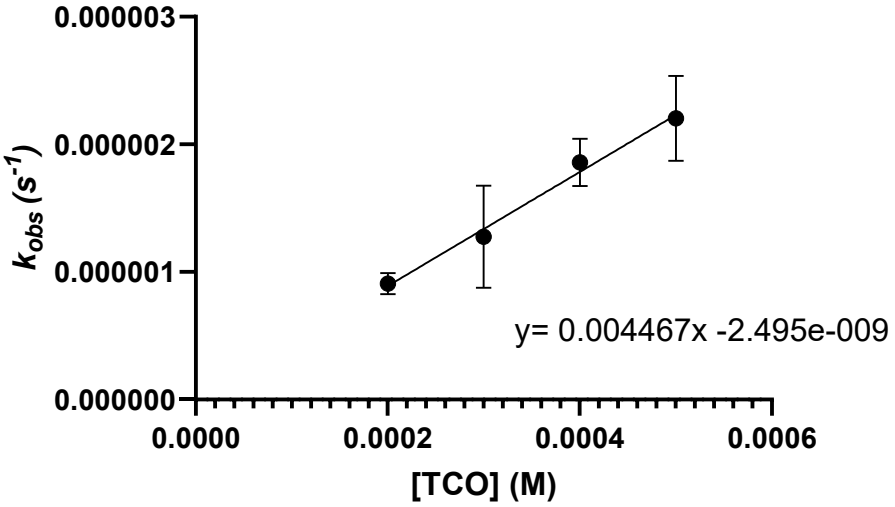

Figure S6. Pseudo first-order rate constants of cycloadditions of **2f** C-(4-nitrophenyl)-*N*-phenylnitrone with unstrained-TCO plotted against the tested concentrations of unstrained-TCO. Error bars represent the difference of the replicate reactions. R^2= 0.86.

Table S7. Acyclic nitrones data for the Hammett plot.

Nitrone	Sub. Constant σ_p	k_2 ($M^{-1}s^{-1}$)	k_2 (1x)/ k_2(1j)	log (k_2 (1x)/ k_2(1j))
R_2= C_6H_5	0	0.01	1.00	0
R_2= p-FC_6H_4	0.06	0.02	1.21	0.08
R_2= p-BrC_6H_4	0.23	0.03	2.24	0.35
R_2= p-CNC_6H_4	0.66	0.15	10.43	1.02
R_2= p-$NO_2C_6H_4$	0.78	0.19	13.21	1.12

NMR second-order kinetic analysis

Table S8. Calculated concentration of nitrone **2a** based off peak integration determined using 1,3,5-trimethoxybenzene as the internal standard.

Nitrone	Time (s)	[Nitrone] (M)	1/[Nitrone] (M^{-1})
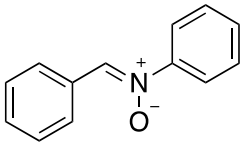	0	0.025	40.000
	130	0.024	42.162
	436	0.022	46.443
	740	0.021	49.609
	1044	0.019	52.125

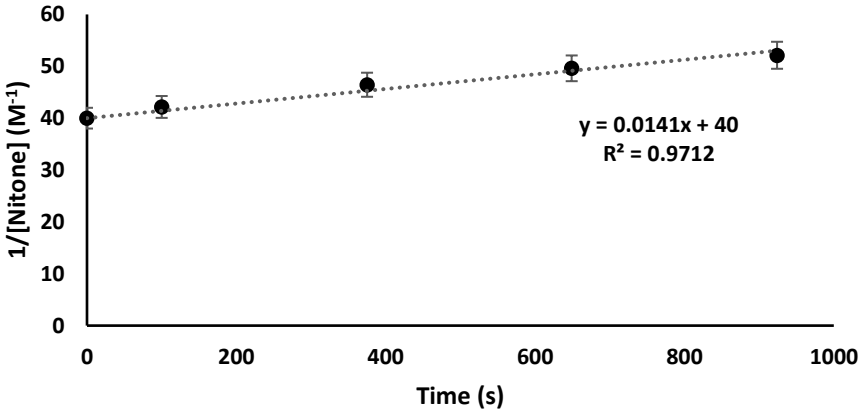

Figure S7. Bimolecular rate constant (k_2) determination of cycloaddition reaction between nitrone **2a** and s-TCO-OH by ^{1}H NMR.

Table S9. Calculated concentration of nitrone **2g** based off peak integration determined using to 1,3,5-trimethoxybenzene as the internal standard.

Nitrone	Time (s)	[Nitrone] (M)	1/[Nitrone] (M^{-1})
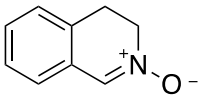	0	0.025	40.000
	100	0.020	50.744
	375	0.014	69.946

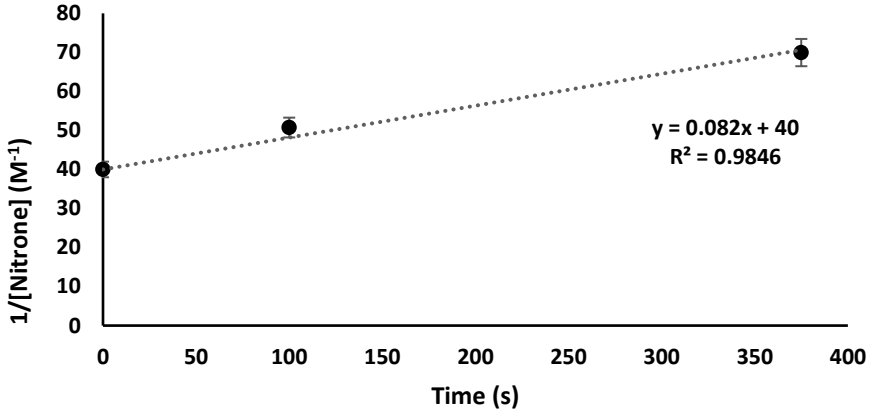

Figure S8. Bimolecular rate constant (k_2) determination of cycloaddition reaction between nitrone **2g** and s-TCO-OH by ^{1}H NMR.

Table S10. Calculated concentration of nitrone **2h** based off peak integration determined using 1,3,5-trimethoxybenzene as the internal standard.

Nitrone	Time (s)	[Nitrone] (M)	1/[Nitrone] (M^{-1})
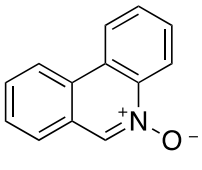	0	0.025	40.000
	130	0.0196	46.776
	436	0.0162	56.944
	740	0.0148	65.457
	1044	0.0140	69.734

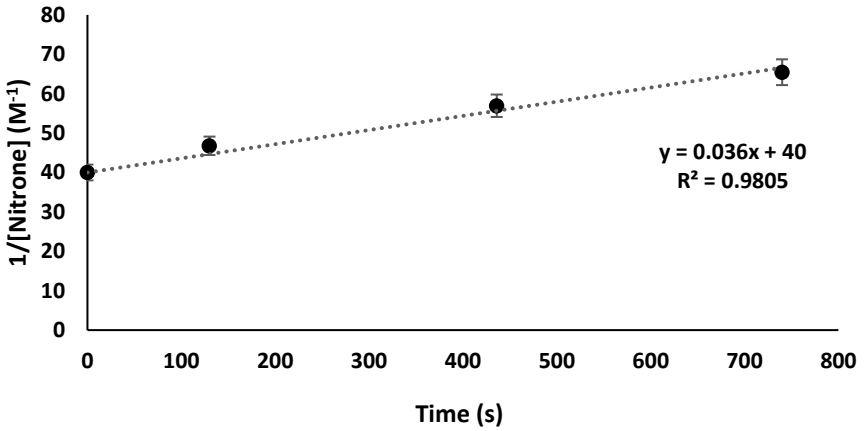

Figure S9. Bimolecular rate constant (k_2) determination of cycloaddition reaction between nitrone **2h** and s-TCO-OH by ^{1}H NMR.

Table S11. Calculated concentration of nitrone **2i** based off peak integration and comparison to 1,3,5-trimethoxybenzene as the internal standard.

Nitrone	Time (s)	[Nitrone] (M)	1/[Nitrone] (M^{-1})
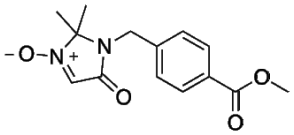	0	0.025	40.000
	100	0.0196	51.012
	376	0.0151	66.190
	652	0.014	73.006

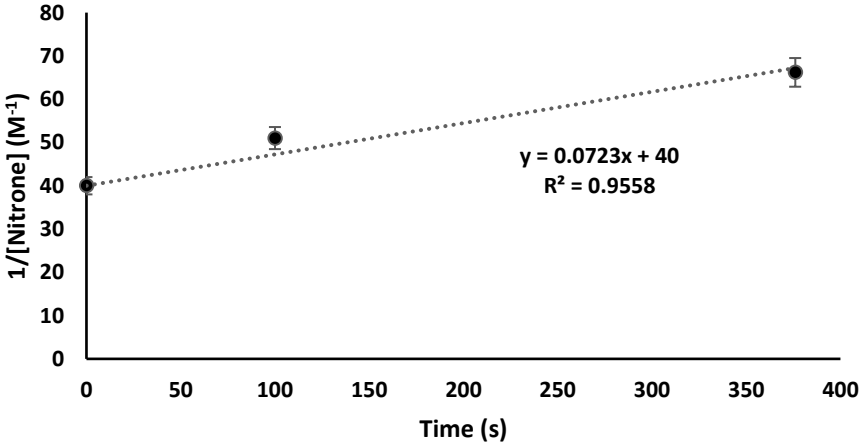

Figure S10. Bimolecular rate constant (k_2) determination of cycloaddition reaction between nitrone **2i** and s-TCO-OH by ^{1}H NMR.

Appendix B

Kinetic Analysis for Chapter 3

Pseudo first-order kinetics of diyne with acyclic nitrones

Table S12. Observed rate constants for the sequential-pseudo first-order kinetic studies of cycloaddition reactions of nitrone **3b** C-(4-methoxyphenyl)-*N*-phenylnitrone with diyne, correlated to various concentrations of nitrone in methanol.

Nitrone	Concentration of Nitrone (10^{-3} M)	k_1' (10^{-4} s^{-1})	k_2' (10^{-4} s^{-1})
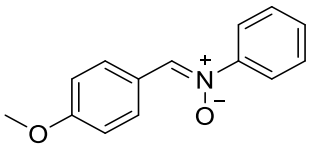	1.00	1.06 ± 0.02	9.76 ± 0.45
	1.25	1.48 ± 0.12	9.87 ± 0.58
	1.50	1.49 ± 0.20	9.96 ± 0.69
	2.00	2.05 ± 0.06	10.4 ± 0.37

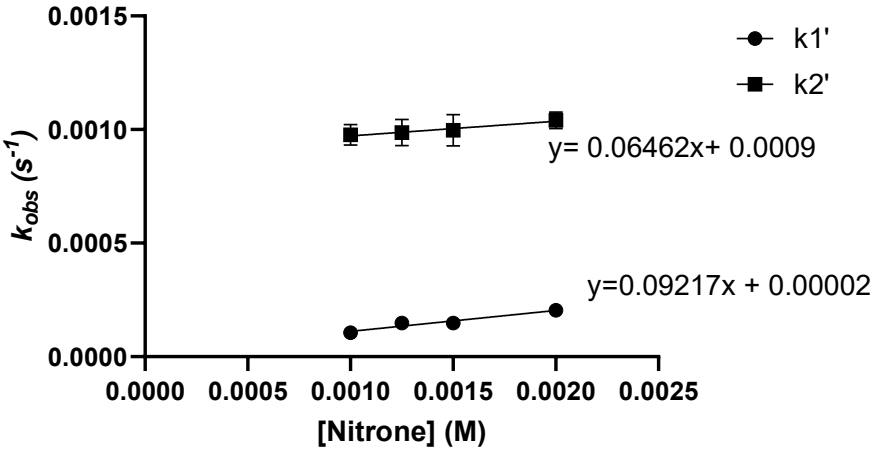

Figure S11. Pseudo first-order rate constants of the first (k_1) and second (k_2') cycloadditions of **3b** C-(4-methoxyphenyl)-*N*-phenylnitrone with diyne plotted against the various concentrations of nitrone (M). Error bars represent the difference of the replicate reactions. R^2 (k_1') = 0.89, R^2 (k_2') = 0.28.

Table S13. Observed rate constants for the sequential-pseudo first-order kinetic studies of cycloaddition reactions of nitrone **3c** C-(4-flourophenyl)-*N*-phenylnitrone with diyne, correlated to various concentrations of nitrone in methanol.

Nitrone	Concentration of Nitrone (10^{-3} M)	k_1' (10^{-4} s^{-1})	k_2' (10^{-3} s^{-1})
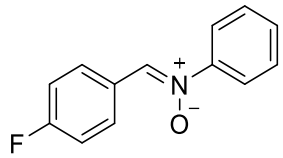	0.50	1.76 ± 0.18	0.96 ± 0.10
	1.00	3.30 ± 0.21	1.02 ± 0.29
	1.50	3.97 ± 0.22	1.24 ± 0.05
	2.00	4.66 ± 0.25	1.64 ± 0.01

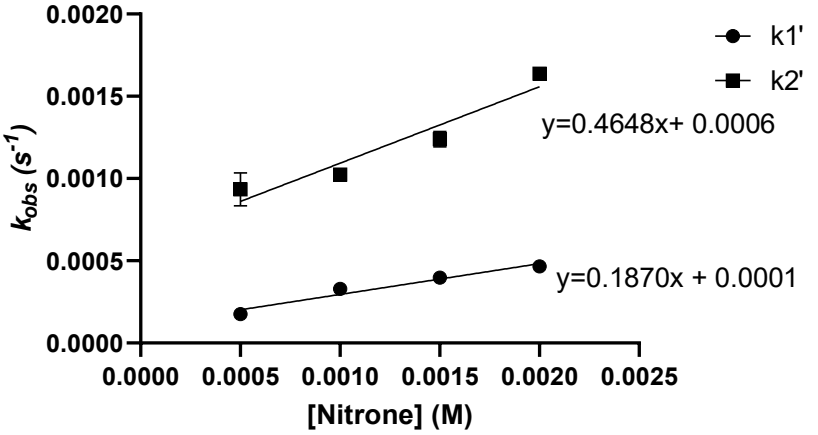

Figure S12. Pseudo first-order rate constants of the first (k_1) and second (k_2) cycloadditions of **3c** C-(4-flourophenyl)-*N*-phenylnitrone with diyne plotted against the various concentrations of nitrone (M). Error bars represent the difference of the replicate reactions. R^2 (k_1') = 0.93, R^2 (k_2') = 0.90.

Table S14. Observed rate constants for the sequential-pseudo first-order kinetic studies of cycloaddition reactions of nitrone **3d** C-(4-bromophenyl)-*N*-phenylnitrone with diyne, correlated to various concentrations of nitrone in methanol.

Nitrone	Concentration of Nitrone (10^{-3}M)	k_1' (10^{-4} s^{-1})	k_2' (10^{-3} s^{-1})
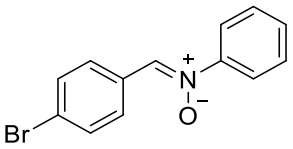	0.50	4.32 ± 0.06	1.14 ± 0.07
	1.00	5.24 ± 0.29	1.09 ± 0.00
	1.50	5.41 ± 0.09	1.42 ± 0.08
	2.00	6.12 ± 0.03	1.61 ± 0.08

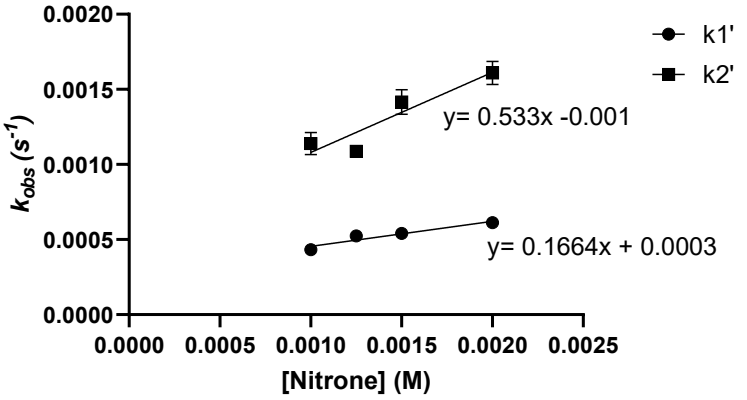

Figure S13. Pseudo first-order rate constants of the first (k_1) and second (k_2) cycloadditions of **3d** C-(4-bromophenyl)-*N*-phenylnitrone with diyne plotted against the various concentrations of nitrone (M). Error bars represent the difference of the replicate reactions. R^2 (k_1') = 0.89, R^2 (k_2') = 0.82.

Table S15. Observed rate constants for the sequential-pseudo first-order kinetic studies of cycloaddition reactions of nitrone **3e** C-(4-cyanophenyl)-*N*-phenylnitrone with diyne, correlated to various concentrations of nitrone in methanol.

Nitrone	Concentration of Nitrone (10^{-3}M)	k_1' (10^{-4} s^{-1})	k_2' (10^{-3} s^{-1})
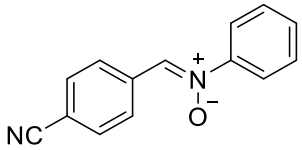	0.50	4.35 ± 0.05	2.11 ± 0.10
	1.00	5.05 ± 0.06	3.20 ± 0.13
	1.50	5.40 ± 0.06	5.46 ± 0.46
	2.00	5.83 x± 0.11	7.99 ± 0.00

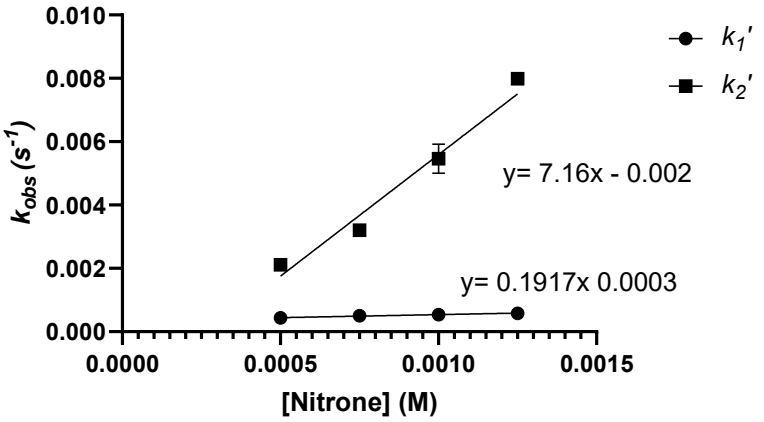

Figure S14. Pseudo first-order rate constants of the first (k_1) and second (k_2) cycloadditions of **3d** C-(4-cyanophenyl)-*N*-phenylnitrone with diyne plotted against the various concentrations of nitrone (M). Error bars represent the difference of the replicate reactions. R^2 (k_1') = 0.97, R^2 (k_2') = 0.96.

Table S16. Hammett plot data for the first addition (k_1) of the reaction of acyclic nitrones with diyne.

Nitrone	Sub. Constant σ_p	k_2 ($M^{-1}s^{-1}$)	k_2 (1x)/ k_2(1j)	log (k_2 (1x)/ k_2(1j))
R_2=p-OMeC_6H_4	-0.27	0.09	0.55	-0.26
R_2= C_6H_5	0	0.17	1.00	0.00
R_2= p-FC_6H_4	0.06	0.19	1.13	0.05
R_2= p-BrC_6H_4	0.23	0.17	0.98	-0.01
R_2= p-CNC_6H_4	0.66	0.19	1.14	0.06

Table S17. Hammett plot data for the second addition (k_2) of the reaction of acyclic nitrones with diyne.

Nitrone	Sub. Constant σ_p	k_2 ($M^{-1}s^{-1}$)	k_2 (1x)/ k_2(1j)	log (k_2 (1x)/ k_2(1j))
R_2=p-OMeC_6H_4	-0.27	0.07	0.16	-0.81
R_2= C_6H_5	0	0.41	1	0
R_2= p-FC_6H_4	0.06	0.46	1.12	0.05
R_2= p-BrC_6H_4	0.23	0.53	1.28	0.11
R_2= p-CNC_6H_4	0.66	7.16	17.30	1.24

Table S18. Observed rate constants for the sequential-pseudo first-order kinetic studies of cycloaddition reactions of nitrone **3a** with diyne, correlated to various concentrations of nitrone in methanol.

Nitrone	Concentration of Nitrone (M)	k_1' (x 10^{-4} s^{-1})
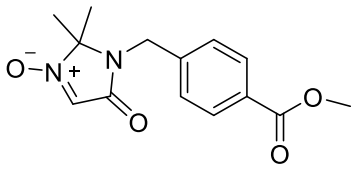	5.00 x 10^{-4}	8.68
	1.00 x 10^{-3}	1.29 ± 0.33
	1.50 x 10^{-3}	1.63 ± 0.60
	2.00 x 10^{-3}	2.05 ± 0.45

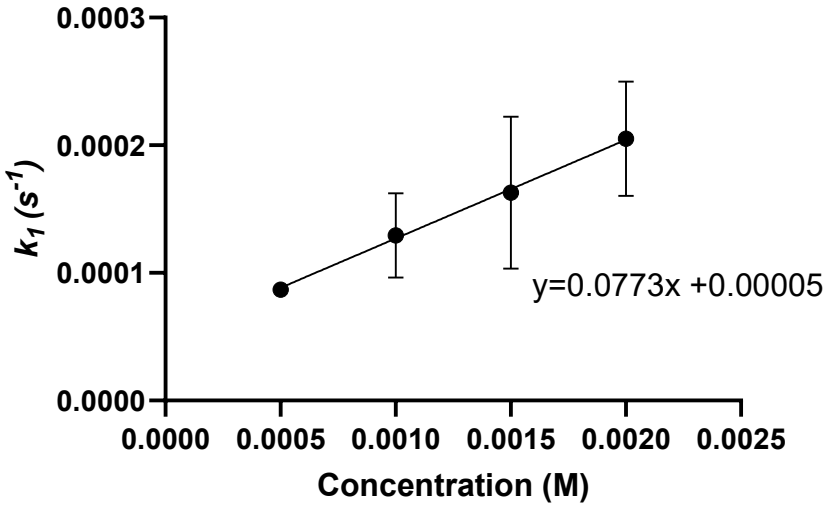

Figure S15. Observed rate constant for the pseudo first-order kinetic studies of cycloaddition reaction of DMImO with diyne, correlated to various concentrations of nitrone in methanol. Error bars represent the difference of the replicate reactions. R^2 (k_1') = 0.63.

Appendix C

NMR and Mass Spectroscopy Data

^{1}H NMR of Synthesized Nitrones

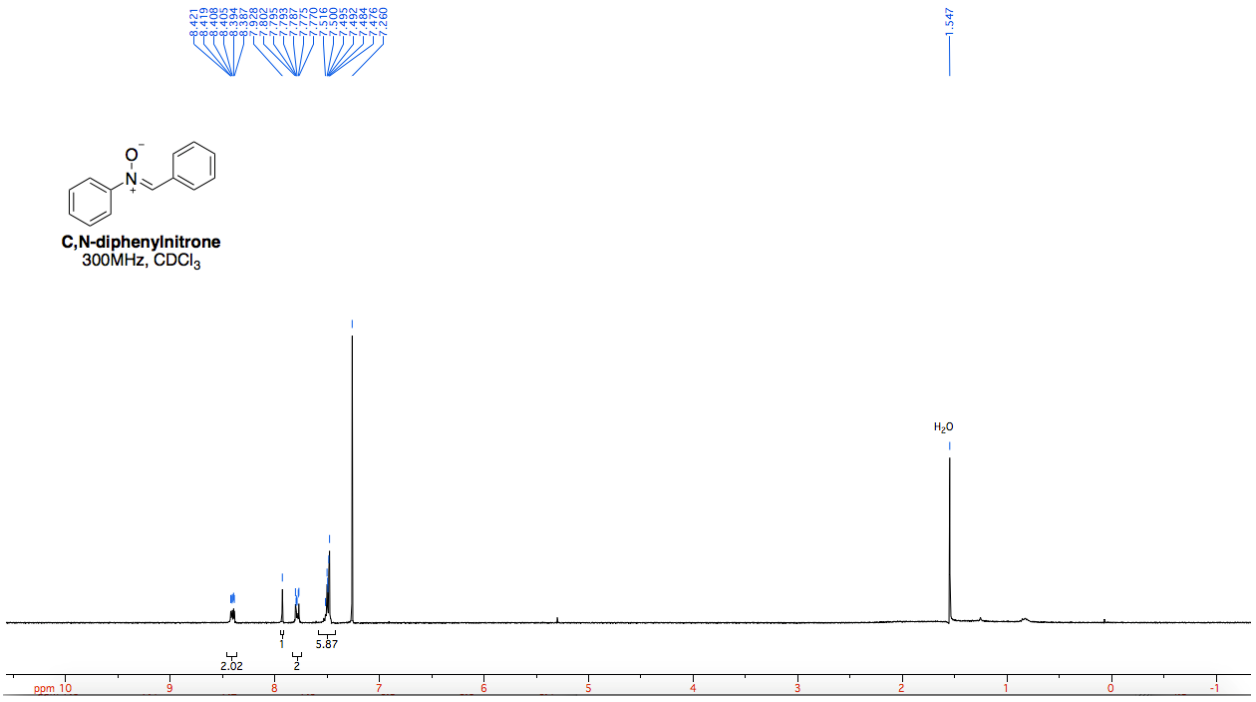

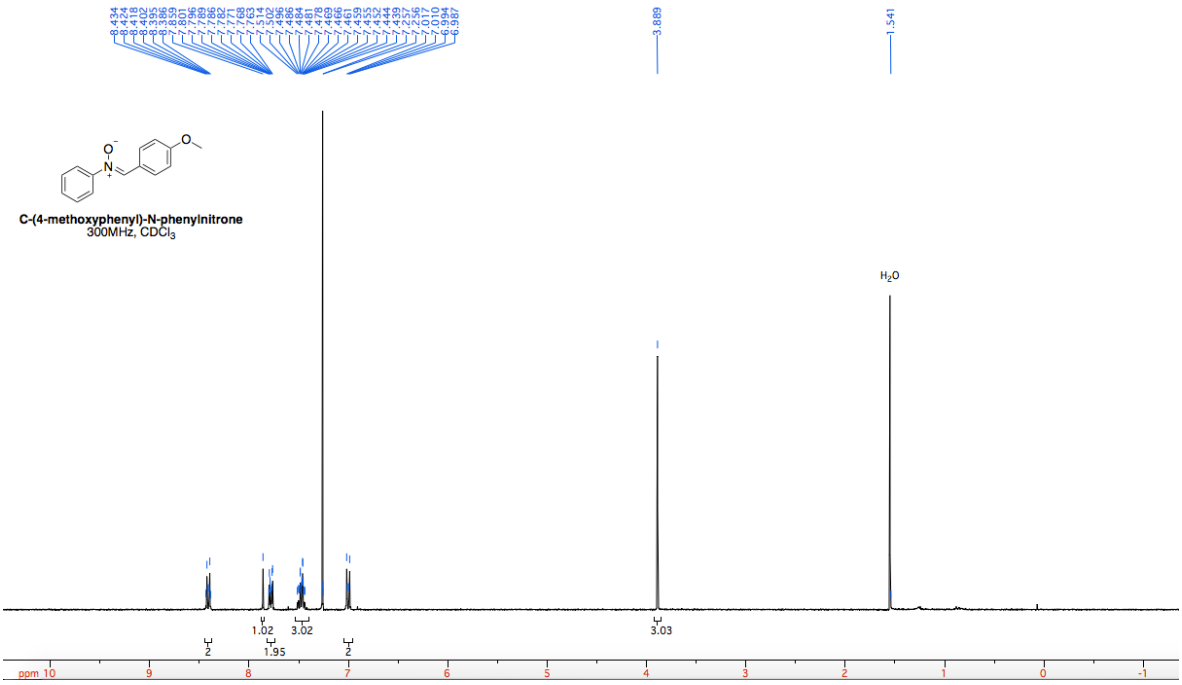
C-(4-methoxyphenyl)-N-phenylnitrone
300MHz, CDCl3
3.889
1.541
H2O
1.02
3.02
3.03
1.95
2
2
2
ppm 10
9
8
7
6
5
4
3
2
1
0
-1

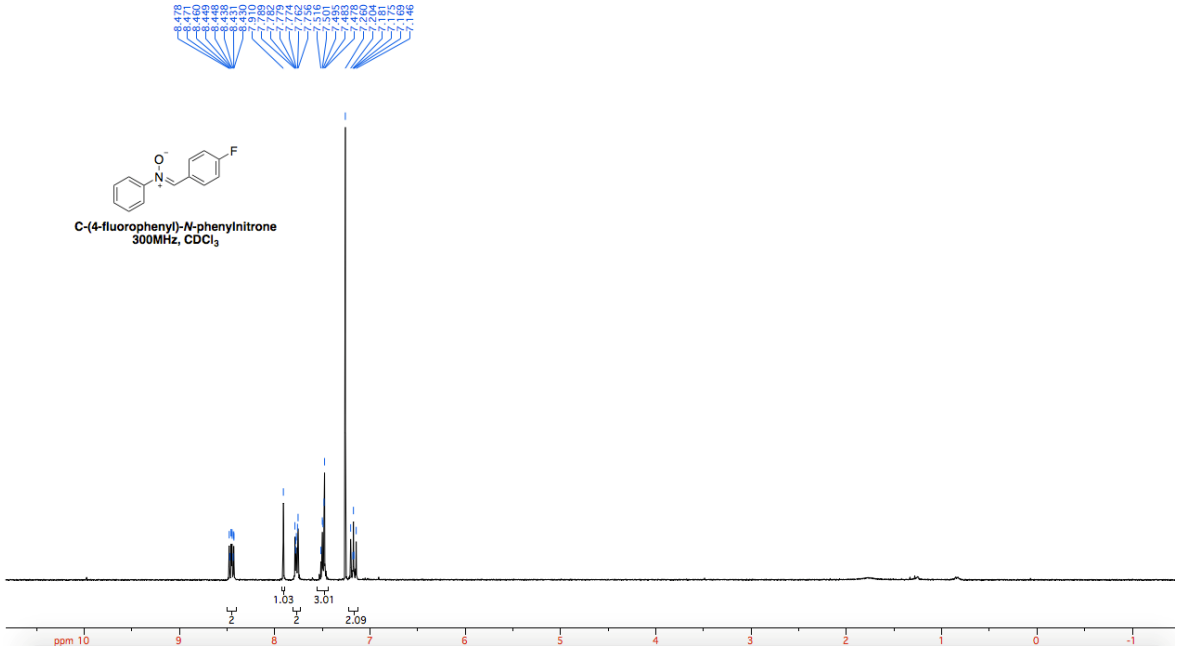
C-(4-fluorophenyl)-N-phenylnitrone
300MHz, CDCl3
F
1.03
3.01
2
2
2.09
ppm 10
9
8
7
6
5
4
3
2
1
0
-1

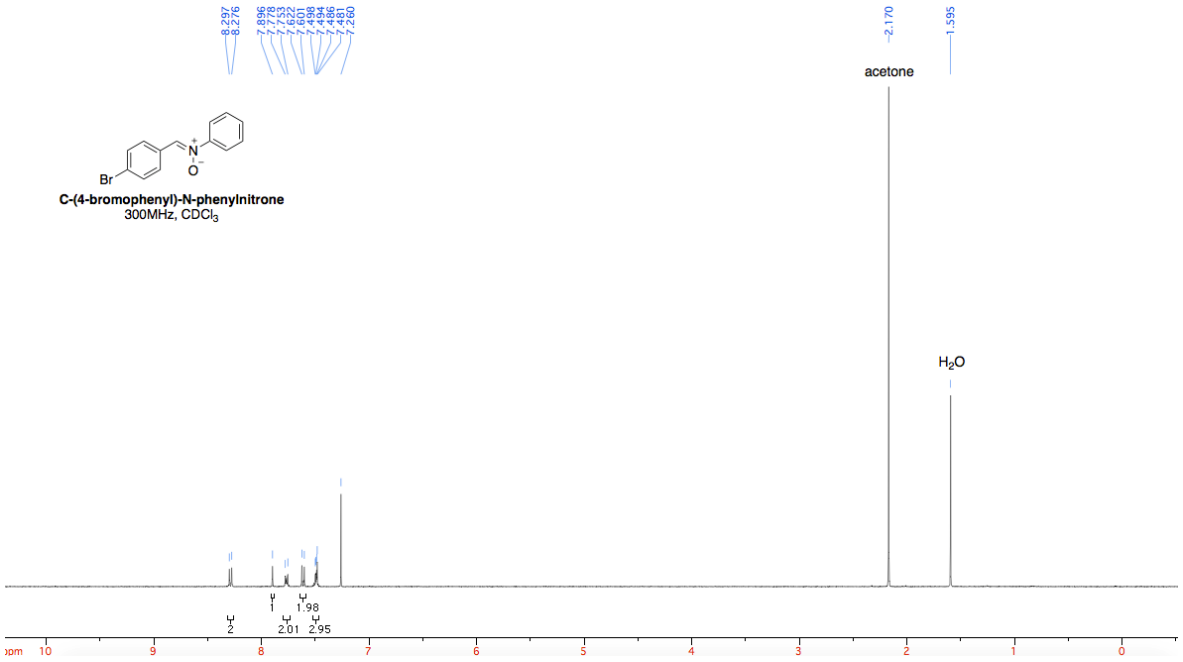
8.297
8.276
7.896
7.778
7.753
7.622
7.601
7.498
7.494
7.486
7.481
7.260
2.170
1.595
acetone
Br
C-(4-bromophenyl)-N-phenylnitrone
300MHz, CDCl3
H2O
1
1.98
2
2.01
2.95
ppm 10
9
8
7
6
5
4
3
2
1
0

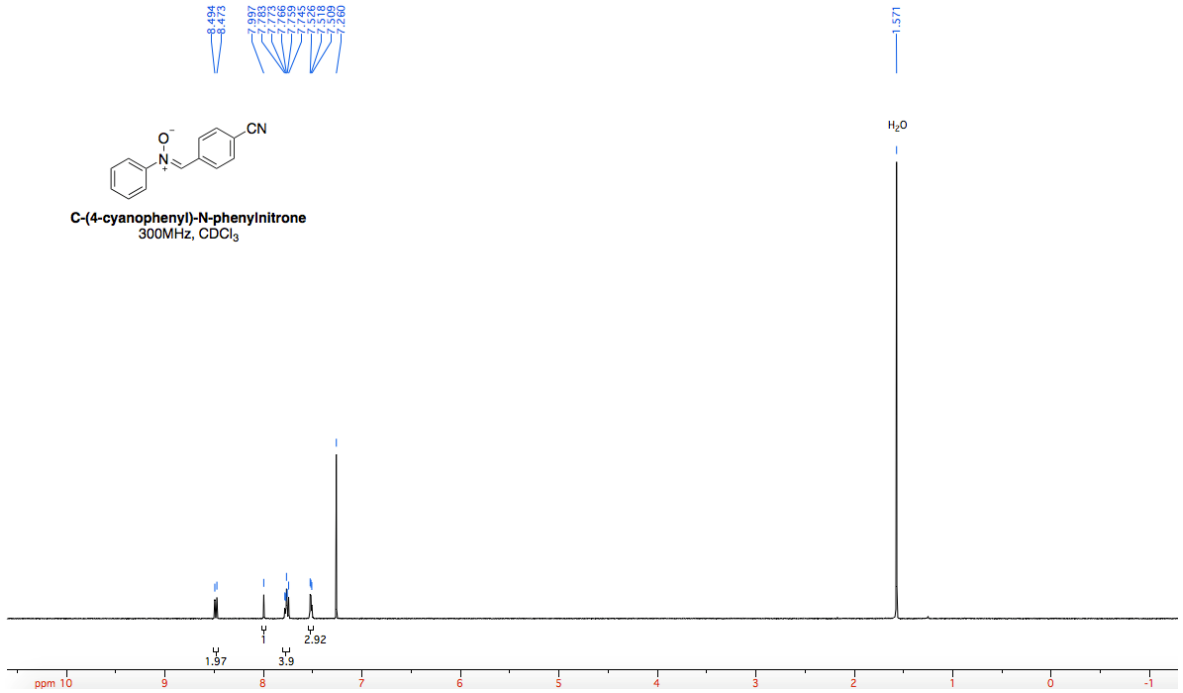
8.494
8.473
7.987
7.783
7.773
7.766
7.759
7.745
7.526
7.518
7.509
7.260
1.571
CN
C-(4-cyanophenyl)-N-phenylnitrone
300MHz, CDCl3
H2O
1.97
1
3.9
2.92
ppm 10
9
8
7
6
5
4
3
2
1
0
-1

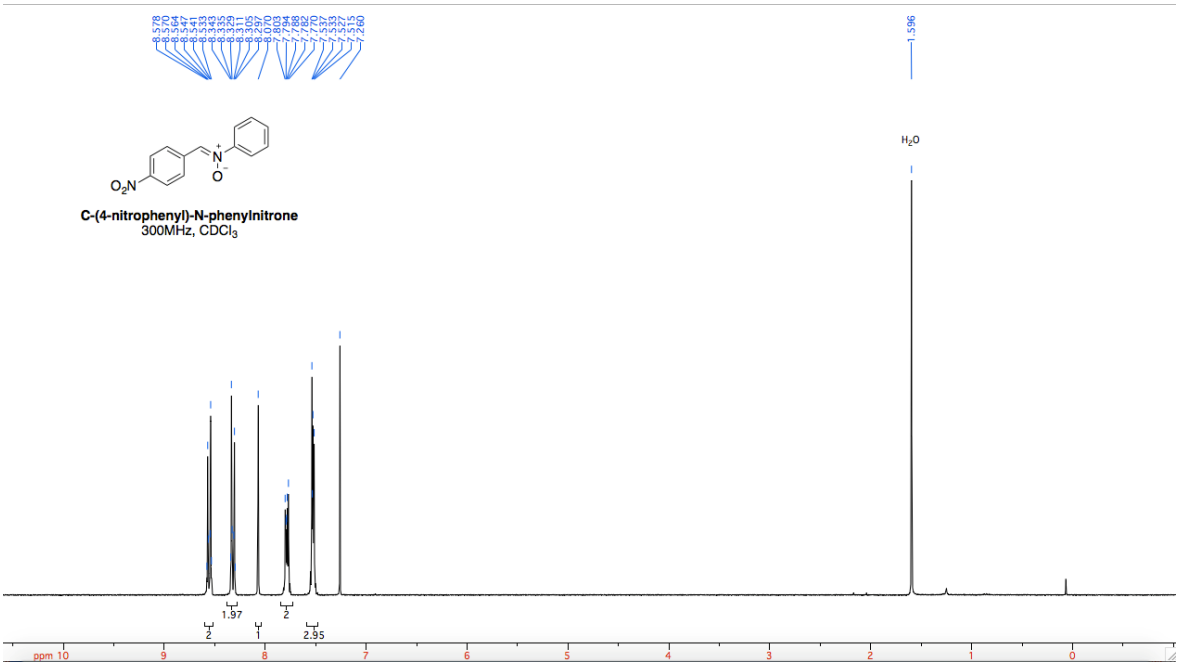
8.578
8.570
8.564
8.547
8.541
8.345
8.343
8.325
8.320
8.311
8.305
8.297
8.070
7.993
7.984
7.788
7.782
7.770
7.537
7.533
7.527
7.515
7.260
1.596
H2O
O2N
N
O
C-(4-nitrophenyl)-N-phenylnitrone
300MHz, CDCl3
1.97
2
2.95
ppm 10
9
8
7
6
5
4
3
2
1
0

Mass Spectrsocopy Spectra

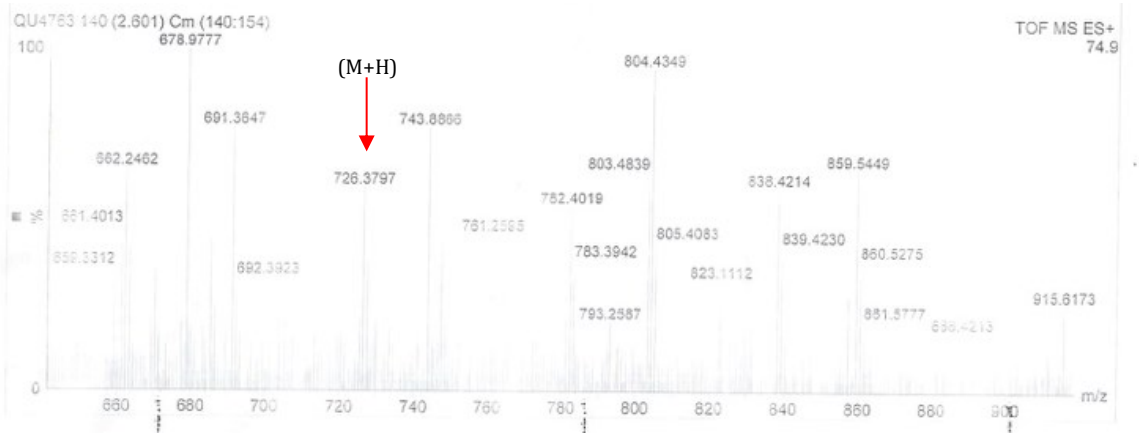

Figure S16. LC-MS analysis of Alexa-TCO on Micromass Q-TOF I quadrupole – time-of-flight mass spectrometer (ESI+ mode, direct injection).

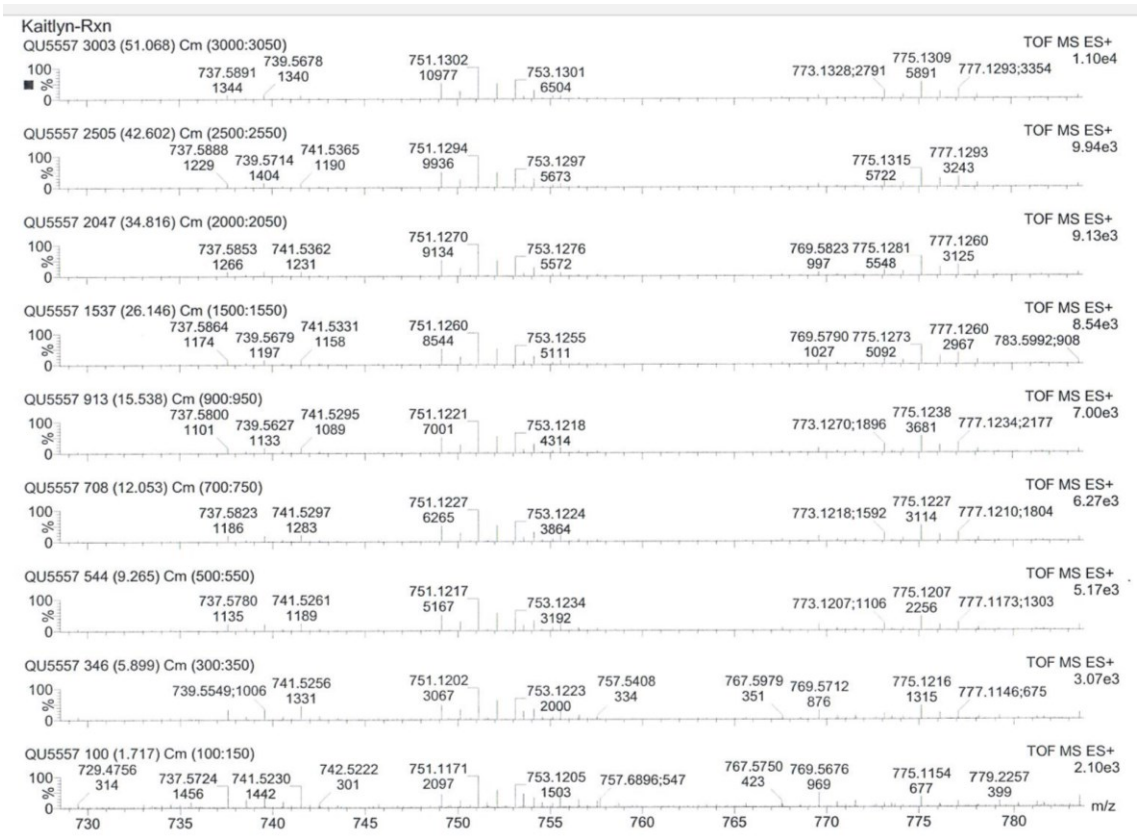

Figure S17. MS analysis of reaction of 100μM diyne 100 μM C-(*4*-bromophenyl)-N-phenylnitrone over 60 minutes, using Waters Synapt High Definition Mass Spectrophotometer Q-TOF (ESI+ mode, direct injection). Intensities of peak region where the di-product ions are found. **MS (ESI+)** calcd ($C_{42}H_{28}Br_2N_2O_2$): 750.05. Found $(M+H)^+$: 751.13, 753.13 and $(M+Na)^+$: 775.12, 777.13

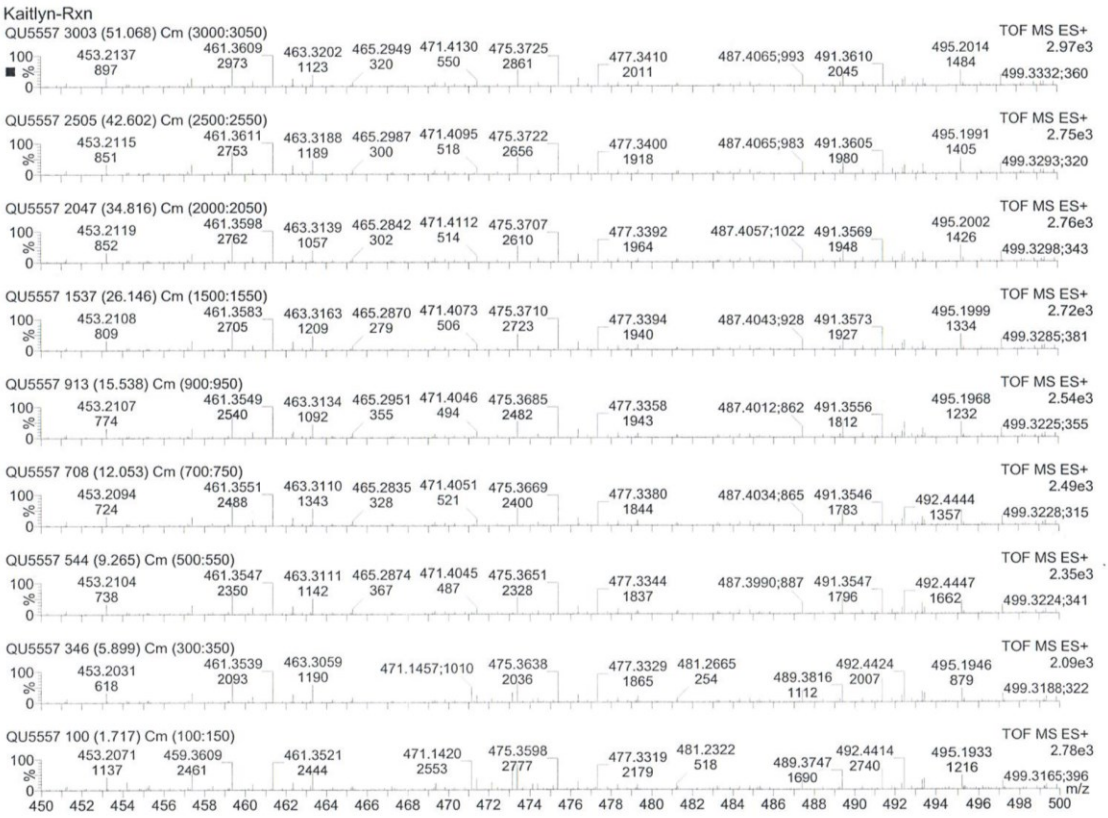

Figure S18. MS analysis of reaction of 100μM diyne 100 μM C-(*4*-bromophenyl)-N-phenylnitrone over 60 minutes, using Waters Synapt High Definition Mass Spectrophotometer Q-TOF (ESI+ mode, direct injection). Intensities of peak region where the mono-intermediate ions would be found. **MS (ESI+)** calcd ($C_{30}H_{21}BrNO$): 475.06

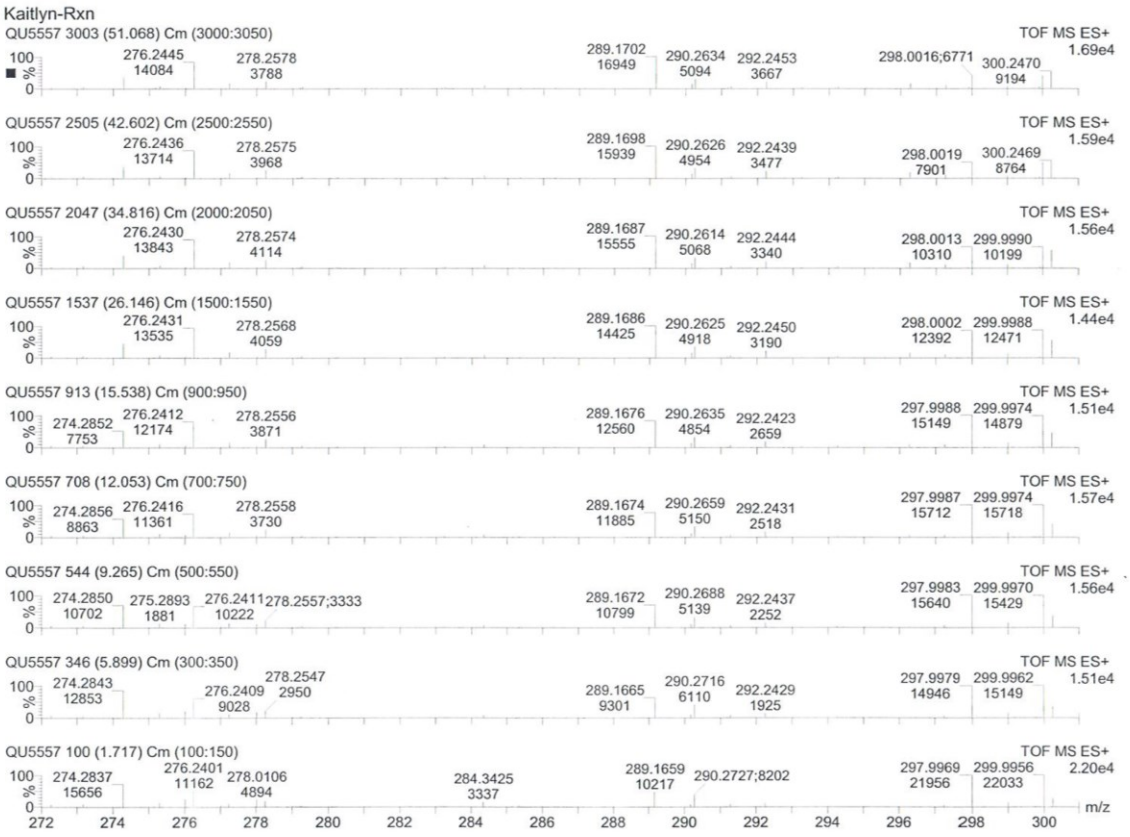

Figure S19. MS analysis of reaction of 100μM diyne 100 μM C-(*4*-bromophenyl)-N-phenylnitrone over 60 minutes, using Waters Synapt High Definition Mass Spectrophotometer Q-TOF (ESI+ mode, direct injection). Intensities of peak region where the C-(*p*-bromophenyl)-N-phenylnitrone ions are found. **MS (ESI+)** calcd ($C_{13}H_{10}BrNO$): 274.99. Found $(M+H)^+$: 276.24, 278.25 and $(M+Na)^+$: 298.00, 300.00

Appendix D List of Publications

Master's Degree

Bilodeau DA, **Margison KD**, Ahmed N, Strmiskova M, Sherratt AR, Pezacki JP. Optimized aqueous Kinugasa reactions for bioorthogonal chemistry applications. *Chem Commun (Camb).* **56**, 1988-1991 (2020).

Margison KD, Bilodeau DA, Mahmoudi F, Pezacki JP. Cycloadditions of Trans-Cyclooctenes and Nitrones as Tools for Bioorthogonal Labelling. *Chembiochem.* **21**, 948-951 (2020).

Undergraduate Degree

Margison KD*, Snider SA*, Ghorbani P, LeBlond ND, O'Dwyer C, Nunes JRC, Nguyen T, Xu H, Bennett SAL, Fullerton MD. Choline transport links macrophage phospholipid metabolism and inflammation. *J Biol Chem.* **293**, 11600-11611 (2018).

Shah R, **Margison K**, Pratt DA. The Potency of Diarylamine Radical-Trapping Antioxidants as Inhibitors of Ferroptosis Underscores the Role of Autoxidation in the Mechanism of Cell Death. *ACS Chem Biol*. **12**, 2538-2545 (2017).

Sundaram M, Curtis KR, Amir Alipour M, LeBlond ND, **Margison KD**, Yaworski RA, Parks RJ, McIntyre AD, Hegele RA, Fullerton MD, Yao Z. The apolipoprotein C-III (Gln38Lys) variant associated with human hypertriglyceridemia is a gain-of-function mutation. *J Lipid Res.* **58**, 2188-2196 (2017).

O'Dwyer C, Yaworski R, Katsumura S, Ghorbani P, Gobeil Odai K, Nunes JRC, LeBlond ND, Sanjana S, Smith TTK, Han S, **Margison KD**, Alain T, Morita M, Fullerton MD. Hepatic Choline Transport Is Inhibited During Fatty Acid-Induced Lipotoxicity and Obesity. *Hepatol Commun*. **4**, 876-889 (2020).